AN ANALYSIS OF THE MECHANICAL PROPERTIES OF AORTIC VALVE INTERSTITIAL CELLS USING MICROPIPETTE ASPIRATION

by

Kristine Wyss

A thesis submitted in conformity with the requirements

for the degree of Master of Applied Science – Mechanical Engineering

Graduate Department of Mechanical and Industrial Engineering

University of Toronto

Thesis Title: An analysis of the mechanical properties of aortic valve interstitial cells using micropipette aspiration

Degree and Year: Master of Applied Science, 2008

Name: Kristine Wyss

Department: Mechanical and Industrial Engineering

University: University of Toronto

Abstract

Changes in cellular mechanical and structural properties may lead to alterations in normal physiological behaviour and be indicative of a pathogenic response. In this thesis, a micropipette aspiration system was designed, constructed and tested as a means to investigate the changes in mechanical properties of aortic valve interstitial cells (VICs). Results indicate that healthy VICs exhibit spatial heterogeneity in elastic response consistent with tissue-level differences in valve structure and organization. Valve pathology often involves an active tissue-level reorganization of the extracellular matrix by the VICs, ultimately resulting in calcific bone nodules and fibrosis. Separate *in vitro* induction of myofibrogenic and osteogenic differentiation of VICs indicated that the differentiated cells once again reflect tissue-level changes – stiffening – in mechanical properties. Additionally, the two pathological mechanisms appear to differentially mediate changes in cell stiffness. VIC mechanical properties therefore appear to be influenced or regulated by both environment and pathology.

Acknowledgements

First and foremost, I would like to thank Craig for all of the support, advice and guidance he has given me over the past few years. None of the work I have accomplished would have been possible without his continued encouragement in face of the obstacles and challenges I experienced. His passion for research has been a constant source of inspiration and I am truly grateful for having had the opportunity to work with such a motivated and dedicated supervisor. I wish you nothing but the best and have no doubt you will be able to attract the best and brightest minds for many years to come.

Secondly, I have to acknowledge and thank all of my fellow labmates in the Cellular Mechanobiology Laboratory, for making my time in the lab and office so enjoyable. I especially want to give thanks to Cindy for all her collagen gel, cell culture and general lab-related advice, Ruogang for his patience in answering my many modeling questions and Zahra for all her technical expertise. To the rest of the group I have worked with these past few years – Chris, Edmond, Jan, Kelly, Krista, Morakot, Wing-Yee and the many summer students that have come and gone – thank you all for the help and advice, and for providing so many much needed and humour-filled distractions.

Finally, I would like to thank my friends and family for providing me with the encouragement to continue with my studies, and for maintaining the belief that I could accomplish whatever I set out to do. I especially want to acknowledge my parents, Barbara and Urs, for their constant and unending support and for the excellent example they have provided me.

Table of contents

v

List of tables

List of figures

Chapter 1:   Introduction

1.1.   Motivation

The structure and mechanical integrity of individual cells can have far-reaching effects on a multitude of biological processes, including growth, differentiation, migration and apoptosis. Changes in mechanical and structural properties at the cellular level may lead to alterations in normal physiological behaviour and may indicate or even trigger the emergence of a pathogenic response. A complete understanding of how various chemical, biological and mechanical pathways interact to promote a pathogenic response therefore requires the study of cellular mechanical properties as a function of both healthy and diseased states.

The cells of interest for this particular study are aortic valve interstitial cells (VICs), a heterogeneous mix of predominantly quiescent fibroblasts distributed throughout the extracellular matrix (ECM) of the aortic valve leaflets. In the healthy valve, VICs are responsible for synthesizing and maintaining the ECM's distinct three-layer structure. However, they also play an active role in the development of aortic valve sclerosis (AS), which can involve both myofibrogenic and osteogenic differentiation within the VIC population, ultimately leading to valve leaflet calcification. At the tissue level, there is a clear shift in mechanical properties – stiffening – of the leaflet with the progression of the disease, inhibiting proper valve function and ultimately necessitating complete valve replacement. AS occurs preferentially on the aortic side of the valve, generally in regions exposed to high mechanical stress and disturbed blood flow. Much research into the underlying mechanobiological mechanisms of these two phenomena (differentiation of VICs and the

spatial heterogeneity of AS) has been conducted, however it is still unknown whether there is a corresponding structural and mechanical change of VICs at the cellular level.

The basic principles behind testing mechanical properties of cells include the application of a known external force that deforms the cell in some way – this force can be concentrated or distributed, transient or oscillatory, intracellular or on the cell surface – and the fitting of the resultant cellular deformation to appropriate mathematical models. The technique used for this particular project is micropipette aspiration (MA), which determines whole-cell elastic and viscoelastic properties. A negative pressure is applied to the surface of a cell held in a saline suspension through a small diameter glass tube (micropipette) by the downward motion of a fluid reservoir. The application of the suction pressure results in the time-dependent partial aspiration of the cell into the micropipette. Mechanical properties are obtained through the relationship between the applied negative pressure, the resulting force applied to the cell, the displacement of the cell membrane and the geometry of the micropipette and cell. The instantaneous and time-dependent mechanical response is determined by fitting experimental data to existing analytical mathematical models or by using finite element simulations.

1.2. Objectives

The overall goal of this project is therefore to use MA to learn more about VIC structure and function in both diseased and healthy cell phenotypes. The specific objectives of this study are as follows:

1. To design, construct, and test a custom MA system capable of determining elastic and viscoelastic properties of cells; and

2. To use the MA system to determine the mechanical response of valve interstitial cells, more specifically to determine the mechanical properties of:

    i.   Healthy VICs isolated from mechanically distinct valve regions; and

    ii.   VICs undergoing osteogenic and myofibrogenic differentiation.

1.3. Thesis organization

The first chapter presented the motivation and objectives of this thesis. The second chapter reviews existing techniques for measuring mechanical properties of cells, with a focus on the rational behind and the execution of the MA technique. This review chapter also summarizes existing knowledge of aortic valve physiology and pathology, with a particular emphasis on VICs. Chapter 3 first outlines the steps taken to design and construct our MA system and the protocols common to all MA experiments on VICs. The final section of Chapter 3 outlines some of the limitations and difficulties encountered in preliminary experiments. Chapters 4 and 5 describe the series of experiments conducted to establish VIC mechanical properties. Specifically, Chapter 4 looks at the spatial heterogeneity of VICs isolated from healthy valves, as well as the effect of standard culture techniques on VIC mechanical response. Chapter 5 examines changes in mechanical properties of VICs undergoing pathological differentiation. Finally, Chapter 6 provides overall conclusions and recommendations for future work.

Chapter 2: Background

2.1. Introduction

This review is divided into two main portions. First, we discuss the motivation behind measuring mechanical properties of cells (section 2.2) and provide a brief summary of existing techniques (section 2.3). A more detailed section outlining the principles behind micropipette aspiration (MA) follows (section 2.4). The second portion outlines the structure and function of the aortic valve and the cell type of interest, the valve interstitial cell (VIC) (section 2.5). Pathogenic processes within the valve are described, with a focus on the effects of matrix stiffness (section 2.6).

2.2. Cell mechanics

2.2.1. Mechanical forces on cells

Living cells *in vivo* are subjected to a variety of mechanical forces, arising from both the external environment and internal physiological conditions. Both applied external and intracellular mechanical forces are known to influence cell morphology, proliferation, motility, gene expression and even apoptosis [1]. For example, compressive forces on chondrocytes are known to modulate proteoglycan synthesis [2, 3] and the fluid shear experienced by endothelial cells in the circulatory system can activate hormone release and intracellular calcium signalling as well as stiffen cells by prompting rearrangement of the cytoskeleton [4-6] .

These external forces evidently elicit structural changes at the tissue- and organ-level; however to what extent these changes are mirrored at the cellular and molecular level is the subject of ongoing research. A clearer understanding of cell and molecular mechanics could

thus provide insight into mechanotransduction, the process through which external mechanical signals are converted to biochemical responses within the cell.

2.2.2. The cytoskeleton

Cellular-level mechanics are largely the function of the cytoskeleton, a network of three types of protein filaments – actin filaments, intermediate filaments and microtubules – that permeate the cytosol and mechanically support cellular membranes [7]. In response to externally applied forces, cells will actively rearrange the organization and contractile activity of the cytoskeleton and redistribute their intracellular forces [8].

Because the cytoskeleton also plays an important role as a mechanotransducer [9], changes to its organization can eventually alter gene transcription processes resulting in altered cell adhesion, secretion of ECM proteins and metabolic activity [10, 11]. These cytoskeletal changes can be reflected as changes in mechanical properties between different phenotypes or cell types, as has been observed in the differentiation of human mesenchymal stem cells (MSCs) to comparatively softer osteoblasts [12]. Immunostaining showed distinct actin cytoskeletal organization in MSCs and fully differentiated osteoblasts, and as MSCs were induced to differentiate into osteoblasts, both actin organization and cellular stiffness (Young's modulus) changed to match those observed in fully differentiated osteoblasts [12].

Chemical changes can also induce alterations in cytoskeletal organization. Specific agents are capable of selectively disrupting each of the three cytoskeletal proteins, providing a mechanism to determine which are primarily responsible for a particular cell's structural integrity. MA of chondrocytes treated with the disrupting agents cytochalasin D (affects only actin filaments), acrylamide (intermediate filaments) and cholchicine (microtubules)

indicated that actin filaments were primarily responsible for the structural integrity of the cell, as only treatment with cytochalasin D significantly decreased cell stiffness [13].

A simple quantification of a specific cell type's response to mechanical stimulation does not provide much information on the physiological processes behind this observation. However, the observation of a corresponding change in cytoskeletal structure and organization, using techniques such as immunostaining, gene and protein quantification and selective disruption of cytoskeletal components, can provide insight into the biological mechanism responsible for the change.

2.2.3. Single-cell biomechanics and disease

Of particular interest is how changes in the biomechanical and biophysical properties of cells can influence or are influenced by pathogenic processes. Changes in mechanical properties of cells can be used as an indicator of biological state and offer insight into mechanisms behind the emergence of a diseased phenotype.

Indeed, a number of pathological conditions have been shown to be accompanied by a change in cellular-level mechanical properties. For example, chondrocytes from osteoarthritic cartilage exhibited significant differences in volume regulation capabilities in response to mechanical deformation [14] as well as increased cellular stiffness (elastic modulus) [13] when compared to chondrocytes isolated from healthy tissue. Cancer cells have also shown to alter their mechanical properties, with cellular deformability increasing in mammary epithelial cells during the progression of disease (from a healthy to a non-invasive malignant to an aggressive, malignant phenotype) [15]. An increase in stiffness and decrease in deformability of erythrocytes that are affected by sickle cell anemia [16] as well as those

infected with the malaria parasite [17] limits their ability to traverse through the smaller blood vessels and capillary networks.

These changes all have potential implications for the onset and progression of disease – a deviation in the structural integrity and the mechanical properties at the cellular level can be detrimental if this results in the breakdown of normal physiological functions at the tissue or organ level [18]. Knowledge of how cells alter their structure with the progression of pathological processes is crucial to understanding how disease processes are initiated and may even provide insight into appropriate therapeutic methods.

2.3. Experimental techniques for single-cell biomechanics

In order to study single-cell or single-molecule biomechanics, we require experimental techniques capable of determining mechanical properties such as Young's modulus, Poisson's ratio or shear modulus at a cellular or even sub-cellular level. The design and implementation of these techniques can be quite challenging, especially considering the magnitude of the forces and displacements that must be measured at the cellular level. The scale of applied forces ranges from just 10 pN to 1 N and length scales can range from micro- all the way down to the picoscale [1, 18, 19]. These experiments usually involve the deformation of the cell or cell surface in some way, and these deformations must then be interpreted with mathematical models that often require the use of a number of simplifying assumptions in order to solve.

All experimental techniques require the application of an external force, which can be either concentrated or distributed, intracellular or on the cell surface, and transient or dynamic [18], and each technique is best suited to a particular force range and length scale. We very briefly outline some of the more common experimental techniques below and

provide some general examples of their application (Table 2-1 and Figure 2-1). A more

comprehensive review of these can be found in [1, 15, 18, 20, 21].

Table 2-1 A brief outline of common experimental techniques used to probe mechanical properties at the cellular and molecular level. Adapted from [1, 15, 18, 20, 21]

Description	Primary applications
Atomic force microscopy	
• A small cell indenter is mounted on the tip of a flexible cantilever probe - interaction force between cell surface and tip induces cantilever deflection • Deflection can be calibrated to estimate the applied force • Applied force range: 0.01 nN to 100 nN • Displacement resolution: 1 nm	• Cell surface topography • Optimal for molecular and sub-cellular level mechanical properties • Used to measure properties of adherent cells in fluids
Magnetic twisting cytometry	
• Magnetic bead with functionalized surface attached to cell • Magnetic field imposes twisting moment on beads and deforms portion of cell • Force resolution: 1 pN • Displacement resolution: 1 nm	• Molecular and sub-cellular level mechanical properties • Protein-protein interaction forces
Micropipette aspiration	
• Suction pressure partially or wholly aspirates a cell into a small diameter glass tube • Changes in cell shape during aspiration provide mechanical information • Applied force range: 0.01 nN – 1 N	• Whole-cell mechanical properties • Limited molecular-level and tissue-level applications
Optical tweezers / laser traps	
• Laser used to trap, control and manipulate object or particles (e.g. bead) • If bead or particle is coated with protein that allows it to adhere to cell surface, then it can be moved laterally, applying deformation force to cell • Force resolution: 0.01 nN	• Membrane properties of cells • Protein-protein interaction forces • Cellular-level properties
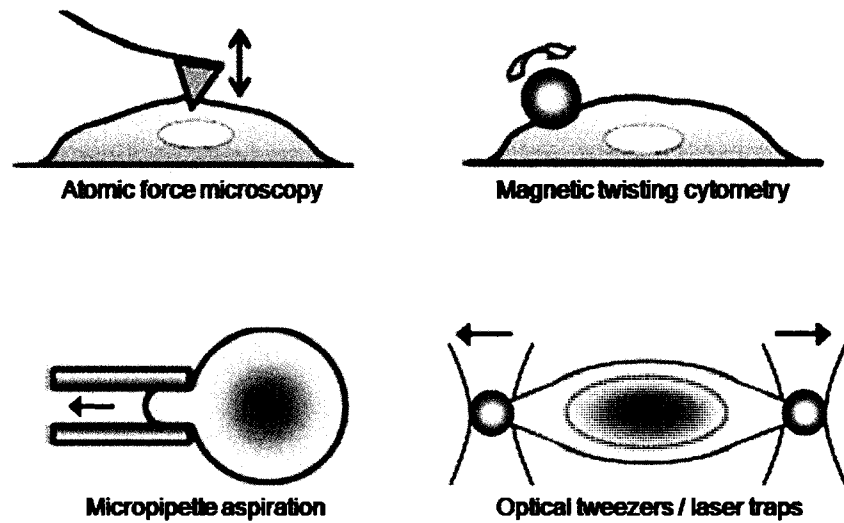
Figure 2-1 Schematic representation of common experimental techniques used to determine mechanical properties of individual cells and molecules (from [18]).

The technique chosen for this particular study was micropipette aspiration (MA). Motivation for this choice as well as a more detailed description of experimental setup and procedure is provided in the following section.

2.4. Micropipette aspiration

2.4.1. Motivation

Micropipette aspiration has long been used to investigate the structural and mechanical response of cells and even biomaterials at the micron level [6, 13, 14, 22-34]. The technique uses suction pressure to partially or wholly aspirate a cell into a small diameter glass tube (micropipette). Geometric constraints and the resulting cellular deformation as a function of pressure and time can then be input into mathematical models (section 2.4.3) to determine a variety of mechanical properties.

MA is a particularly versatile technique, and can be used to determine properties such as cortical tension [23, 30, 31], stiffness [6, 14, 27, 32, 34], compressibility [14, 32, 35] and viscoelastic parameters [13, 33] for a variety of cell types and biomaterials. The basic technique is quite straightforward and in principle has remained the same since its inception [29]. Continued improvements to the both the experiment setup and data analysis [19, 24, 35-40], as well as to the mathematical models used to describe specimen deformation behaviour [35, 41-46], have ensured that MA remains a relevant and widely-used technique capable of accurately and repeatedly measuring cellular-level mechanical properties.

2.4.2. Experimental technique

The following sections describe in very general terms the components of an MA system. Specific information regarding the setup and protocols for the system designed as part of this thesis can be found in Chapter 3 and in Appendices A and B.

2.4.2.1 Experimental setup and procedure

MA was developed based on the principle of hydrostatic pressure transmission [29]. As such, the basic system consists of a glass micropipette that directly applies a negative pressure to the surface of a cell, and a hydrostatic system that controls the suction pressure within the pipette. A number of peripheral components are used for tasks such as micropipette fabrication, pressure control and automation, and cell imaging (Figure 2-2).

Hydrostatic pressure is generally applied either by the downward motion or the removal of fluid from a reservoir connected via liquid-filled tubing to the micropipette. As soon as the fluid level in the reservoir is below that of the micropipette tip, there exists a pressure difference between the two. Because the opening of the pipette is so small (generally between 1 µm and 10 µm), equilibration of the liquid level between pipette and

reservoir occurs at an extremely slow rate. This fact permits the assumption that the entire system is essentially static and allows pressure to be correlated to the height difference according to the following hydrostatic relation:

$$\Delta P = \rho g \Delta h,$$

where ΔP is the pressure difference, ρ is the density of the fluid (usually water), g is the standard acceleration of gravity and Δh is the height difference between reservoir and micropipette tip.

Single-cell suspension
- Chamber allows for side entry of micropipette

Micromanipulator
- Precisely controls micropipette motion

Hydrostatic system

Water reservoir

Video camera

Applied pressure
- $\Delta P = \rho g \Delta h$

Micropipette

Microscope

Vertical linear actuator
- Downward motion of reservoir provides negative pressure applied to cell

Pressure transducer
- Measures pressure applied to cell

Computer
- Saves images and pressure data
- Controls linear actuator
- Integrates time with cell deformation and pressure data

Actuator control circuit

5 µm

Figure 2-2 Schematic representation of a typical MA system. This particular system tests single cells in suspension. Suction pressure is applied through the downward displacement of a fluid reservoir mounted on a vertical linear actuator.

In order to properly image cell aspiration, all MA setups require a video microscopy system to view and record cellular deformation. In addition, although an approximation of applied pressure can be obtained from the downward displacement of the fluid level in the reservoir, more accurate readings come from a pressure transducer mounted in-line with the system. Data acquisition must be integrated in a way that allows for the correlation of time with applied pressure and deformation data.

Micropipettes are usually fabricated from small-diameter capillary tubes (outer diameter usually 1 mm or less) made of borosilicate glass that are pulled to a point using a pipette puller and then fractured to the desired inner diameter (1-10 μm) using a microforge. A micromanipulator is used to correctly position the micropipette next to a specimen. Most experimental designs require that the micropipette approach the cell in the horizontal plane, so that aspiration length can be accurately measured from recorded images.

2.4.2.2 Data collection

Measurement of a number of geometric and deformation response parameters is necessary to determine elastic and viscoelastic properties of the cell being tested (Figure 2-3). Aspiration length (L_{asp}), suction pressure (ΔP), cell (R_C) and micropipette (R_P) radius are the required data for tests on single cells held in suspension (which is the configuration of the MA tests conducted in this study). The only potentially relevant geometric parameter that cannot be measured is the inner fillet radius of the pipette (e), largely due to limitations within the optical setup. Additional raw data may be required for other MA techniques, a few of which are outlined in section 2.4.4.
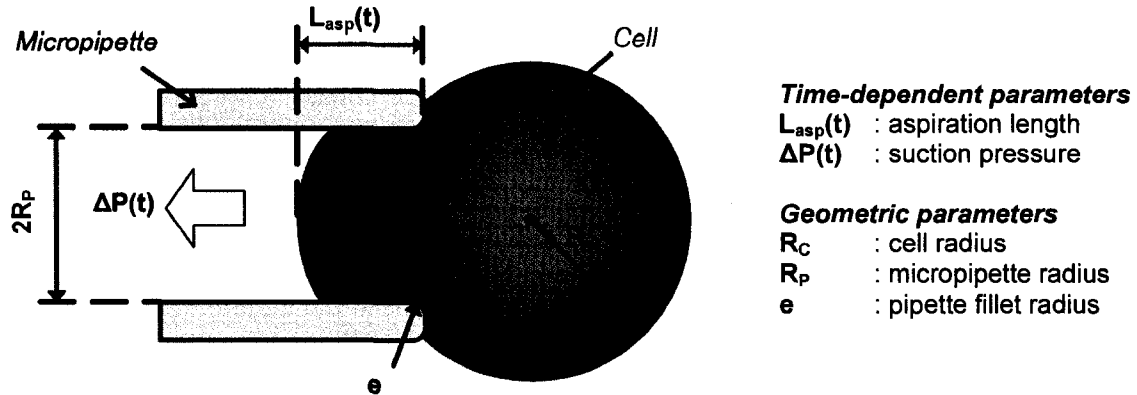
Figure 2-3 Diagram of a single cell undergoing aspiration, including all experimental parameters that must be measured.

2.4.3. Data analysis

2.4.3.1 Continuum models for MA

All mechanical models developed for MA use the continuum approach, which provides whole-cell mechanical properties. These models assume that the entire cell consists of materials with specific continuum material properties. Appropriate constitutive material models and their associated parameters are then derived from experimental observations [18].

A single cell in suspension undergoing MA can behave either as a solid or a liquid [19]. The deformation response for both types is the same until a hemispherical projection (when aspiration length equals micropipette inner radius) is formed in the micropipette. An increase in suction pressure beyond that point will cause a liquid-like cell to flow completely into the pipette [23], while a solid-like cell will continue to extend into the pipette until the aspiration length reaches a finite equilibrium position (i.e. no further aspiration into the pipette) [47]. Cells behaving as liquids are generally fitted to a cortical shell-liquid core model [30] while those exhibiting solid-like behaviour are fitted to an elastic or viscoelastic

solid model [18]. Examples of cells that behave as liquids include neutrophils [23, 48] and erythrocytes [49], while endothelial cells [6, 33] and chondrocytes [14] exhibit the behaviour of solid cells. As a general rule, cells that behave as viscoelastic solids are considerably stiffer than liquid-like cells. The cell type we examined, the valve interstitial cell (see section 2.5.2) behaves as a solid [25], therefore in the following sections we refer only to MA experiments on cells that behave as solids and are fitted to solid elastic and viscoelastic models. A comprehensive review of cortical shell-liquid core models can be found in [18, 19, 30].

2.4.3.2 Analytical solution for solid elastic and viscoelastic models

The most common analytical model for MA approximates the cell as an incompressible elastic half-space, where aspiration length is proportional to the applied suction pressure and inversely proportional to the elastic modulus [47]. The value for elastic modulus is given as:

$$E = \frac{3\Phi_P \cdot \Delta P \cdot R_P}{2\pi L} \, ,$$

where E is Young's modulus, L is the equilibrium (final) aspiration length, R_P is the pipette radius, and Φ_P is a function of the ratio of pipette wall thickness to pipette radius, with a value of 2.1 for most experiments [47]. The half-space model is based on a linear elastic solid, which is not ideal for describing the viscoelastic behaviour of cells. However, the linear elastic half-space solution serves as the basis to the analytical viscoelastic solution developed using a homogeneous viscoelastic solid model [13, 33, 50]. Despite a number of simplifying assumptions, the half-space model (both elastic and viscoelastic) is still widely

used in MA studies [14, 25, 47, 51], primarily because it avoids the need to develop complex finite element simulations.

The derivation of the half-space model required a number of simplifying assumptions. The governing equations used in the half-space approximation are for a linear isotropic elastic material assuming small deformation. Cell deformation is substantial, so the infinitesimal strain assumption is not correct. The model also does not account for the finite boundaries of the cell with respect to the pipette. This is not a major concern if the ratio of micropipette to cell diameter is small, however the solution becomes increasingly inaccurate as this ratio increases [46]. Friction between the pipette wall and the cell are also not accounted for. Finally, the solid continuum model assumes a homogenous material, which does not take into consideration the sub-cellular components which make the cell heterogeneous.

2.4.3.3 Numerical solutions

The primary motive to use finite element simulations to determine the mechanical properties of cells is that a number of the simplifying assumptions that allowed for the derivation of the analytical models described above can be eliminated. Geometric constraints and boundary conditions can be accurately simulated, and assumptions about material behaviour can move beyond those of the linear elastic solid [41, 46]. Finite element models also allow for the investigation of which constitutive models best predict the aspiration response of a particular cell type [46] and can be used to account for any nonlinearity caused by large deformation, contact slippage and material nonlinearity [41]. Parametric studies can be used to show the extent of effects due to changes in factors such as pipette, cell or fillet radius [41].

The major restriction in using finite element analysis to evaluate MA mechanical properties is the considerable amount time and technical expertise required for the development of a working numerical solution. For this reason, some recent studies [13, 25, 28] still rely on the existing analytical models, especially if simply evaluating the relative difference in mechanical properties between two distinct cell populations.

2.4.4. Extensions of the MA technique

Beyond the standard single-cell partial aspiration tests, there exist several newly developed techniques that use the MA apparatus to discover additional mechanical properties of single cells. A limited number of studies have used MA to investigate mechanical properties of adherent cells on a substrate [51, 52], which represents a more physiologically relevant test environment. Trickey *et al* examined the volumetric properties of chrondrocytes and established a novel MA technique and model that involved complete cell aspiration and allowed for the calculation of Poisson's ratio [14, 35]. MA has also been applied at the sub-cellular level to measure the mechanical response of isolated cell nuclei [53, 54].

A second micropipette can be used to manipulate a cell or a microsphere coated with specific binding proteins next to a cell held in the first pipette. Specific receptor-ligand bond forces can be calculated by measuring the force required to move the microsphere away from the cell. This technique has been used to examine neutrophil tether formation [39].

Single cell aspiration into micropipettes has even been combined with single-channel patch-clamp electrophysiology to examine the sensitivity of mechanosensitive ion channels in osteoblasts to cell membrane tension and strain [55].

Finally, MA has also recently been implemented to study tissue-level mechanics, both of soft tissues [56] and thin biological samples, such as polyacrylamide gels [45, 57].

2.4.5. Limitations of the MA technique

All mathematical models derived to interpret MA experiment results include a number of simplifying assumptions. Factors such as the high stress concentrations in the cell at the pipette edge, or the friction between pipette wall and cell membrane may influence experimental results, but are often too complex to include in any mathematical simulation, whether analytical or numerical [1].

Most MA experiments still require cells to be in held in suspension. For circulating cells such as leukocytes and erythrocytes, this is not a limitation, as it is representative of their natural state. However, the detachment of adherent cell types such as fibroblasts from their extracellular matrix will cause the cell in question to soften, largely because the cytoskeletal filaments are relieved of stress at the focal adhesions that connect the cell to the ECM. MA of adherent cells has been performed [51, 52] but remains technically challenging (see section 3.4.3).

2.5. The aortic valve

2.5.1. Aortic valve anatomy and structure

The aortic valve is a tricuspid valve, with three distinct leaflets that are thin and translucent in their healthy state. Leaflet shape and structure is such that they permit maximal opening during systole and a perfect seal during diastole. Leaflets have a highly organized, tri-layered structure (Figure 2-5). The fibrosa on the aortic side consists primarily of circumferentially arranged collagen fibres and bears the mechanical load of aortic pressure during diastole. The spongiosa is a sparse network of radially oriented collagen fibres in a connective tissue layer that is composed primarily of glycoaminoglycans and water. Its

primary mechanical function is to damp vibrations in the leaflet during the cardiac cycle [58]. On the ventricular side, the ventricularis is composed of an elastic fibre layer, with both elastin and collagen content, thought to be important in the maintenance of the smooth ventricular surface of the aortic valve, presumably in part to maintain laminar blood flow during systole [59].

Two cells types populate the aortic valve leaflets: the valve endothelial cell (VEC) and the valve interstitial cell (VIC). VECs exist as a monolayer of cells on the outer surface of valve leaflets and provide a barrier between the passing blood and the interstitial tissue. VECs also appear play a role in the regulation of VIC phenotype and function [60]. VICs are a phenotypically dynamic mix of cells that reside throughout the valve extracellular matrix of collagen, elastin and glycosaminoglycans and are the focus of this study. VIC physiology and pathology are described in the following sections.

2.5.2. Aortic valve interstitial cells

Aortic valve interstitial cells are a heterogeneous population consisting primarily of quiescent fibroblasts, as well as a small number myofibroblasts and smooth muscle cells [61-63]. The main responsibility of VICs is the maintenance of valve structure [64] – including the distinct three layer morphology exhibited in healthy tissue. Valve integrity is highly dependent on the ECM, and as such, VICs are ultimately responsible for synthesizing and remodelling the ECM to ensure the mechanical durability and function of the aortic valve. However, our current understanding of the mechanisms behind normal VIC function is limited. Increased knowledge of VIC phenotype and regulation may also provide insight into valve pathology.

2.5.3. Aortic valve function

The aortic valve regulates the flow of oxygenated blood from the left ventricle to the aorta (Figure 2-4). It exists in an extremely dynamic environment, opening and closing approximately once every second (at a frequency of ~1 Hz), for a total of over three billion cycles within one lifespan [59].
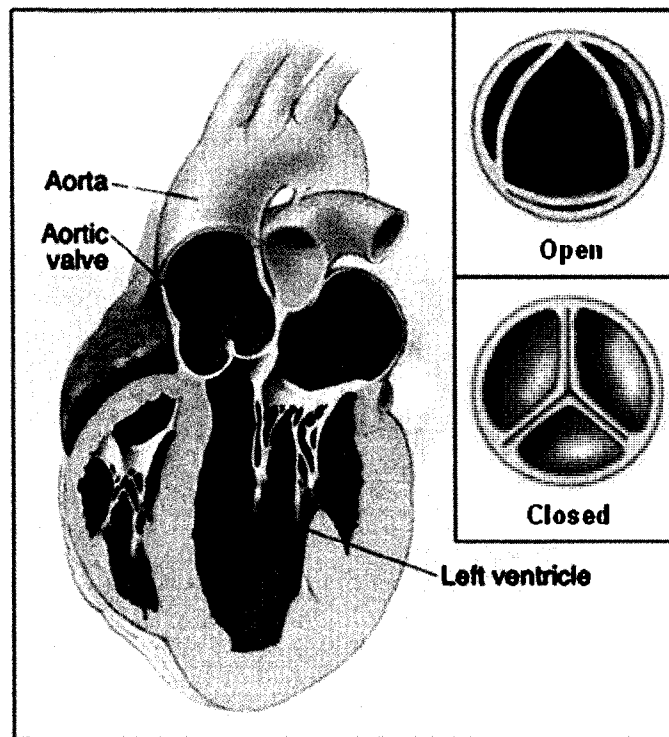
Figure 2-4 The aortic valve regulates blood flow from the left ventricle to the aorta. The tricuspid structure allows for maximal opening during systole and a perfect seal during diastole (images adapted from www.nucleusinc.com)

The valve operates passively in response to the pressure gradient across it and consists of three distinct leaflets. These are held closed during diastole, when pressure is higher on the aortic side, and open as the left ventricle contracts during systole, which increases the pressure on the ventricular side. Oxygenated blood is pumped through the valve

into the aorta. As ventricular pressure decreases, the aortic valve closes to prevent backflow of blood into the left ventricle.

2.5.4. Aortic valve mechanics

Valve leaflet motion is such that the tissue is constantly exposed to varying mechanical loading, both spatially and temporally. Leaflet surfaces are exposed to two distinct flow profiles: blood flow along the ventricular side is generally laminar, however vortices will form above the leaflets on the aortic side, in part to help them close [65] (Figure 2-5).
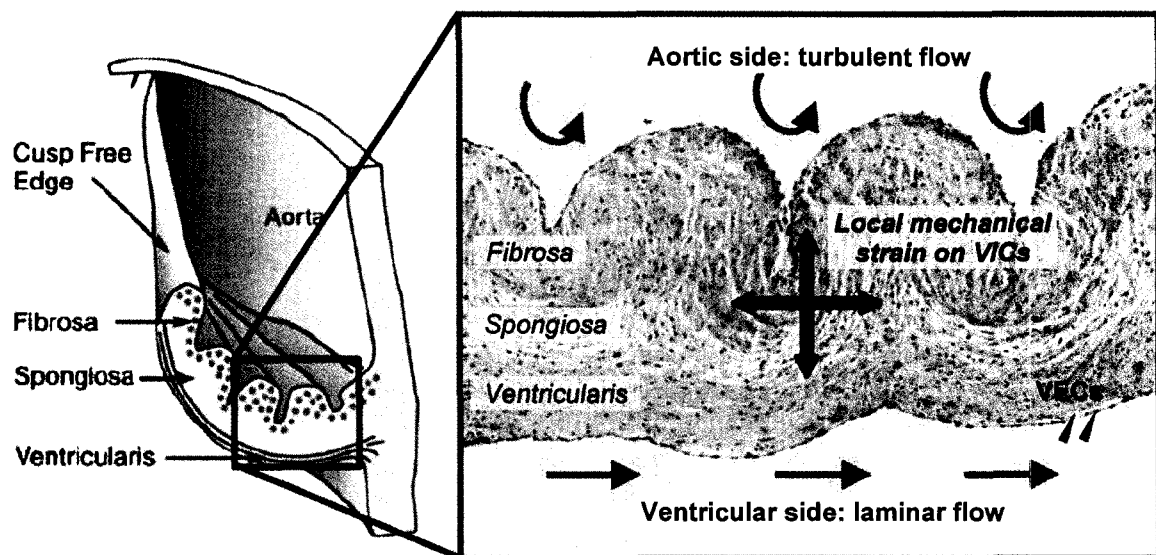
Figure 2-5 Valve leaflet structure and mechanical influences: (a) the organization of leaflet ECM and (b) a histological section of a healthy porcine aortic valve stained with hemotoxylin and eosin (adapted from [66]). The tri-layer structure is clearly visible, along with the local distribution of both VIC and VEC populations

Stress and strain within the tissue change as a result of flexure during valve opening and closing. Valve structure must exhibit low flexural rigidity to allow for normal opening and closing of leaflets, yet also provide the strength to withstand the high amplitude stresses

caused by transvalvular pressures (TVP – the pressure difference between ventricle and aorta when the valve is closed) of up to 100 mmHg [67]. The distinct morphology of the ventricularis, spongiosa and fibrosa layers permit the wide range of motion necessary for proper valve function, with each layer exhibiting different mechanical properties and behaviour [68-71]. For example, the elastin content unique to the ventricularis appears to be necessary to restore collagen fibre organization between successive loading cycles [71]. The regulation and maintenance of the valve structure is crucial to healthy valve function. However, despite the considerable research dedicated to tissue-level studies of valve microstructure, it is unknown whether the distinct mechanical response observed within each layer is also evident at the cellular level.

2.6. Aortic valve sclerosis

Healthy leaflet structure is maintained by tightly regulated cellular processes [64, 72], disturbance of which prevents normal valve function and can lead to aortic valve sclerosis (AS), a common pathogenic condition [73, 74] with many features similar to atherosclerosis [75, 76], that affects 20-30% of the population between 65-75 years of age [74, 77].

AS can involve chronic inflammation, increased cellularity, lipid accumulation, ECM deposition, fibrosis and calcification of valve tissue [76, 78-84], all of which combine to compromise the structural integrity of the leaflet, ultimately leading to tissue stiffening and altered hemodynamic flow. AS can carry severe consequences, including an increased risk for other cardiovascular conditions, and ultimately may lead to aortic stenosis [77, 85]. Aortic stenosis is the symptomatic phase of calcific valve disease and occurs when valve leaflets thicken to the point where blood flow is disrupted, eventually resulting in leaflet

immobility and outflow obstruction [58] (Figure 2-6). The only existing treatment for late-stage aortic stenosis is surgical replacement with a prosthetic valve.

(a)

(b)   (c)
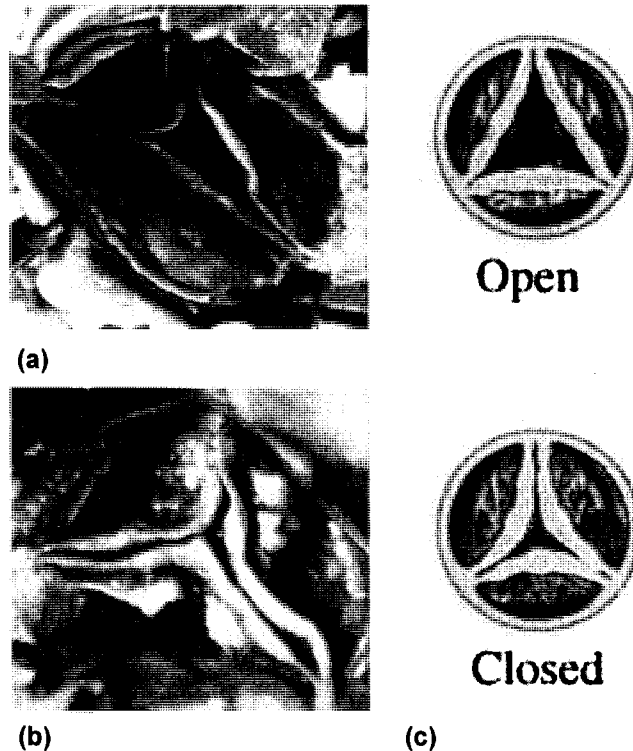
Figure 2-6 Calcific aortic valve disease: (a) a minimally diseased aortic valve and (b) a severely stenotic valve. Prominent lipocalcific lesions (arrow) are evident on the aortic side of leaflets [86]. (c) Aortic valve stenosis prevents proper valve leaflet motion, leading to altered blood flow (adapted from www.nucleusinc.com).

Valve pathological conditions are often accompanied by a change in valve tissue organization, which in turn can affect flow profiles [87], disrupting the mechanical cues that help regulate both VEC and VIC behaviour. Lesions preferentially form in the fibrosa, in leaflet regions exposed both to large bending stresses [59, 88] and turbulent rather than laminar flow [59]. These observations imply the existence of a mechanical link in the development of AS. This theory is further supported by the fact that bicuspid aortic valves (a congenital defect whereby the aortic valve has two instead of three leaflets) have a higher prevalence of AS, with symptoms appearing up to two decades earlier. The hemodynamic

behaviour of bicuspid valves is abnormal, again suggesting that mechanical factors may play a role in the development of AS [58]. A strong correlation has been established between aortic valve pathology and changes in the tissue-level mechanical properties; however whether these changes are reflected at the cellular level is unclear.

2.6.1. Pathological differentiation of VICs

Initially thought to be a passive process largely due to age-associated "wear and tear" of valve tissue and passive calcium deposition, considerable research now demonstrates that AS is an active pathogenic process in which the VICs are actively involved [72, 89, 90]. VICs involved in pathobiological responses are often phenotypically different from the quiescent fibroblasts commonly observed in healthy valve tissue [64]. Activated VICs appear to have increased matrix remodelling potential [61, 62, 91] and in some cases may even differentiate into an osteoblast-like phenotype [78, 92-94]. VICs located within aortic valve lesions have consistently shown evidence of differentiation into myofibrogenic and/or osteogenic phenotypes, however there is currently no consensus on what initiates and regulates the molecular mechanisms behind these transformations.

2.6.1.1 Myofibroblasts

Healthy VICs may exhibit plasticity, with the normally quiescent fibroblasts able to undergo differentiation to become "active" fibroblasts, called myofibroblasts. Within the valve, this phenotype has been shown to be contractile, proliferative, migratory and capable of remodelling the ECM [61, 62, 91]. Valve ECM remodelling by myofibroblasts is likely stimulated by external factors such as mechanical loading and presumably occurs in order to restore the normal stress profile within the tissue [58]. In a healthy valve, the majority of

these myofibroblasts either disappear through regulated apoptotic processes or return to their quiescent fibroblast state once normal function is regained [58, 62].

Aortic valve lesions frequently include fibrotic tissue, which is characterized by increased deposition and accumulation of excessive amounts of disorganized ECM. Pathological fibrosis has been observed in many connective tissues, and shows parallels with wound healing [95]. Both wound healing and pathogenic fibrotic conditions are characterized by the appearance of myofibroblasts [96]. Under normal wound healing conditions, myofibroblasts appear transiently and their eventual disappearance is thought to be mediated primarily by apoptosis [97]. However, dysregulation of the myofibroblast life cycle can allow the activated phenotype to persist with continued force generation and ECM production, resulting in fibrotic tissue [97]. VICs within these fibrotic lesions show evidence of phenotypic differentiation into cells having myofibrogenic characteristics [98]. Although a small proportion of myofibroblasts exists even in healthy valve tissue, late-stage diseased valves exhibit a much higher percentage of myofibroblasts, often located next to calcified regions [61, 62], suggesting that mechanisms that mediate apoptosis or the reversion back to a quiescent fibroblast are no longer functional.

The most reliable phenotypic marker for myofibroblasts is alpha-smooth muscle actin (α-SMA), a tissue-specific actin isoform also expressed in smooth muscle cells [99] and not normally found in quiescent fibroblasts. Myofibroblasts are characterized *in vitro* by the appearance of stress fibres containing α-SMA. This is in contrast to the (non α-SMA) F-actin distribution in typical fibroblasts, where actin filaments are normally concentrated in the subcortex [100]. Stress fibres aid in contractile force generation [101], and are important for

transduction of extracellular mechanical signals to intracellular biochemical signals [102-104].

Differentiation of fibroblasts into myofibroblasts in the aortic valve appears to be synergistically mediated by a number of factors, including mechanical tension and cytokines such as transforming growth factor-β (TGF-β), a profibrotic cytokine [100]. ED-A fibronectin, a protein expressed in the transition from fibroblast to myofibroblast, may also play a role in the ability of TGF-β to induce α-SMA expression [105]. *In vitro*, myofibroblast differentiation appears to be induced simply by culturing VICs on a stiff substrate [106]. *In vivo*, however, there is no clear consensus on exactly how myofibrogenic differentiation is initiated and regulated. AS also frequently involves regions of calcifying tissue, indicating either that myofibroblasts differentiate further into a calcifying phenotype, or that there is an additional cell source involved in the initiation and progression of the disease.

2.6.1.2 Calcifying cells

Similar to vascular calcification [107], valvular calcification occurs through multiple mechanisms, leading to dystrophic calcification associated with apoptosis [94, 98, 108-110] as well as the formation of bone tissue through osteogenic processes [78, 92-94]. In order to study the factors affecting *in vivo* calcifying processes, a number of studies have attempted to induce calcification of VICs *in vitro*. VICs can be induced to form aggregates that are typically referred to as bone nodules due to the presence of calcium deposits and alkaline phosphatase activity (ALP) [108, 111]. However, significant differences in nodule microstructure, cell viability within nodules and phenotypic processes [108, 111] suggest that these cell culture systems appear to exhibit aspects of dystrophic and/or osteogenic calcification [89, 108, 111-113].

Calcification *in vitro* can be rapid and dystrophic, characterized by myofibrogenic differentiation of VICs, apoptosis, and increased alkaline phosphatase activity. This occurs *in vitro* in response to TGF-β [108, 111]. Apoptotic cells and TGF-β have also been associated with dystrophic calcification *in vivo* [108, 109, 111]. *In vitro* aggregates have also been shown to be associated with the expression of bone-related transcripts and proteins. This is a predominantly osteogenic process that is characterized by the occurrence of bone-matrix proteins [89, 112, 113], transcription factors [113], and minerals [89] in cultured VICs. Like dystrophic calcification, this osteogenic process is also consistent with *in vivo* observations [78, 92]. VICs in aortic valve lesions also appear to differentiate into an osteogenic phenotype. Calcium deposits found in aortic valve lesions often contain both calcium and phosphate as hydroxyapatite, a mineral found predominantly in bone. Culture of cells from canine and human aortic valves resulted in the emergence of a subpopulation of calcifying valve cells that exhibit characteristics of osteoblasts [89]. Recent research in our lab also suggests that the heterogeneous native VIC population includes a multipotent mesenchymal progenitor cell population that is highly enriched for osteoprogenitors [114].

2.6.2. Effects of substrate stiffness

The ECM provides biochemical and mechanical cues to many adherent cell types and alterations in both composition [81, 115] and biomechanical properties [116] of the ECM are characteristic of sclerotic and fibrotic diseases. Although molecular pathways are still only partially known, muscle cells, neurons and many other adherent cell types have been shown to sense substrate stiffness [52, 117, 118]. Most tissue cells not only adhere to but also pull on their microenvironment and thereby respond to its stiffness in ways that relate to tissue elasticity [117]. Cytoskeletal tension is generated intrinsically by cells as they exert tractional

forces on surrounding ECM; a stiff substrate will provide greater resistance to deformation, resulting in greater tractional forces [117]. In the case of mesenchymal stem cell lineage specification, tissue-level changes appear to be reflected at the cellular level, with cell stiffness linearly increasing with substrate stiffness [52].

Recent research in our lab suggests that substrate stiffness plays a role in regulating *in vitro* valve pathogenic processes, with VICs cultured in calcifying media preferentially differentiating to osteoblast-like cells on compliant (soft) substrates and to myofibroblasts on stiff substrates [119]. Calcified aggregates or nodules formed in both cases, but were differentially mediated not only by substrate stiffness, but also by the organization of the actin cytoskeleton and TGF-β, suggesting that different mechanisms are responsible for their emergence. VICs on compliant substrates were viable and showed upregulation of transcripts and proteins typical of osteoblasts. Culture on stiff substrates facilitated myofibrogenesis and dystrophic calcification as evidenced by apoptotic cells within nodules. Although substrate stiffness appears to differentially influence differentiation of VICs and the mechanisms by which they calcify [119], it is unclear whether stiffness is affected at the cellular level.

Chapter 3: Methods and Materials

3.1. Introduction

Micropipette aspiration (MA) systems are not available as a complete and integrated product, but instead are assembled from a series of off-the-shelf components selected to best suit an individual application. Therefore, the first major task of this project was to set up a custom MA system in our laboratory.

We first determined a series design criteria for each of the additional components required (section 3.2.1). Using the established criteria, we selected suitable components and developed an integrated method of data acquisition (section 3.2.2). Our next task was to establish an appropriate experimental protocol and data analysis technique, including the selection of a relevant mathematical model to determine cell mechanical properties (section 3.3). In the process of developing the experimental protocol, a number of system limitations – both technical and biological – became apparent (section 3.4). Although the various components are described to some degree in this section, a more complete list of the relevant technical specifications and part numbers for all MA equipment can be found in Appendix B.

3.2. System design

3.2.1. Design criteria

Before selecting specific individual components, we determined a number of criteria that would allow for proper testing, listed in Table 3-1. Although we used it primarily to examine VIC function, MA is a technique broadly applicable to a number of different cell types, and even certain biomaterials (see Appendix C and [120]). Therefore, in designing the

system, care was taken to ensure that it could be used to test cells and materials of varying size and mechanical properties.

Table 3-1 – MA design criteria for major system components, and a summary of the motivation behind their selection.

Criteria	Motivation
General	
1. Synchronization of pressure, time and aspiration (image) data	→ Aspiration length is a function of both pressure and time, these must be correlated
2. Isolation from external vibrations	→ Required to prevent vibration-induced damage (e.g. cell penetration and lysis, micropipette breakage)
3. Ability to easily dismantle / clean / remove system components	→ Many components are shared among other lab members, allows for cleaning of individual parts
Hydrostatic system	
1. Pressure range 0–2 kPa (approximate)	→ Covers relevant cell types in current literature [14, 25]
2. Ability to vary rate at which pressure is applied	→ Certain models assume instantaneous pressure decrease (i.e. requires high rate)
	→ Ability to conduct ramp tests (i.e. requires low rate)
	→ Biological limitations may affect maximum or minimum rate, need flexibility
Pressure transducer	
1. Pressure range at least 0–2 kPa	→ See above
2. Pressure ports compatible with liquids	→ Hydrostatic system filled with liquid throughout
3. Resolution of 1 Pa	
Video camera	
1. Maximum image capture rate of approximately 60 fps	→ Allows for capture of potentially rapid instantaneous cell or biomaterial response
2. Ability to vary image capture frame rate	→ Slower fps used for longer test periods, larger images, reduces aspiration video file size
3. Ability to change image size	→ Reduces file size, allows for increased frame rates
4. High resolution	→ Allows for accurate measurement of aspiration length

3.2.2. System components

3.2.2.1 Videomicroscopy system

Samples were viewed using an Olympus IX71 inverted microscope (Olympus Canada Inc, Markham, ON). We performed all tests on VICs using a 40× dry relief contrast (also known as differential interference contrast (DIC)) objective (numerical aperture = 0.6). During pressure application, images of cell and micropipette were recorded using a charge coupled device (CCD) camera (Retiga 2000R, QImaging, Surrey, BC) with an IEEE 1394 FireWire connection. The camera was chosen in part due to its ability to be integrated into a LabView interface, which allows region of interest (ROI), frame rate and image acquisition parameters to be controlled during testing of individual samples. Camera resolution is 1600×1200 pixels (pixel size 7.4×7.4 μm). Used with the 40× objective after calibration with a stage micrometer, the resolution of saved images was calculated to be 5.3 pixels/μm (0.19 μm/pixel). Typical VIC diameters range from approximately 7 μm to 20 μm, allowing for a maximum image size of about 150×150 pixels. Although maximum frame rate at full resolution was just 10 fps, the acquisition of smaller images allowed for higher frame rates, easily reaching 60 fps.

The microscope and the majority of the MA equipment was located on an air isolation table (Kinetic Systems Inc, Boston, MA), which was necessary to isolate the equipment from vibrations elsewhere in the laboratory.

3.2.2.2 Hydrostatic loading system

MA applies pressure using a hydrostatic system, as outlined in section 2.4.2.1. Our setup linked the micropipette to a height-adjustable fluid reservoir using plastic tubing filled with distilled water. Both the adjustable reservoir and the cell suspension on the microscope

were exposed to atmospheric pressure, therefore when they were at the same height, the pressure difference between them was zero and no suction was applied to the cell.

Although the height difference between the variable reservoir and the microscope stage provided an approximation of the applied pressure, more precise values were required for data analysis, prompting the purchase of a differential pressure transducer (Valiydne Engineering, Northridge, CA). The transducer has a pressure range of ±3.5 kPa, corresponding to a voltage output of ±5 V, and accepts liquids at both the negative and positive pressure ports. It was integrated into the MA system by the addition of a second, reference fluid reservoir. This fixed reservoir consisted of a 50 mL conical tube mounted on an adjustable stand placed next to the microscope stage, with the fluid level at the same height as the cell suspension on the stage. The transducer was connected between the two reservoirs and therefore indirectly provided the pressure difference between the cell suspension (represented by the height of the fluid level in the fixed reservoir) and the variable reservoir (Figure 3-1). This design is similar to that of [14, 24].

The magnitude of the applied suction pressure and the rate of loading were determined by the downward displacement and the speed of the variable water reservoir, respectively. The variable water reservoir consisted of a 50 mL conical tube mounted in a custom plexiglass holder attached to the top of a vertical linear actuator. To allow for fine control of both magnitude and speed of applied pressure, we purchased a linear actuator (Ultra Motion, Cutchogue, NY) and an accompanying step motor driver (Applied Motion Products, Watsonville, CA). The vertical linear actuator has a stroke length of 8 in, which means that the applied suction pressure can reach a maximum of approximately 2 kPa (i.e. 8 in-H_2O). The stepper motor driver allows for several stepping options, resulting in a

displacement range from 2 μm/step to 65 μm/step. Using the LabView program written specifically for the MA system, actuator speeds could range from 100 μm/s to 50 cm/s, equivalent to pressure application rates of 1 Pa/s to 4.9 kPa/s.

Micromanipulator

Single-cell suspension

Reference reservoir

Height of single-cell suspension and fluid level of reference reservoir

$\Delta P = \rho \, g \, \Delta h$

Micropipette

Adjustable stand
Adjust height until fluid level is same as that of single-cell suspension on microscope stage

Variable reservoir

Transducer check valves
- Used to zero pressure readings (all three ports open)
- Ports connecting to middle tube closed during actual testing (only two ports open)

Pressure transducer
Measures pressure drop between reservoirs

Vertical actuator
Controls height of variable reservoir

Water-filled PVC tubing

Inline check valve
Fluid-filled syringe is attached to the (normally closed) third port: used to apply positive pressure to remove cells and/or debris from micropipette

Figure 3-1 MA hydrostatic system. The reference reservoir is maintained at the same height as the cell suspension and the suction pressure applied to the cell is inferred from the pressure difference between the variable and reference reservoirs.

The hydrostatic system was connected using a series of plastic tubing, barbed tubing connectors and check valves. Most of the check valves were placed to allow for easy setup

and dismantling of the system and to prevent damage to sensitive equipment such as the pressure transducer.

3.2.2.3 Micropipette fabrication and integration into MA system

Micropipettes were made from borosilicate capillary glass tubes with an outer and an inner diameter of 1.0 and 0.78 mm, respectively (Harvard Apparatus Canada, Saint-Laurent, QC). They were first pulled to a point using a vertical puller (David Kopf Instruments, Tujunga, CA) and subsequently fractured to an inner diameter ranging from 4 to 15 μm using a DeFonbrune microforge. The tips of all micropipettes were then coated with Sigmacote (Sigma-Aldrich, Oakville, ON), which created a hydrophobic thin film on the glass surface intended to prevent cell adhesion during aspiration.

A micropipette holder (Harvard Apparatus Canada) connected the pipette to the rest of the system (Figure 3-2). This holder was mounted on a micromanipulator controlled by a closed-loop 3-axis joystick controller (Siskiyou Corp., Grants Pass, OR). The micro-manipulator has freedom of movement in the x-, y- and z-axes (travel range / axis is 20 mm). Coarse motion adjustment (1.7 mm/s) allowed the pipette to be manoeuvred into the microscope field of view, while fine motion adjustment (30 μm/s) allowed it to be positioned next to the test cell. The micromanipulator was attached to a stand (Siskiyou Corp.) placed next to the microscope stage and the pipette holder and pipette were mounted on the manipulator at approximately 30° to the horizontal (Figure 3-2). The tips of all micropipettes were bent (using the microforge) and mounted in the holder so that the cell was aspirated into the horizontal portion of the pipette.
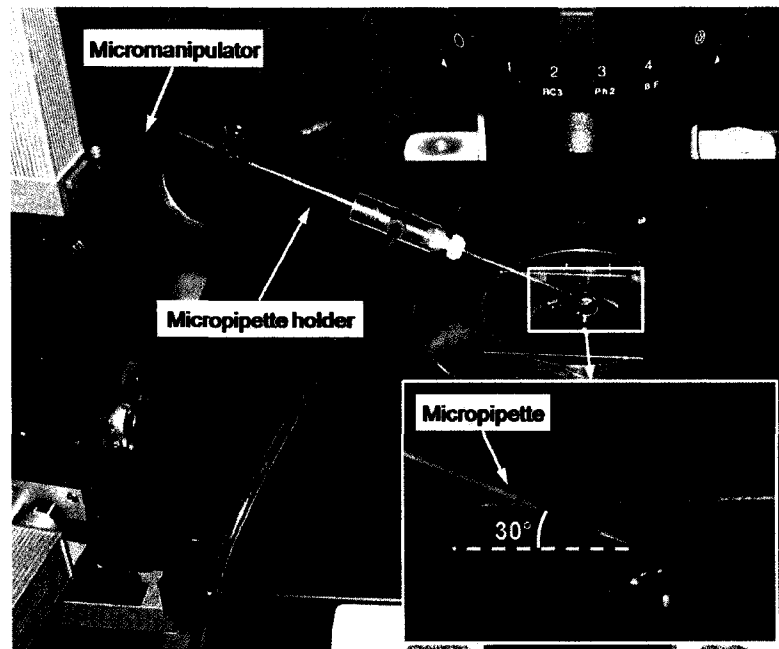
Figure 3-2 Micropipette mounted in holder. The micropipette is mounted in the micromanipulator at an angle, but the tip through which the cell is viewed is bent so as to be horizontal.

3.2.2.4 Data acquisition system

An important design criterion was the synchronization of pressure, time and image data. To achieve this goal, we purchased a multifunction National Instruments data acquisition board (DAQ) bundled with LabView 8.2 graphical programming software. The DAQ board provided and monitored outputs to the linear actuator and step motor driver and accepted the voltage input from the pressure transducer. Outputs to the step motor driver included a digital step pulse to control the speed of the stepper motor that drove the linear actuator (one full rotation of the stepper motor corresponds to one inch linear travel) and a digital signal that controlled the actuator direction (up or down). These signals were also shown on the LabView user-interface as a means of monitoring actuator performance. The frequency of the step pulse controlled the speed of the stepper motor, and by extension the vertical linear travel speed of the actuator. LabView user inputs to the actuator and driver

included speed, direction and travel distance of the linear actuator, and these could be changed at any time during a single experiment.

A stepper motor has a maximum starting speed (i.e. a maximum input step pulse frequency) – exceeding this speed will cause the motor to stall. Consultation with representatives from Ultra Motion indicated that the maximum starting speed for our linear actuator is approximately 2 in/sec. Speeds greater than this require an acceleration profile that ramps up motor speed (pulse frequency) gradually. For the MA system, the acceleration profile was generated using software-timed controls programmed with basic LabView functions and virtual instruments (VIs). Using software-timed programming is not ideal – it does not create an optimal acceleration ramp and results in a slight decrease in positional accuracy (in our case, a tendency to overshoot travel distances) at high speeds. Ultimately however, the slight decrease in positional accuracy proved to be insignificant, as biological concerns prevented the application of an instantaneous step suction pressure to the cell type of interest (see sections 3.3.4.2 and 3.4).

To accurately measure applied pressure, the transducer's ±5 V output was connected to the DAQ board and displayed on screen. The transducer readings were also saved to a textfile to be correlated with time and image data after aspiration tests were completed.

An IEEE 1394 FireWire cable and PCI card connected the CCD camera to the PC. Image data acquisition parameters were incorporated into the LabView interface using drivers developed by QImaging (QCam LabView Interface 2.2.1 for LabView 7.1, 8.0 and 8.2). Although the LabView VIs developed by QImaging for the camera provided most of the necessary functions, substantial modifications proved difficult, primarily a result of the fact that the QImaging camera could only communicate with the drivers provided by the

company (and not with the many image-acquisition and analysis VIs built into LabView 8.2). The most significant consequence of this limitation was that individual images could not be directly saved to a video but instead had to be saved in a single folder and be converted after test completion to an image stack using ImageJ software (NIH, Bethesda, MD). Any modification to individual images (e.g. timestamp, scale bar) also had to be done using ImageJ after testing.
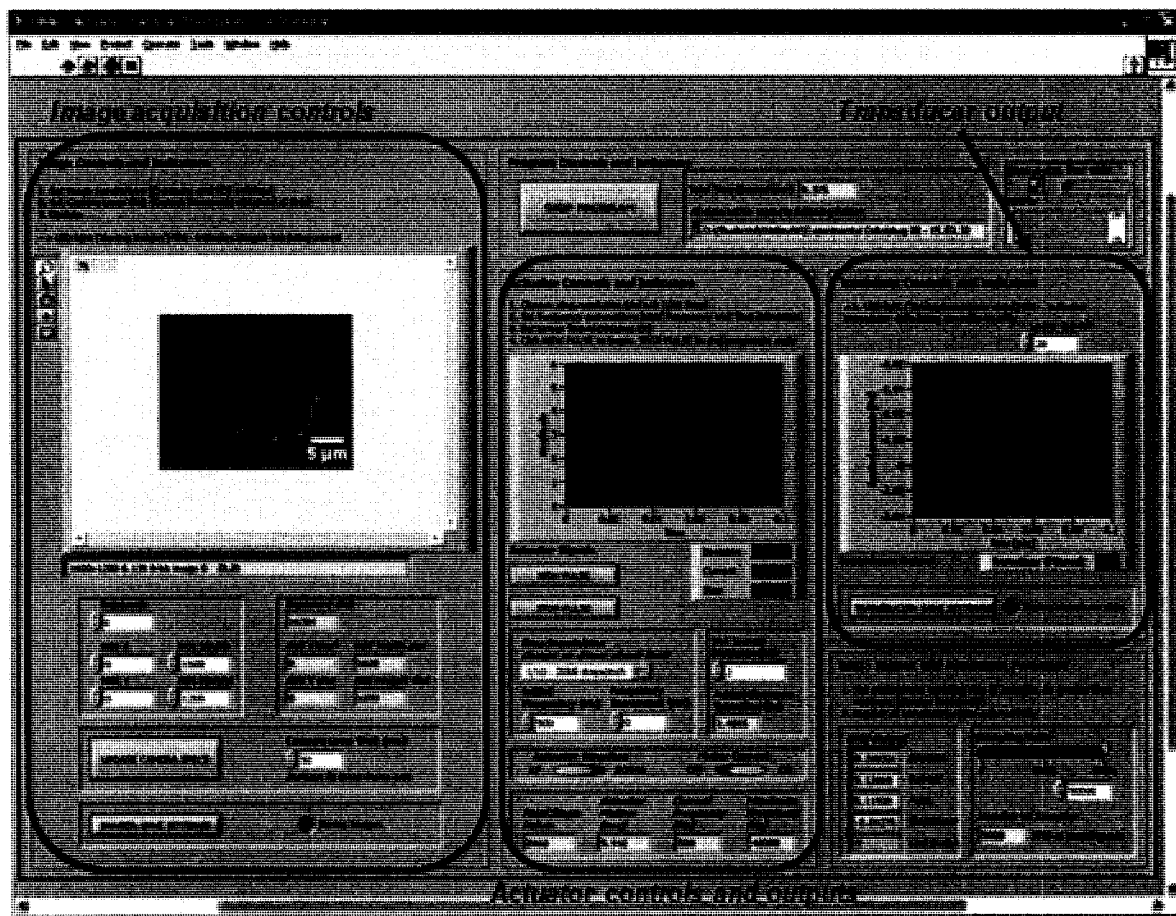
Figure 3-3 User interface of the developed LabView MA program, with key sections labelled.

The user interface for the LabView program is shown above (Figure 3-3). The cell can be monitored in the streaming window and the various image and actuator controls can

be set prior to testing and monitored in time with cell aspiration. Pressure data and image acquisition automatically and simultaneously begins as soon as a pulse input is sent to the actuator. The only way to stop saving images and pressure values is to stop the program. Saved images and the transducer output textfile are saved in a folder created each time the program is run. The program must be started and stopped for each cell tested and all data associated with a singe cell is saved in a single folder.

3.2.3. Integrated MA system

The integrated system is shown in the images on the following page (Figure 3-4).
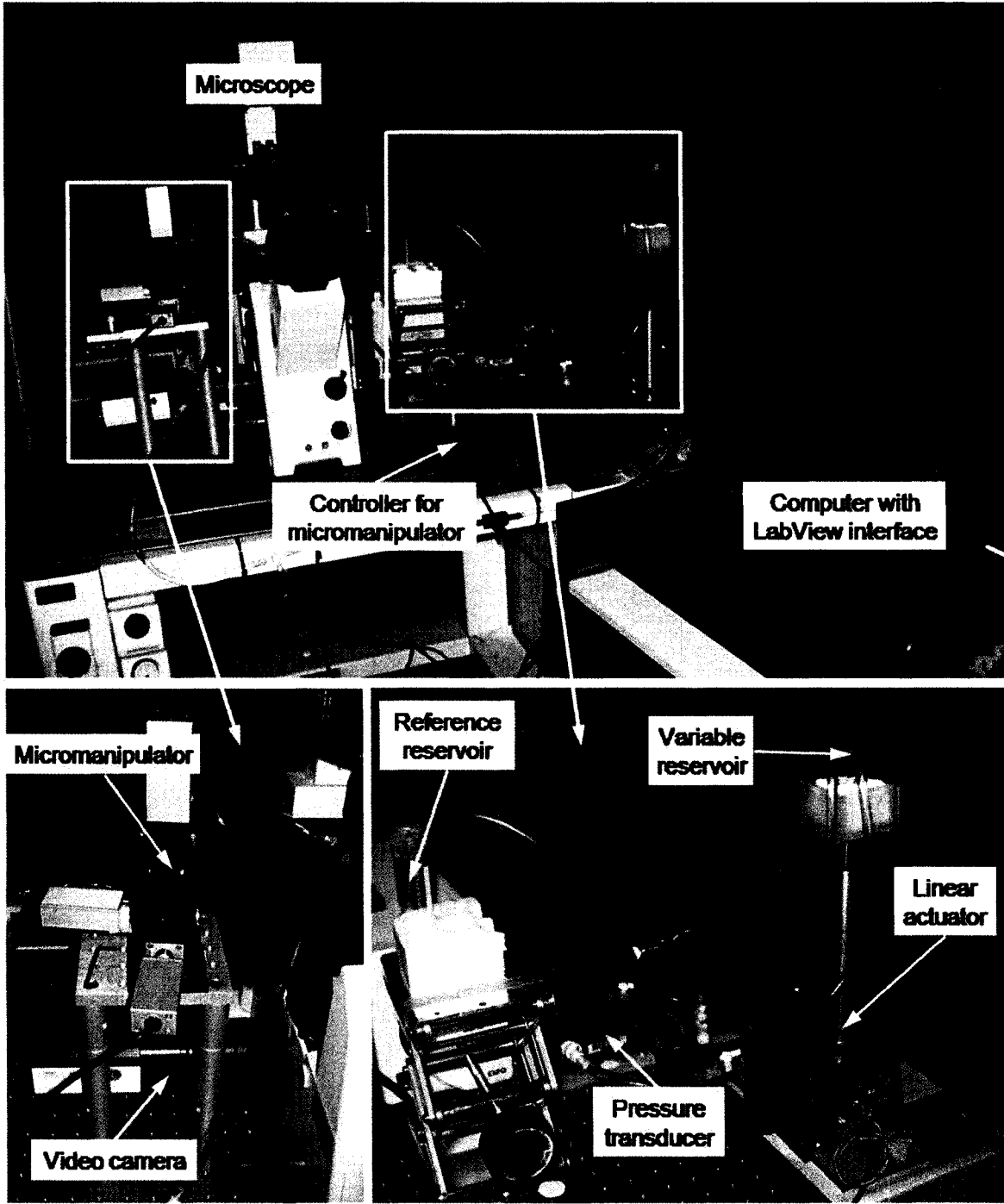
Figure 3-4 MA system experimental setup.

3.3. Experimental method

This section outlines the finalized cell preparation and the image and data analysis techniques common to all experiments conducted. These test parameters were selected after a series of preliminary experiments, the most significant of which are outlined in section 3.4. More specific detail about individual experiments can be found in Chapters 4 and 5, as well as in Appendix A, which documents all protocols used.

Unless otherwise noted, all reagents are from Sigma-Aldrich (Oakville, ON).

3.3.1. Isolation of VICs

The basic VIC isolation protocol is outlined below. Isolation of cells from different regions of the valve leaflet (Chapter 4) required some additional steps (sections 4.2.2 and 4.2.3).

Primary aortic valve interstitial cells (VICs) were isolated from the hearts of 8 month old pigs obtained from a local abattoir (Quality Meat Packers, Toronto, ON). Aortic valve leaflets were excised and rinsed in sterile phosphate buffered saline (PBS) containing 0.5% amphotericin B and 1% penicillin/streptomycin mixture. To remove the outer endothelial cell (EC) layer, leaflets were pre-digested with collagenase (150 units/mL) in N-Tris(hydroxymethyl)methyl-2-aminoethanesulfonic acid (TES) buffer with 0.36 mM calcium chloride (20 min, 37°C) followed by 7 minutes in 0.125% trypsin and EDTA at 37°C. After vortexing and lightly scraping to remove any remaining ECs, leaflets were minced and digested with collagenase (150 units/mL) in PBS (2 h, 37°C). The digested tissue was first vortexed and then strained using a 70 μm filter and rinsed with complete medium (Dulbecco's modified Eagle's medium (DMEM) with 10% FBS (Hyclone, Logan, UT) and 1% penicillin/streptomycin). The resulting cell suspension was centrifuged at 284×g and

resuspended in complete medium, which was again strained to obtain a single-cell suspension.

Mechanical properties of healthy (freshly isolated) VICs were measured after every VIC isolation. In experiments that involved culture of VICs , a given experiment consisted of cells from a single isolation.

3.3.2. Aspiration procedure

All information on cell culture conditions for individual experiments is described in Chapters 4 and 5.

Once removed from either the native valve tissue or the various culture substrates, cells were held on ice in complete medium. Depending on suspension concentration, a small amount (15–100 μL) was placed onto a glass coverslip treated with Sigmacote. The cell suspension was then diluted in PBS supplemented with 10% FBS until cells were sufficiently dispersed so as not to cause interference during aspiration. The cell suspension on the microscope stage was changed every 20–30 minutes and cells were held on ice for a maximum of 2.5 hours.

Once the micropipette was manoeuvred close to a single cell, the actuator was slowly (about 6 Pa/s) lowered to provide a small negative pressure (usually 20-60 Pa). This tare pressure (P_t) was maintained for 30-60 seconds to allow the micropipette to form a complete seal around the cell, and to define a reference state for measurements of pressure application and aspiration length. Next, a suction pressure ($P_{applied}$) of approximately 500 Pa was applied at a rate of 60 Pa/s. The cell was allowed to equilibrate over a period of at most 120 seconds. Equilibrium was defined as no significant (approximately < 0.2 μm) change in aspiration length for at least two measurements (20 seconds). The cell was then expelled from the

pipette by returning to a slightly positive pressure (applied either by raising the actuator or by using a syringe mounted in-line with the pipette).

Image acquisition rate was always set to 20 fps. ROI depended on cell diameter and was usually somewhere between 100×100 pixels and 150×150 pixels.

3.3.3. Criteria for test cells

In any given cell suspension, a number of cells were deemed unacceptable for MA and were either avoided entirely or their aspiration data discarded.

3.3.3.1 Cells not tested

In order to ensure we were only recording the mechanical properties of living cells, we used fluorescent labelling of dead cells with ethidium homodimer-1 (EthD-1, from a Live/Dead Viability Cytotoxicity Kit, Invitrogen, Burlington, ON), a compound enters only cells with damaged outer membranes to then bind with nucleic acids. A small volume of VICs in suspension was added to 4 μM EthD-1 in PBS and allowed to incubate on ice for 30 minutes. Cells were viewed under the microscope and it became apparent that dead cells exhibit a very distinct morphology (Figure 3-5). Attempts to aspirate these cells revealed that they were extremely compliant and were either lysed or completely aspirated at pressures far below the 500 Pa typically applied to VICs. Therefore, we determined that it was not necessary to use EthD-1 as a marker for dead cells in subsequent experiments.

We excluded a second cell type from any MA experiments. This cell type was characterized by the formation of multiple plasma membrane-bound blebs on the surface of cells (Figure 3-6). This phenomenon may be an indication of apoptotic processes [121, 122] and these cells were therefore also excluded from MA tests.
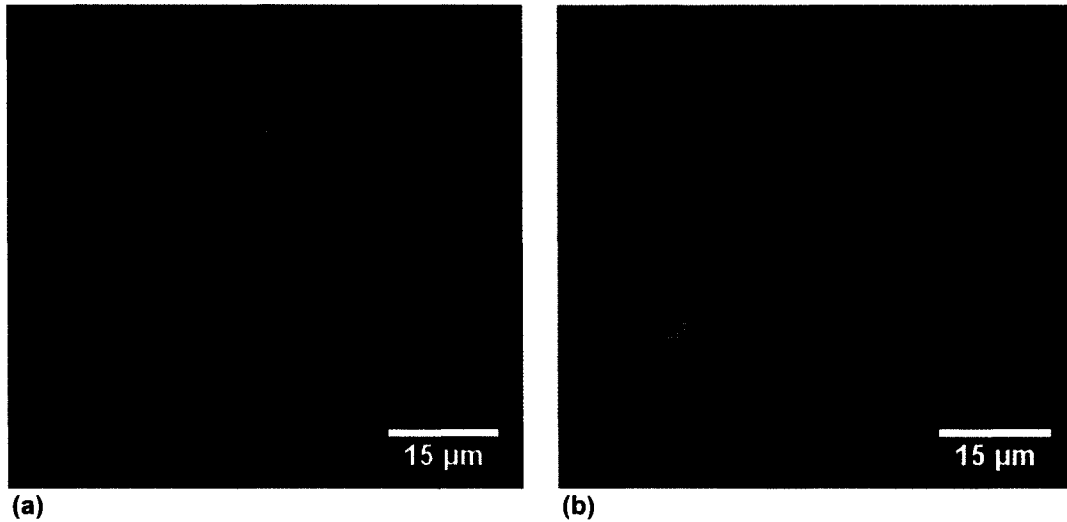
Figure 3-5 Cell morphology of dead VICs in suspension: (a) Three cells fluorescently labelled with EthD-1, (b) DIC image of the same cells, along with a healthy cell suitable for MA testing.
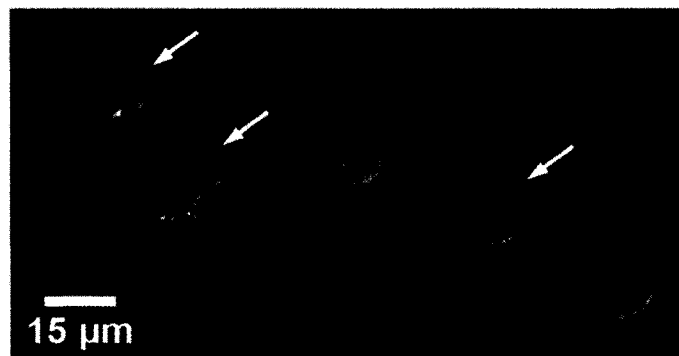
Figure 3-6 An example of blebbing cells (arrows) and two healthy VICs suitable for MA testing.

3.3.3.2 Criteria to discard MA data

Although we were able to immediately exclude certain cells, others exhibited undesirable behaviour during testing. We therefore established criteria to discard the aspiration data of these cells, listed below

1. A small number of cells were seen to respond actively during MA. This behaviour is characterized by a deviation from the typical monotonic creep response curve of

viscoelastic materials during aspiration. This includes a decrease (rather than an increase) of aspiration length over time, or a change in aspiration length after the cell has reached equilibrium (generally after 120 seconds). Cells exhibiting this behaviour were discarded.

2. If the aspirated portion of the cell consisted solely of plasma membrane (no organelles or other cellular components), the measurement was discarded (Figure 3-7a).

(a)

(b)   (c)
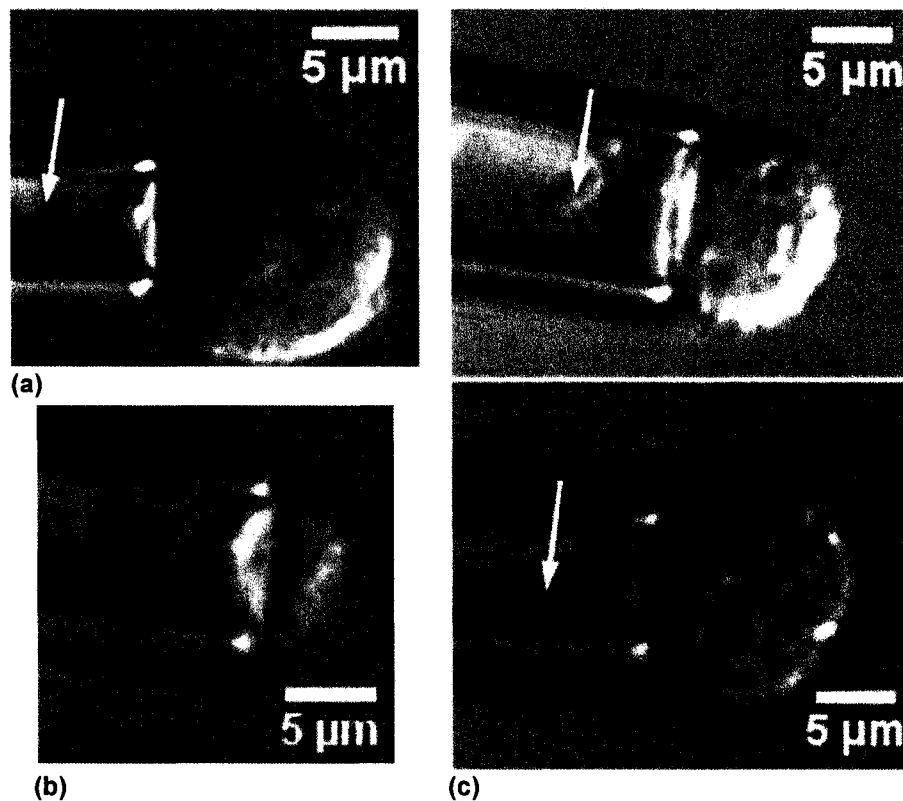
Figure 3-7 Discarded MA data: (a) membrane-only aspiration (arrow) (b) a cell held in the pipette for over 120s, about to be completely aspirated into the micropipette and (c) two separate examples of bleb formation (arrows) during aspiration.

3. In some cases, the ratio between the pipette and cell radius (R_p/R_c) was too large and the cell was completely aspirated into the pipette. These measurements were

obviously discarded. Additionally, if after 120 seconds aspiration lengths were still increasing rapidly (>0.5 µm/10 seconds), that measurement was also discarded (Figure 3-7b). Observation past 120 seconds of several cells exhibiting this behaviour invariably resulted in complete aspiration of the cell.

4. If blebs or smaller membrane protrusions formed before aspiration length reached equilibrium, the measurement was discarded (Figure 3-7c).

3.3.4. Data analysis

Raw MA data consisted of a series of aspiration images (Figure 3-8) acquired every 50 ms and a textfile with pressure transducer values. Images were converted to an image stack in ImageJ and a timestamp corresponding to the 20 fps acquisition rate was superimposed on all images. Saving transducer data and image data was initiated at the same time, so once images were labelled, pressure data could be correlated.

Aspiration lengths were measured after application of the tare pressure (L_t, at $t = t_0^-$), immediately after the 500 kPa suction pressure was applied ($L_{initial}$, at $t=t_0^+$) and then every 10 seconds until the aspiration length reached equilibrium (L_{final}, at $t=t_f$). Actual pressure (ΔP) and aspiration data (L_0 and L_{eq}) is the difference between the measured and tare values (Figure 3-9). We used ImageJ software to measure all data.
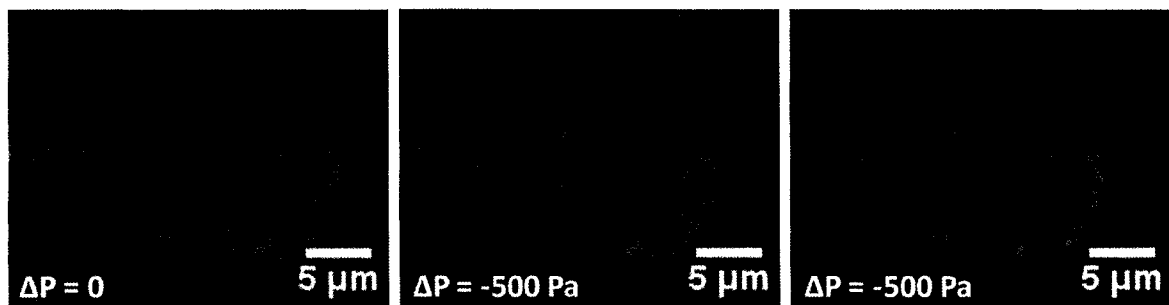
Figure 3-8 A selection of typical aspiration images: (a) after application of tare pressure, (b) immediately after application of the 500 Pa suction pressure and (c) final aspiration length

$t = t_0^-$

L_{tare}

Cell

$2R_p$

P_{tare}

(a)

Pipette

Pipette fillet radius: e

From $t_0^- \rightarrow t_0^+$

$\Delta P = P_{applied} - P_{tare}$

$L_0 = L_{initial} - L_{tare}$ (elastic response)

From $t_0^+ \rightarrow t_f$

$\Delta P = 0$

$L_{eq} = L_{final} - L_{tare}$ (viscoelastic response)

$t = t_0^+$

$L_{initial}$

$P_{applied}$

(b)

$t = t_f$

L_{final}

$P_{applied}$

(c)
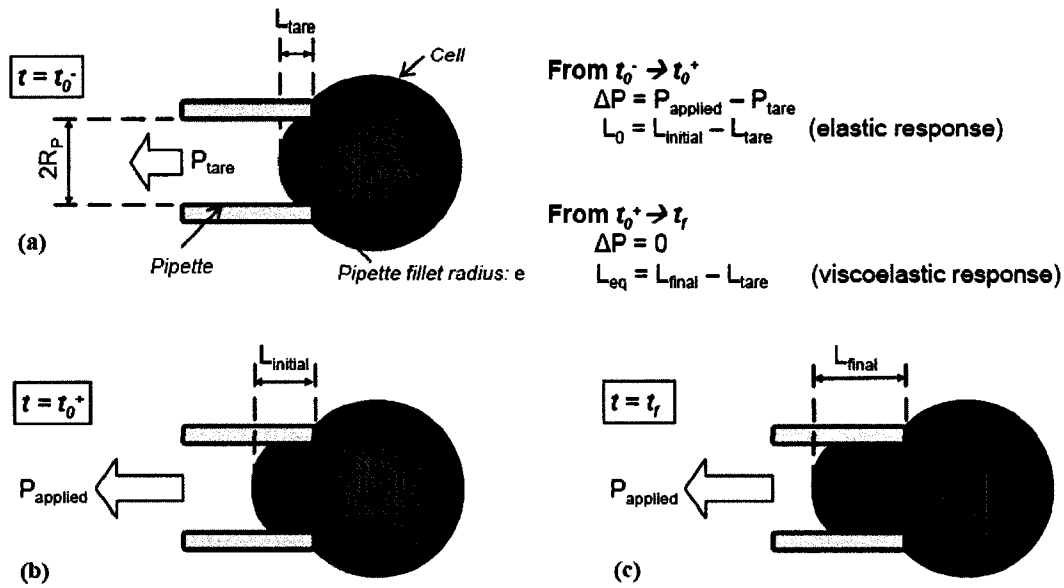
Figure 3-9 Schematic representation of a cell in various stages of aspiration: (a) after application of tare pressure, (b) immediately after application of the test pressure and (c) after reaching equilibrium. Elastic and viscoelastic response was found from fitting aspiration, pressure and geometric data to existing numerical models.

3.3.4.1 Finite element simulation of VIC experimental results

Finite element analysis of MA on VICs showed that the time constant for VICs was about an order of magnitude larger the ~1 Hz cardiac cycle [123, 124]. Although VICs clearly exhibit a viscoelastic response, the high time constant indicates that elastic effects dominate *in vivo*. We therefore decided to focus our analysis on the elastic response, characterized by the instantaneous Young's modulus (E_0). However, aspiration length was still monitored until it reached equilibrium – this was necessary in order to apply the selection criteria described in 3.3.3.2.

3.3.4.2 Mathematical model for E_0

We evaluated mechanical properties of VICs using a nonlinear viscoelastic model, the standard neo-Hookean solid (SnHS) derived by Zhou in [41]. This model is similar to the

standard linear solid model described in 2.4.3, however the non-linear SnHS model takes into consideration nonlinear material properties and therefore accounts for the large strains experienced by cells undergoing MA.

The simulated aspiration process using the SnHS viscoelastic finite element model examined both instantaneous and creep deformation [41]. Because of the large time constant associated with VICs, we were interested only in the instantaneous, elastic response and therefore the SnHS viscoelastic finite element model reduced to a purely elastic one. Zhou first examined effects of the pipette radius (R_P) and the pipette fillet radius (e) and showed that fillet radius had a negligible effect on the solution for a pipette/cell radius ratio ($R_p^* = R_P/R_C$) ranging from 0.25 to 0.6 [41]. Zhou then applied non-linear regression analysis to the SnHS elastic finite element solution for that range of R_P^* and obtained the following equation and fitting parameters:

$$E_0 = \frac{3\Delta P}{\left[\beta_1 \frac{L_0}{R_P} + \beta_2 \left(\frac{L_0}{R_P}\right)^2\right]\left[1 - \left(\frac{R_P}{R_C}\right)^{\beta_3 + \beta_4 \frac{L_0}{R_P} + \beta_5 \left(\frac{L_0}{R_P}\right)^2}\right]}$$

$\beta_1 = 2.0142$

$\beta_2 = 2.1186$

$\beta_3 = 2.1187$

$\beta_4 = -1.4409$

$\beta_5 = 0.3154$

$$0.25 \leq \frac{R_P}{R_C} \leq 0.6$$

We applied the above equation even for $R_P^* > 0.6$, because of the relative insensitivity of fillet radius at higher R_P^* values [41].

For a viscoelastic material, the apparent elastic modulus varies depending on loading rate and history. The above equation for E_0 assumes pressure is applied instantaneously. If the pressure is increased very slowly, or if the aspiration length is measured after the applied pressure has been kept constant for a long time, the apparent elastic modulus will approach that of the long-term modulus (E_∞), which is defined by a separate equation [41].

For reasons outlined in section 3.4.2, it was not possible to apply an instantaneous load to VICs. Instead, we applied the 500 Pa load over an 8 second time period and allowed the cell to equilibrate for 120 seconds in the pipette. Although this loading profile is not quite instantaneous, we felt we were justified in using the equation for E_0 because the loading time period was a relatively small fraction of the total load time (approximately 6%).

3.4. Preliminary tests and system limitations

Although MA is a widely used technique, a number of system limitations exist. The following sections outline some of the major problems encountered during the course of this project and describes how and if these were overcome.

3.4.1. Cells in suspension

MA was designed to test cells in suspension, which in the case of adherent cells such as VICs does not represent a physiologically relevant state (see section 2.4.5). Attempts to use MA on VICs attached to a substrate ultimately failed (see section 3.4.3) and we therefore conducted all tests on VICs in suspension. However, because all of our MA experiments examined only the relative difference between VICs (either isolated from distinct valve regions or cultured in distinct conditions), any significant difference in stiffness between VIC

groups is presumably still representative of actual differences in VIC mechanical behaviour, even though the absolute experimental values might not be typical of the adherent state.

3.4.2. Blebbing

Initial tests revealed a tendency for the aspirated portion of the cell to be granule free, and detached membrane blebs were frequently observed. This blebbing phenomenon (shown in Figure 3-7) occurred much more frequently (in more than 50% of cells tested) when the ratio of pipette to cell radius was particularly small ($R_P^* < {\sim}0.4$), and when the suction pressure was applied too rapidly. Increasing R_P^* and decreasing pressure loading rates reduced the occurrence of blebbing significantly to less than 10% of cells tested.

In addition to the cytoskeletal proteins that permeate the cytoplasm, cells typically have a cytoskeletal cortex, consisting largely of actin filaments arranged in an organelle-free network, located directly beneath (and attached to) the plasma membrane [7]. Cell blebbing occurs when the plasma membrane is detached from the cytoskeletal cortex, allowing for intracellular solvent flow into the region between the membrane and cortex [121, 125, 126] and can be induced by hydrostatic suction pressure [127]. This phenomenon has been observed in other MA experiments [27]. It can thus be deduced that if force is applied rapidly to a relatively small area on the cell surface, blebbing is more likely to occur, consistent with our observations. Although we can still measure aspiration lengths, the stiffness value obtained is representative only of the cell membrane, not the entire cell. For this reason, the data from any cell exhibiting membrane blebs or protrusions (Figure 3-7) were discarded.

3.4.3. Micropipette aspiration of adherent cells

We initially had hoped to use MA on adherent VICs (Figure 3-10a), as this would be more representative of the cell's *in vivo* physiology. However, although MA has been used to

examine the mechanics of adherent cells on a substrate [51, 52], we were not able to apply it to adherent VICs. The principle problem encountered was similar to the blebbing seen in cells in suspension, namely that the aspirated portion of the cell appeared to consist only of cell membrane (Figure 3-10b) This observation indicated that the membrane had detached from its actin cortical shell [121, 125-127]. In a few cases, portions of this projection would actually pinch off and form membrane vesicles, effectively shortening the aspiration length and rendering any further analysis useless. In the case of [51], membrane aspiration was not considered a problem, as they were solely interested in effects within the cell membrane itself. However, because the cytoskeleton plays such a substantial role in the mechanical response of VICs, it was imperative that the cellular stiffness measurements include it.

Attempts to change loading rates or pipette size were ineffective in permitting aspiration of adherent cells. Pipette size had to be limited to very small diameters (< 5 μm) since VIC height when seeded on collagen-coated glass coverslips is just 6 μm [128]. Because adherent cells are naturally stiffer than those held in suspension, pressure loads had to be higher in order to see any appreciable deformation within the pipette. This higher, more concentrated load profile was likely responsible for the increased occurrence of blebbing. Prolonged exposure to a high suction pressure also frequently resulted in detachment of VICs from the underlying substrate.

In the rare event that a portion containing organelles and other cellular matter was aspirated into the pipette, the aspiration rate and the projection into the pipette was not uniform (Figure 3-10c) and essentially impossible to fit into any existing models.

Ultimately, we made the decision to continue all tests only on VICs held in suspension, which, although not a physiologically relevant test state, would provide reliable and repeatable data and allow for relative comparison between VIC populations.
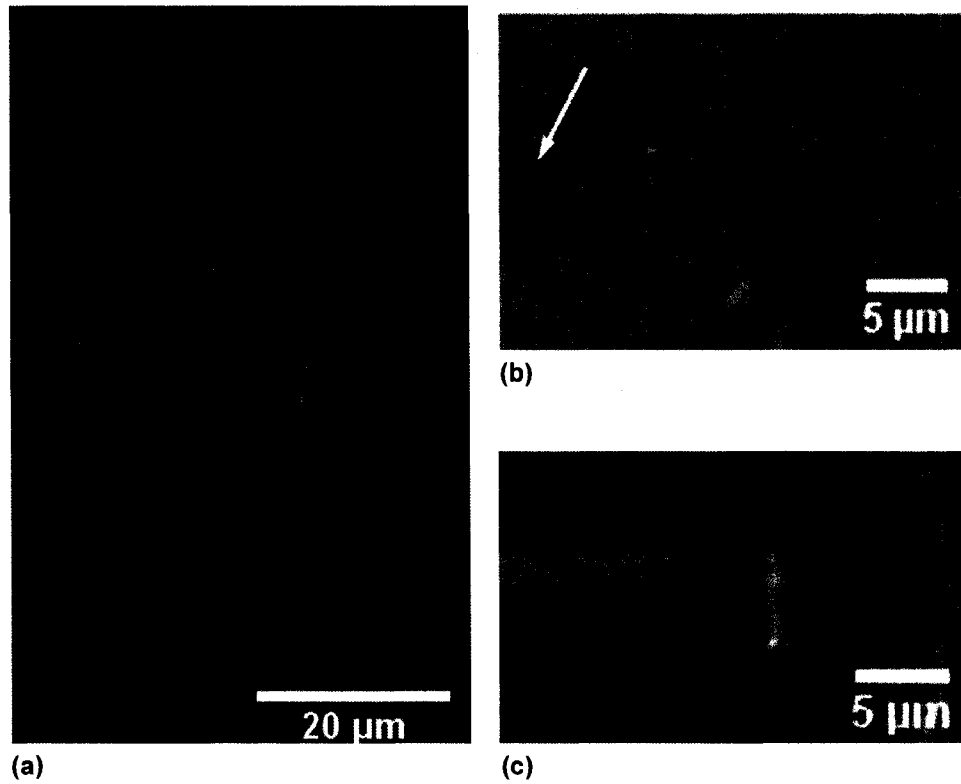
Figure 3-10 MA of adherent VICs: (a) tests required a very small micropipette diameter compared to cell size, (b) membrane-only bleb (arrow) and (c) uneven aspiration of intra-cellular components

Chapter 4: Mechanical properties of native and cultured valve interstitial cells

4.1. Introduction

As outlined in Chapter 2, the tissue-level organization of the aortic valve leaflet is highly regulated, consisting of a layer of circumferentially arranged collagen fibres on the aortic side (the fibrosa), a layer composed primarily of glycosaminoglycans and water in the centre (the spongiosa) and a layer with both elastin and collagen content (the ventricularis) on the ventricular side. VICs are spread throughout these three layers and spatial heterogeneity of mechanical properties within each of the three layers at the tissue level of the aortic valve is well documented [68-71, 129-134]. Leaflet mechanical properties are the focus of numerous studies, with some examining the mechanical response of individual layers [68, 70, 133] and others investigating the relative mechanical contribution of each layer in the intact leaflet [68, 69, 71, 129-132, 134]. Differences in test methods and interpretation have resulted in a range of reported values and behaviour, however, the fact that layer-specific differences exist in properties such as tissue stiffness and extensibility is undisputed. VICs are responsible for maintaining this tri-layer organization and as such the cells in each of these layers must be exposed to distinct cues in order to maintain the proper morphology – these may be biological, chemical and/or mechanical in origin.

A link between cell stiffness and substrate stiffness has been established [52, 117, 135], with multiple cell types altering their cytoskeletal organization in response to changing matrix compliance, although the effect of this on VIC mechanical properties has not been investigated. However, a mechanical link between VICs from different valves has been established. VICs isolated and cultured *in vitro* from the valves on the left side (aortic and

mitral) of the heart were significantly stiffer than those on right side (pulmonary and tricuspid) [25]. VICs from the aortic and mitral valves are exposed to substantially higher transvalvular pressures – 80 and 120 mmHg vs. 10 and 25 mmHg – suggesting that the tissue-level mechanical environment is mirrored to some degree at the cellular level.

In addition, VICs cultured *in vitro* preferentially differentiate into myofibroblasts (as opposed to the quiescent fibroblasts of native tissue), and show significant alterations in cytoskeletal arrangement [106]. Standard tissue-culture plastic is several orders of magnitude stiffer than native tissue, therefore if VICs do respond to matrix stiffness, then this phenomenon should become especially evident after culture *in vitro*.

Our objective was to establish the mechanical heterogeneity, if any, of VICs within native tissue and to establish whether standard tissue-culture methods affect their mechanical response, as an initial attempt to assess whether VICs mechanical properties are influenced by substrate stiffness. We used MA to characterize both the native VIC population and cells grown on a plastic substrate *in vitro*. Results provide preliminary evidence that there may be spatial heterogeneity in primary VIC mechanical properties and that prolonged culture on a stiff substrate indeed causes VICs to alter their mechanical properties (to become significantly stiffer).

4.2. Methods and materials

4.2.1. Experimental design

We conducted two distinct experiments to investigate mechanical properties of native and cultured VICs:

1. A layer separation experiment: this experiment involved the microdissection of porcine aortic valve tissue to examine the spatial heterogeneity in mechanical properties of primary VICs isolated from healthy leaflets.

2. A passage dependent experiment: this experiment examined the mechanical properties of primary VICs compared with those cultured *in vitro* for several passages (up to 27 days culture *in vitro*).

The methods and materials are outlined in the following sections. Unless explicitly stated otherwise, it can be assumed that methods and reagents are the same for both experiments.

4.2.2. VIC isolation

For passage dependent studies, primary VICs were obtained using the isolation protocol described in Chapter 3 and Appendix A. Viable cells were counted using a Vi-Cell™ cell viability analyzer (Beckman Coulter, Mississauga,ON). A portion of the cell yield from primary (day 0) cells were resuspended in complete media and held on ice for MA testing and the rest were reserved for *in vitro* cell culture (see section 4.2.4).

Primary VIC isolation techniques for the layer separation experiments were similar to those described in Chapter 3 and Appendix A, with some minor modifications. After removal of the outer VEC layer (digestion in collagenase with TES buffer, vortex and scraping), leaflets were dissected (section 4.2.3) so that the fibrosa and ventricularis layers were separated. Cell isolation protocol for the separated layers was the same as that for intact leaflets after this point, with the exception of incubation time, which was increased to four hours at 37°C for the first isolation (Trial 1). Incubation time was decreased back to two hours for Trials 2 and 3.

4.2.3. Layer separation

We adapted our layer separation technique from Vesely *et al* [70]. After VEC removal, leaflets were held in PBS with 0.5% amphotericin B and 1% penicillin/streptomycin mixture. Each leaflet was mounted with the ventricular side facing upwards. In this orientation, the distinction between fibrosa and ventricularis was clearly visible along the edge of the leaflet (Figure 4-1).

(a)   (b)
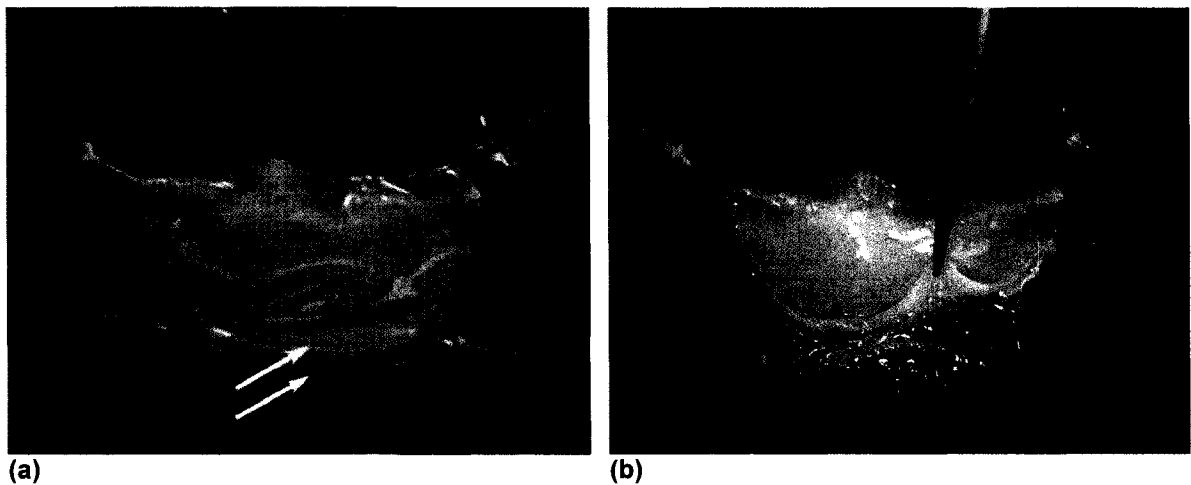
Figure 4-1 Layer separation technique: (a) the separation between ventricularis (top) and fibrosa (bottom) is clearly visible (arrows) and (b) the ventricularis is held up with forceps while the microdissection knife severs the connections between the two layers by cutting through the spongiosa

Using fine-tip forceps, the ventricularis was lifted and the fibrous connections between it and the fibrosa were severed using a dissecting knife. This technique unavoidably cut through portions of the spongiosa – it was not possible to manually separate the three layers. The leaflet surfaces were kept moist at all times using PBS applied topically. All microdissections were carried out under sterile conditions with specimens mounted on an adjustable vertical stage so as to be at eye level of the operator. Despite initial attempts to use a stereo-microscope to aid in the dissection, we ultimately found it easier to work without any specimen magnification.

4.2.4. VIC culture

For passage dependent experiments, VICs were counted using a Vi-Cell™ cell viability analyzer (Beckman Coulter) and then seeded at 10'000 cells/cm^2 in tissue-culture flasks and maintained in complete media at 37°C and 5% CO_2. Media was changed every 2 days until cells were about 90% confluent (approximately 6-7 days). VICs were then removed from the substrate with 0.125% trypsin with EDTA for use in both MA experiments and further subculture. Cells to undergo MA after trypsinization were immediately resuspended in complete media and held on ice. Cells selected for further *in vitro* culture were replated. This procedure was repeated up to passage 4.

4.2.5. MA technique

For both tests, MA procedures were followed according to the protocols outlined in Chapter 3 and Appendix A. Cells were held on ice throughout testing. Cells in suspension were placed on the microscope stage for a maximum of 25 minutes at a time and generally were held in the micropipette at a constant pressure for a maximum of 2 minutes. The average applied pressure (ΔP) was 476±7 Pa (mean ± standard deviation) for all layer separation MA tests and 501±12 Pa for all passage-dependent MA tests. Stiffness measurements are reported as instantaneous Young's modulus (E_0) and were analyzed as outlined in Chapter 3.

For the layer separation experiments, one trial is defined as MA testing of VICs from a single isolation – from both the ventricularis and the fibrosa – conducted the same day as the isolation. Once a particular isolation was complete, we resuspended the two cell populations (fibrosa and ventricularis) separately in complete media. Cells were held on ice throughout testing. Care was taken to alternate testing of fibrosa and ventricularis VICs.

4.2.6. Scanning electron microscopy of intact and separated leaflets

Both intact and separated leaflets were freeze-fractured and fixed in 4% formaldehyde, followed by dehydration in a series of ethanol washes (30%, 50%, 70%, 95% and 100%) for 30 minutes at each concentration. Samples were subsequently critical point dried in liquid carbon dioxide in a Polaron CPD7501, mounted on SEM aluminum stubs and sputter coated with gold using a Polaron SC 515 SEM coating system. Samples were examined using a scanning electron microscope (Model S-2500, Hitachi Instrument).

4.2.7. Statistical Analysis

Values for Young's modulus more than 1.5 times the interquartile range (1.5×IQR) above the 75th percentile or below the 25th percentile were considered outliers and removed from the dataset. All data are presented as mean ± standard error of the mean (SEM). For both experiments, $p < 0.05$ was considered significant.

Layer separation experiments were repeated three times. Each trial tested 10 to 16 cells from each side (or a total of 20 to 31 cells per trial). Average stiffness of ventricularis and fibrosa cells were compared between the three trials using the paired Student's t-test. The non-paired Student's t-test was used to evaluate statistically significant differences between individual trials of the layer separation experiments.

For the passage-dependent experiments, Kruskal-Wallis one-way ANOVA on ranks and Dunn's method were used to evaluate statistically significant differences in multiple group comparisons.

4.3. Results

4.3.1. Layer separation experiments

Because there are no known morphological or other markers to distinguish cells from either layer, we first used SEM to qualitatively investigate the success of the layer separation technique. The three layers were visible in the whole leaflet (Figure 4-2 and Figure 4-3), and the morphology of the ventricularis, spongiosa and fibrosa in the intact leaflet appeared to be consistent with that from the separated layers (Figure 4-4). The collagen fibres of the fibrosa were aligned, while the matrix of the spongiosa and ventricularis appeared to be somewhat less organized. Although a substantial portion of it appeared to be lost in the dissection, a segment of the spongiosa remained on the ventricular side (Figure 4-4).
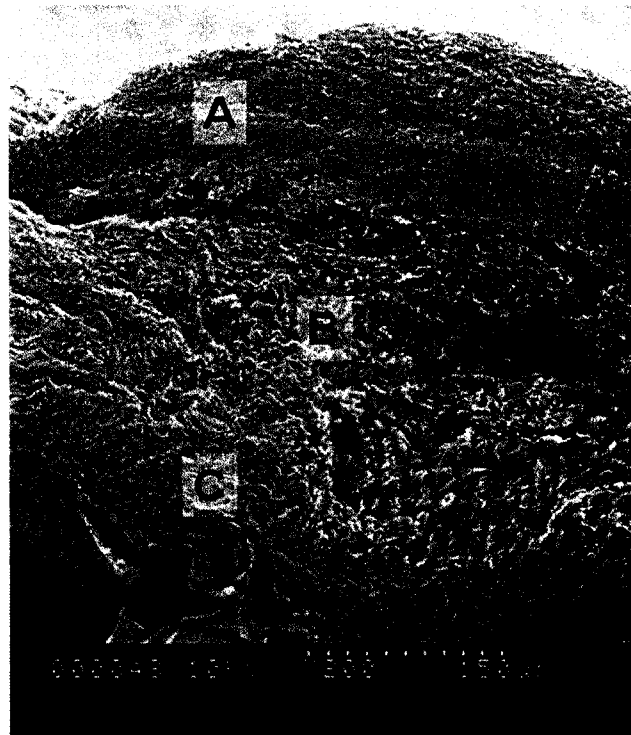
Figure 4-2 SEM of entire leaflet. The distinct morphology of each layer is clearly visible. The ventricularis (A) consists of a network of collagen and elastin fibres, the spongiosa (B) is a loose layer of glycosaminoglycans and collagen fibres and the fibrosa (C) consists of an organized layer of radially aligned collagen fibres. Images courtesy of C.Y.Y. Yip and J. Wang.
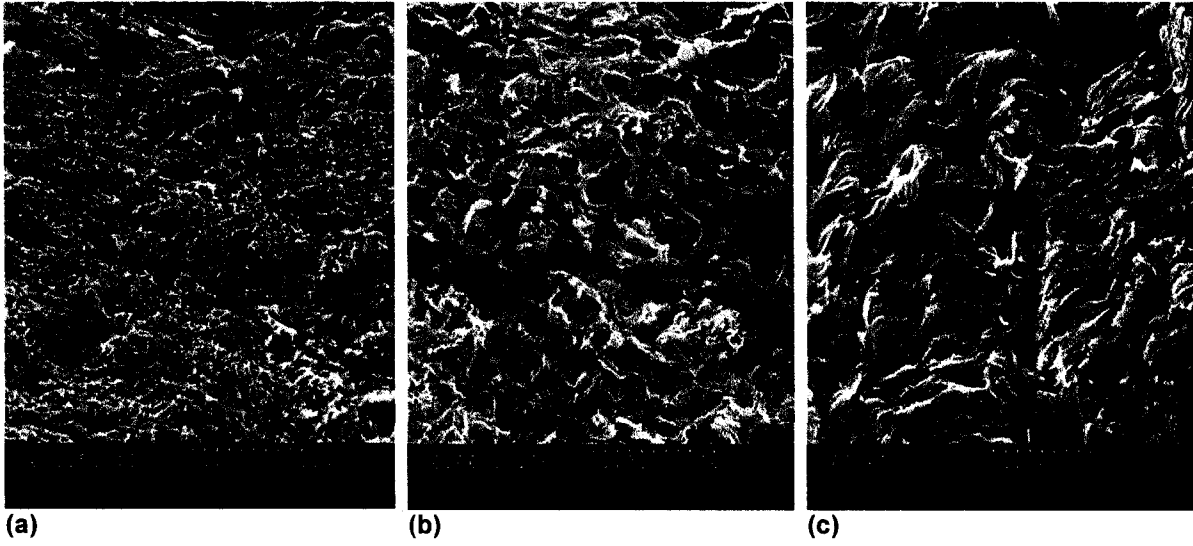
Figure 4-3 Enlarged view of each layer (a) ventricularis, (b) spongiosa and (c) fibrosa. Images courtesy of C.Y.Y. Yip and J. Wang.
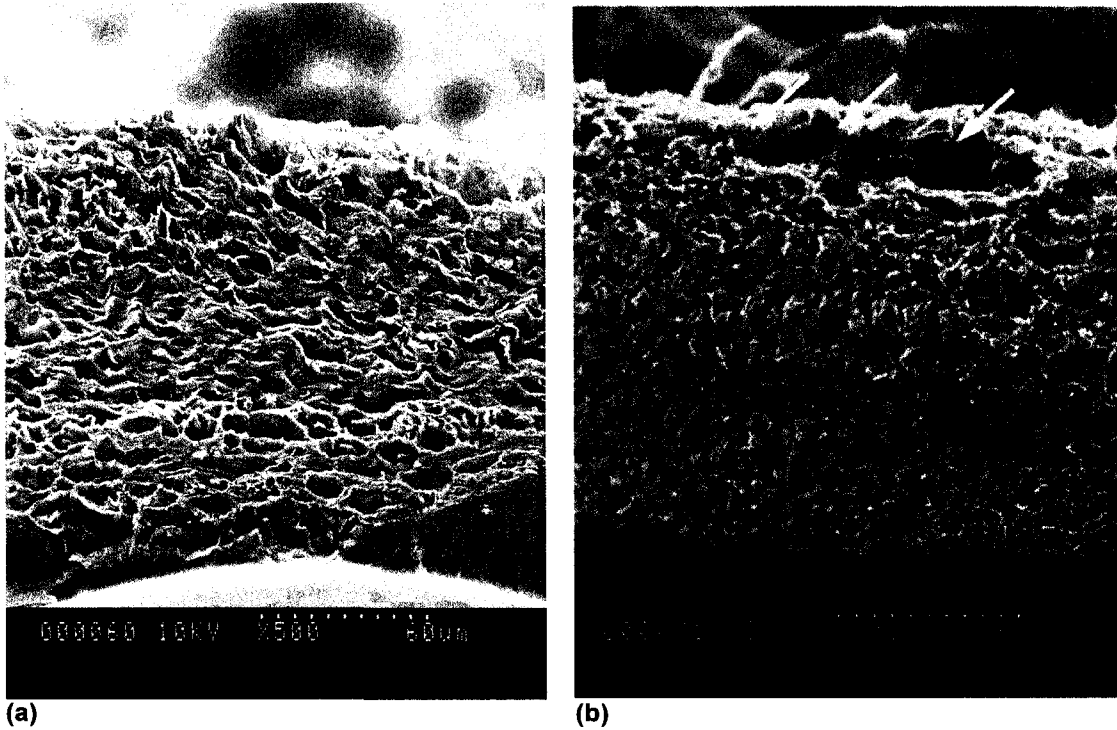
Figure 4-4 SEM of a dissected (a) fibrosa and (b) ventricularis. The only remaining portion of the spongiosa appears to be on the ventricular side (arrows). Images courtesy of C.Y.Y. Yip and J. Wang.

The average Young's modulus for the VICs from the fibrosa was 3.69±0.54 kPa, while that for VICs from the ventricularis was 2.60±0.24 kPa (Figure 4-5). There was no significant difference between the two cell populations (p=0.14). Averages were calculated as population averages from the three independent trials.
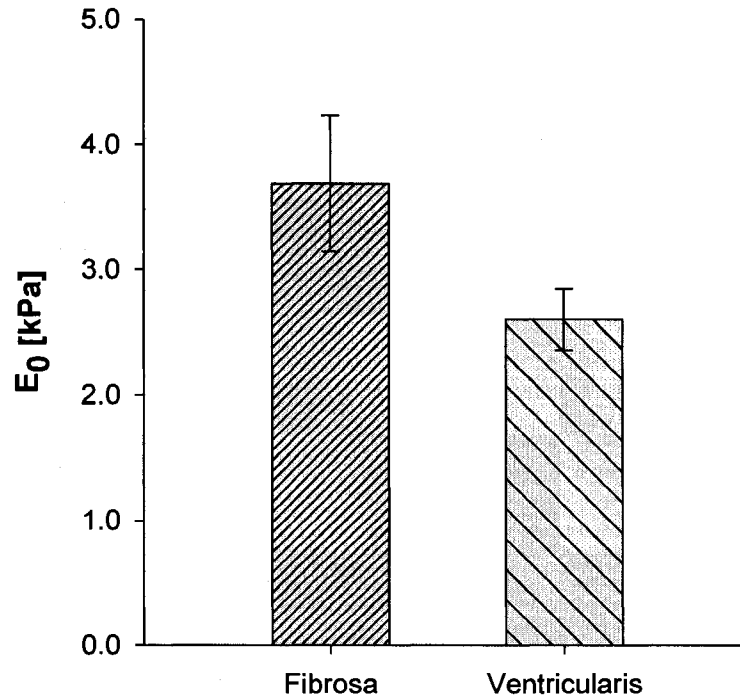
Figure 4-5 Instantaneous Young's modulus for VICs from the fibrosa and the ventricularis (n = 3, p = 0.14).

Although not statistically significant, the p-value obtained was low enough to warrant further investigation. We therefore examined the differences in stiffness between fibrosa and ventricularis for each individual trial. Interestingly, there was a statistically significant difference between the two layers for two out of the three trials (Table 4-1 and Figure 4-6), suggesting that perhaps the cells within the fibrosa were actually stiffer.

Table 4-1 Stiffness data (mean±SEM) for individual trials. Stiffness of fibrosa and ventricularis are compared using the student's t-test. * p < 0.05 is considered significant.

Trial #	Fibrosa		Ventricularis		p-value
	E_0 [kPa]	# cells tested	E_0 [kPa]	# cells tested	
1	2.80±0.76	15	3.08±0.29	13	0.218
2	3.59±0.31	16	2.43±0.49	15	*0.002
3	4.68±0.99	10	2.29±0.98	10	*0.035
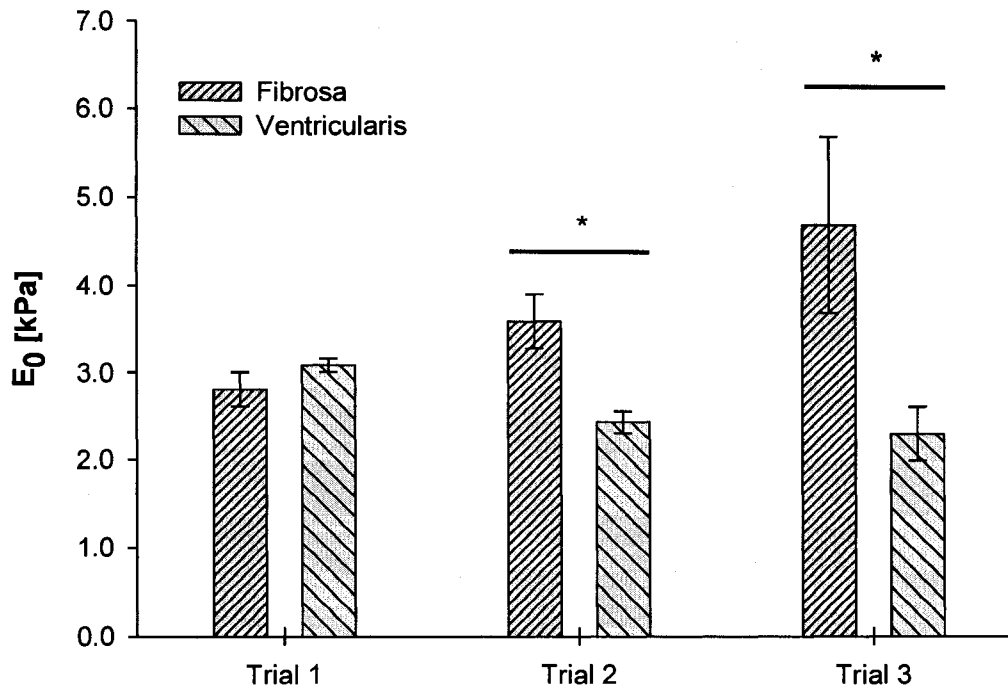
Figure 4-6 Difference in Young's modulus of VICs from the fibrosa and ventricularis. A significant difference was noted in two of the three trials (* p < 0.05).

4.3.2. Passage dependent experiments

Multiple group comparison tests showed that a significant difference (p < 0.05) in stiffness existed between primary VICs and each of the passaged VIC groups. Primary cells had an average stiffness of 2.04±0.21 kPa while the average Young's modulus of passaged

cells ranged from 4.99±0.90 kPa to 6.08±0.73 kPa. There was no significant difference between mechanical properties in VICs from different passages (Figure 4-7 and Table 4-2).

Table 4-2 Stiffness data (mean±SEM) for passage-dependent studies. Day 0 values are significantly less than all passaged (Day 7-27) values

	E_0 [kPa]	# cells tested
Primary (Day 0)	2.04±0.21	12
Passage 1 (Day 7)	4.64±1.38	9
Passage 2 (Day 13)	5.81±0.44	10
Passage 3 (Day 20)	4.99±0.90	9
Passage 4 (Day 27)	6.08±0.73	5
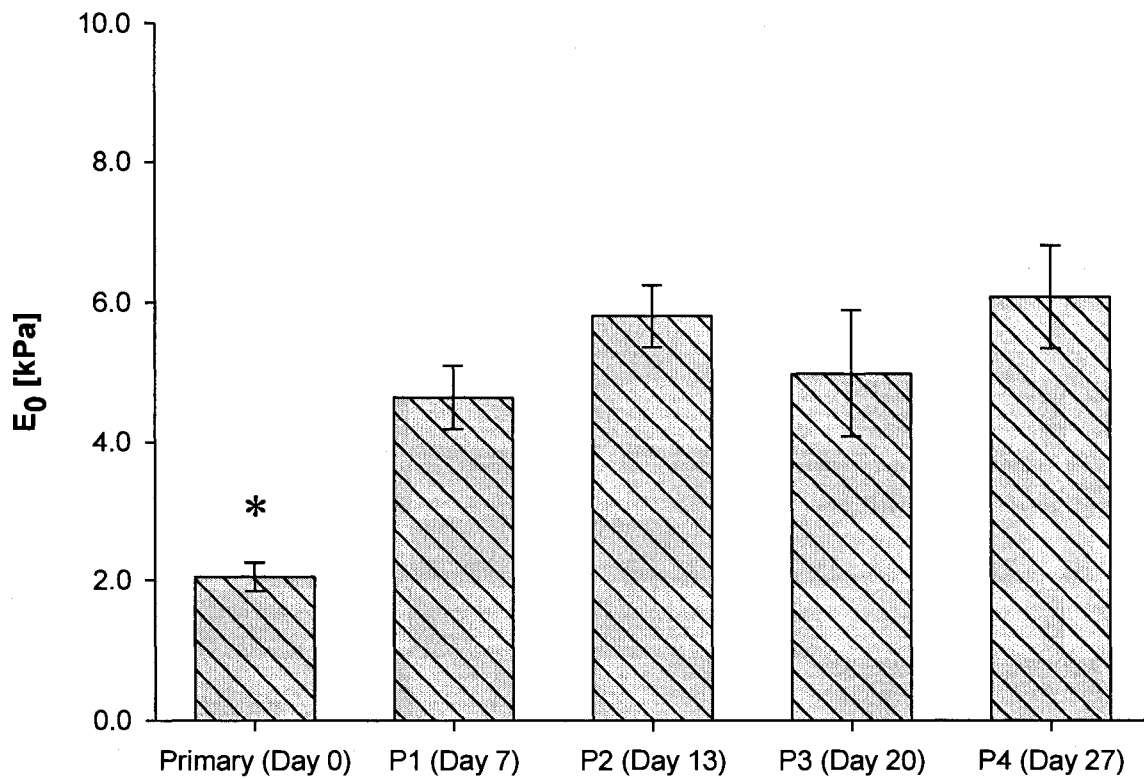
Figure 4-7 Stiffness of primary and passaged VICs. Primary VICs were significantly softer than those cultured on tissue-culture plastic. Passaging and culture time did not produce significant changes in stiffness (* $p < 0.05$ relative to all other conditions).

We also noticed that VIC diameter increased after *in vitro* culture. The average cell diameter of primary cells (measured using the Vi-Cell cell viability analyzer) was 13.3±4.8 μm while that of VICs from passage 1 and 2 was 18.31±1.1 μm and 18.37±1.5 μm, respectively. Average cell diameter of both groups of passaged cells was significantly higher than the cell diameter of primary cells ($p < 0.001$, ANOVA with Fischer LSD multiple comparisons). No significant statistical difference was observed between the diameter of cells from passage 1 and passage 2.

4.4. Discussion and Conclusions

4.4.1. Layer separation experiments

The healthy aortic valve leaflet has a distinct three-layer morphology, with the VICs responsible for maintaining leaflet structural organization distributed throughout all three layers. We have attempted to experimentally assess the spatial heterogeneity of VIC mechanical properties by adapting a layer separation technique pioneered in [70]. We were able to successfully separate the ventricularis and fibrosa and isolate independent cell populations from each layer. SEM imaging indicated that a portion of the spongiosa remained attached to the ventricularis, suggesting that the ventricular VICs tested may actually be representative of a heterogeneous population of VICs from those two layers.

Based on three independent trials, the stiffness of the fibrosa cells was approximately 42% greater than that of the ventricularis VICs. Despite the small sample size, this difference approached significance ($p = 0.14$) and in two of the three trials conducted, a consistent difference in VIC stiffness between fibrosa and ventricularis was observed, with VICs from the fibrosa significantly stiffer than those from the ventricularis ($p < 0.05$ in both cases).

These somewhat conflicting observations make conclusive interpretation of these data challenging, however it does appear that further investigation is warranted, not least because other studies suggest that there is indeed spatial heterogeneity within VIC biological and mechanical function.

Layer-specific differences in VIC stiffness may reflect the cells' response to the dynamically and structurally dissimilar environments within the individual layers. Leaflet tissue is highly anisotropic, with different elastic moduli in the radial and circumferential direction in both fibrosa and ventricularis [70]. The fibrosa is mechanically the strongest layer, and bears the principal stress of diastolic pressure [59]. In the intact valve, the surface of the fibrosa is folded, held in place by connections to the ventricularis, producing in a small residual stress in each layer [70], with the fibrosa under compression and the ventricularis under tension. The elastin content of the ventricularis has been shown to help keep the fibrosa compressed in the radial direction when the leaflet is unstressed [70, 133]. During diastole, there is considerable realignment of collagen fibres in the fibrosa as leaflets extend beyond 50% strain and recoil elastically, with the elastin content in the ventricularis imposing tensile forces on the collagen fibres during valve unloading [71]. As TVP increases, the normally randomly oriented fibres of the ventricularis stretch out along the circumferential direction. Overall, the rate and amount of reorientation of the natural aortic valve's fibrous microstructure changes regionally with increasing TVP [69]. The rearrangement of leaflet microstructure as a result of both TVP and the opening and closing of the valve results in varying mechanical stresses and strains in distinct regions of the valve. VICs located in different regions within the valve may therefore be exposed to a multitude of unique strains throughout the cardiac cycle.

Multiple cell types have been shown to adapt their cytoskeletal organization and contractile activity in response to externally applied forces [8, 52], suggesting that if VICs from different layers are continually deformed at different rates during the cardiac cycle, they may indeed exhibit a unique mechanical response. Tissue-level differences in applied mechanical forces do appear to have a mechanobiological effect on VICs isolated from each of the four cardiac valves. VIC stiffness has been shown to increase with increasing TVP between left and right heart valves [25]. This observed increase in stiffness has also been correlated to an increase in α-SMA expression and collagen biosynthesis, although this phenomenon may have been partially influenced by the *in vitro* culture of these VICs prior to biological and mechanical testing [25].

Within the aortic valve, the extent to which these distinct tissue-level strains are transmitted to the VICs embedded within the ECM is the focus of ongoing research. VICs appear to be tightly bonded to the ECM of the leaflet and consequently have been shown to deform under increasing TVP [131]. Deformation of VICs, as calculated by the nuclear aspect ratio (NAR), showed changes in VIC shape as a result of collagen fibre re-alignment under increasing pressure. The extent of NAR changes were layer specific, with significantly higher NAR values observed in the fibrosa [131].

Finally, there also appears to be a biological difference in VICs isolated from the two layers. Preliminary results in our lab suggest that VICs from the fibrosa and ventricularis differentially form calcific nodules *in vitro* and show differences in calcium deposition and ALP activity. Unclear is whether these differences between the two populations are the result of the local mechanical environment, or a reflection of an inherent difference in VIC phenotype not dependent on external factors.

Although we were not able to conclusively determine whether there is a difference in VIC stiffness between the fibrosa and ventricularis, the preliminary evidence presented above does appear to suggest that VICs from the fibrosa are stiffer, which is further supported by previous research on tissue-level stresses and strains and how these are transmitted to the cellular level.

4.4.1.1 Study limitations

MA involves the removal of adherent VICs from their ECM and tests them in a non-physiologically relevant suspended state. Disruption of the focal adhesions anchoring the cytoskeleton to the ECM results in a softening of cells, and although this is less of a concern when examining the relative difference in stiffness between two or more cell populations, any potential difference in stiffness between the two layer-specific populations may not be large enough to consistently be observed once VICs are removed from the ECM.

The manual dissection of valve leaflets is a lengthy process, increasing total isolation time. The rate at which adherent cell mechanical properties change while in suspension is unknown, however a longer isolation time may also potentially eliminate any existing differences between the two populations. This may actually be the reason for the inconsistent results seen in Trial 1, where valve tissue was incubated in collagenase for four hours instead of the usual two hours.

Finally, SEM results indicated that VICs isolated from the ventricular side may actually be a heterogeneous mix of spongiosa and ventricularis VICs, two populations which exist in distinct ECM and mechanical environments and therefore likely experience different mechanical stresses and deformation rates.

4.4.2. Passage dependent mechanical properties

We hypothesized that cytoskeletal changes observed with culture of VICs [106] influenced the stiffness of individual VICs. Primary and cultured (P1-P4) VICs were tested using MA and primary VICs were indeed found to be significantly softer ($p < 0.05$) than cells cultured *in vitro*.

In healthy valves, the majority of VICs are quiescent fibroblasts and only a small percentage of cells are activated myofibroblasts [62]. However, culture on a stiff substrate such as tissue-culture plastic induces myofibrogenic differentiation, as characterized by the actin cytoskeletal reorganization into stress fibres expressing α-SMA [106]. Myofibrogenic differentiation requires the presence of two factors, TGF-β and ED-A fibronectin [100, 105, 136], however even if both of these factors are present, differentiation can be inhibited if there is not sufficient mechanical tension or if mechanical tension is removed [101, 137].

A number of adherent cell types are able to sense substrate stiffness [52, 117, 118]. Cells exert tractional forces on the surrounding ECM and thus increase intra-cellular cytoskeletal tension – a stiff substrate will provide a greater resistance to deformation and therefore result in greater tractional forces [117]. For example, culture on polyacrylamide (PA) gels with tuneable stiffness showed that fibroblasts are capable of increasing their internal stiffness until it matches that of the substrate, forming actin stress fibres at higher matrix stiffness [138], suggesting that substrate elasticity is a mechanism that influences both cellular mechanical and biochemical behaviour. Myofibroblasts also have well-developed bundles of actin filaments that contain α-SMA. These α-SMA stress fibres are generally arranged in parallel to the long axis of the cell, in contrast to the concentration of actin filaments in the subcortex that is more typical of fibroblasts [100]. Prolonged culture of VICs

on stiff substrates promotes the development of these stress fibres [106], and now we have shown that the cells cultured *in vitro* also show an increase in intra-cellular stiffness, suggesting that myofibrogenic differentiation is accompanied by cellular-level changes in mechanical properties and that VICs respond both biologically and mechanically to matrix stiffness changes.

This observation has particular implications for the study of VIC biology. Much research into VIC function is conducted on cells grown in culture on either glass or plastic. Because this configuration alone may induce myofibrogenic differentiation, interpretation of data from these experiments is difficult. Culture of VICs on softer substrates such as collagen or polyacrylamide matrices that inhibit formation of the α-SMA stress fibres characteristic of myofibroblast differentiation may provide a more physiologically relevant culture system.

4.4.2.1 Study limitations

MA of cells cultured on tissue culture substrates remains the most challenging MA experiment. Following trypsinization and resuspension in complete media, cells experience blebbing to a much higher degree than the cells isolated and tested on the same day. This phenomenon resulted in a much higher proportion of cells that needed to be excluded from results (following the criteria outlined in section 3.3.3). As such, the total number of useful cells remained low, because of the finite amount of time available to test cells.

4.4.3. Overall conclusions

VIC function does appear to be at least partially regulated by the immediate mechanical environment. The degree to which the tissue-level mechanical organization influences VIC function and mechanical properties remains somewhat uncertain, however it is evident that myofibrogenic differentiation *in vitro* involves substantial changes in the

mechanical response of VICs. Although the exact biological mechanisms behind these changes remain unclear, VIC stiffness clearly increases during myofibrogenic differentiation, perhaps as a result of the formation of α-SMA stress fibres. In any case, these results indicate that stiffening of the valve in disease processes may indeed be reflected at the cellular level. The following chapter investigates this observation in more detail by examining the VIC mechanical response to two distinct pathogenic mechanisms.

Chapter 5: Mechanical changes in pathogenic VICs

5.1. Introduction

Aortic valve sclerosis is a pathological condition that can involve chronic inflammation of valve tissue, increased cellularity and extensive remodelling of the ECM, resulting in fibrotic and calcific tissue [76, 78-84]. AS is now widely accepted to be an active process in which VICs are directly involved [72, 89, 90], capable of differentiating into an osteogenic or myofibrogenic phenotype. Unknown are what factors cause VIC differentiation and how these are regulated. However, due to the dynamic environment in which VICs reside, mechanical effects have been suggested as a contributing factor to the initial and propagation of valve pathogenic processes.

Despite many studies examining changes within ECM organization, individual VIC mechanical response to disease is poorly understood. Matrix stiffness clearly has an effect on VIC differentiation *in vitro*, regulating two apparently distinct calcification mechanisms [119]; whether this effect is translated down to the cellular level is unknown. A clearer understanding of the extent to which VICs change their mechanical properties in distinct disease processes could provide insight into how particular phenotypes are initiated and maintained in the pathogenic state.

For this study, we used an existing *in vitro* collagen matrix system that differentially mediated VIC calcific processes and examined the relative difference in cell stiffness between these cultured cells and healthy cells isolated directly from the valve. Distinct disease processes do appear to exhibit different mechanical properties, suggesting that cell stiffness could be an indication of disease phenotype.

69

5.2. Methods and materials

5.2.1. VIC isolation

VICs were obtained using the isolation protocol described in Chapter 3 and Appendix A. One trial used VICs from a single isolation. A portion of the primary (day 0) cells were resuspended in complete media and held on ice prior to MA testing, while the remainder was seeded onto collagen matrices.

5.2.2. VIC culture and calcification

VICs were seeded on constrained collagen matrices (see section 5.2.3) at 10'000 cells/cm^2 in calcifying medium consisting of complete medium (DMEM + 10% FBS + 1% P/S) supplemented with 10 mM β-glycerophosphate, 10 μg/mL ascorbic acid and 10 nM dexamathesone. Calcifying media was changed every other day and cells were incubated at 37°C, 5% CO_2 until cell aggregates formed on both thick and thin collagen matrices, generally between day 10 and day 15 of culture (Figure 5-1).

Culture of VICs on either thick or thin (i.e. compliant or stiff) collagen matrices has been previously shown to induce two distinct calcification processes *in vitro* [119]. Although both matrices promote the formation of cell aggregates after culture in calcifying media, the aggregates themselves were morphologically and phenotypically distinct. VICs seeded on thick matrices formed aggregates that appeared to demonstrate development of an osteogenic VIC phenotype, characterized by increased calcium expression and ALP activity as well as increased gene expression of bone-markers osteocalcin and osteonectin. VICs seeded and cultured on thin collagen matrices showed evidence of myofibrogenesis and dystrophic calcification. Treatment with exogenous TGF-β accelerated aggregation only on thin matrices, consistent with the presence of myofibroblasts on these substrates.

We used the above system to determine whether there is a difference in mechanical properties of the various VIC populations – specifically, whether cells grown on thick or thin collagen gels altered their stiffness depending on matrix compliance as well as location (aggregate or non-aggregate). We also compared stiffness of all conditions with primary cells from the same isolation (Figure 5-1).
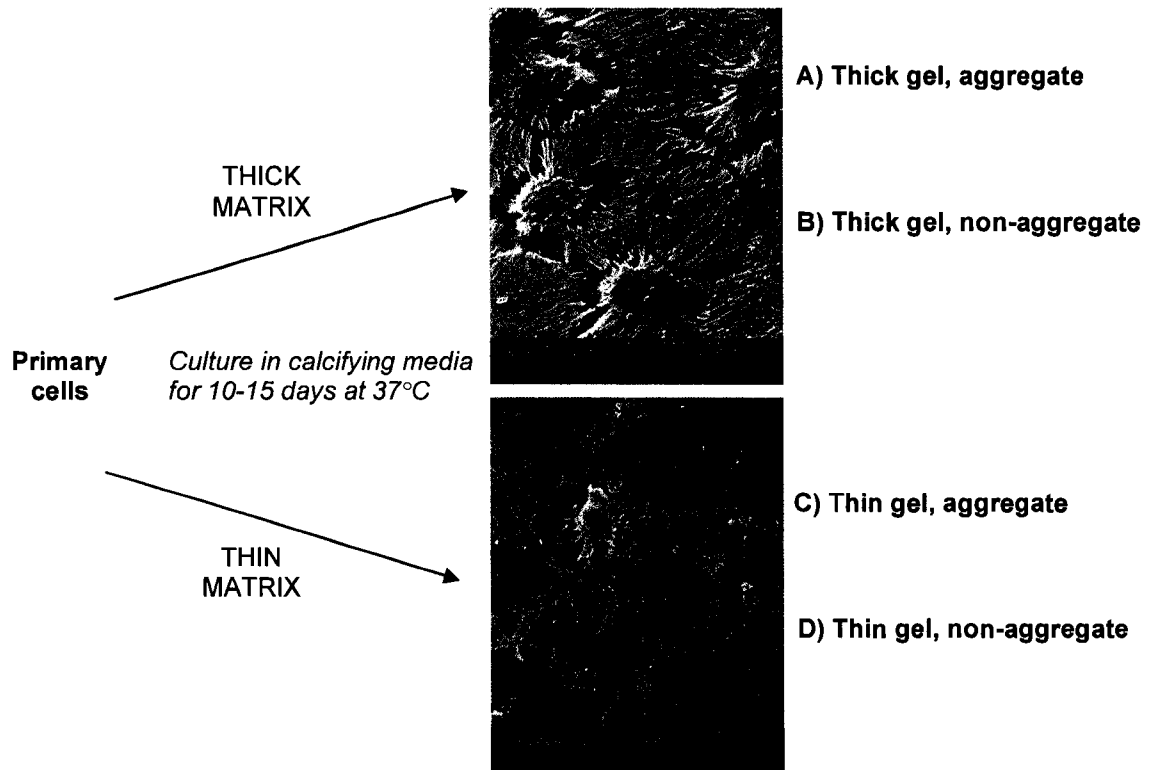
Figure 5-1 Experimental design for MA of differentiating VICs. For a single isolation, MA results from (1) primary VICs are compared to MA results from VICs from (A) thick matrix aggregates, (B) thick matrix non-aggregate regions, (C) thin matrix aggregates and (D) thin matrix non-aggregate regions. SEM images of VICs cultured on thick and thin collagen matrices in calcifying media show aggregate and non-aggregate regions. (Images courtesy of C.Y.Y. Yip).

5.2.3. Collagen matrices

Collagen solutions were prepared for each experiment as described in [139] (see protocol in Appendix A). The collagen mixture consisted of 0.3 mL 10X concentrated

DMEM, 0.3 mL 0.25M NaHCO₃ buffer, 0.3 mL FBS, 0.3 mL penicillin/streptomycin mixture, 0.12 mL 0.1 M NaOH buffer and 2.5 mL bovine collagen (PureCol, Inamed Biomaterials, Fremont, CA). Thick collagen matrices were made by pipetting 500 μl of collagen mixture into a 24-well plate lined with sterile coverslips. Thin matrices were made by allowing 500 μl of the collagen mixture to sit on the sterile coverslips for one minute at room temperature. Excess mixture was removed by aspiration, leaving a thin collagen layer on the coverslip. Polymerization of collagen was achieved by incubating at 37°C, 5% CO_2 overnight. Collagen matrices were constrained by the glass bottom and culture well sides. The thin collagen layer represented a stiff substrate (in which cells could feel the glass coverslip beneath the gel) and the thick collagen matrix represented a more compliant substrate.

5.2.4. Microdissection of collagen matrices

Within each of the two collagen matrices, there were two cell populations of interest: VICs within the aggregates and those surrounding them. Because both existed on a single matrix, we needed to establish a technique to independently remove each population.

This was achieved using a stereoscope and microdissection tools. Immediately prior to MA testing, a single collagen gel was removed from the incubator and placed under the stereoscope. The collagen matrix was easily detached from the glass substrate, so that with practice, the region of interest (aggregate or non-aggregate) could easily and accurately be removed from the collagen matrix using fine-tip forceps and a microdissection blade. Only one sub-population (aggregate or non-aggregate) was isolated from a particular collagen matrix.

Following dissection, we needed to establish a method to obtain the single-cell suspension necessary for MA. VICs are normally removed from entire collagen matrices by collagenase digestion and incubation at 37°C for 1 hour. Attempts to use this method to obtain a single-cell suspension proved unsuccessful (Figure 5-2a), as cells were observed to be clumped together. The addition of an equal amount of 0.125% trypsin in EDTA to the collagenase solution proved effective in obtaining the necessary single-cell suspension (Figure 5-2b)

(a)   (b)
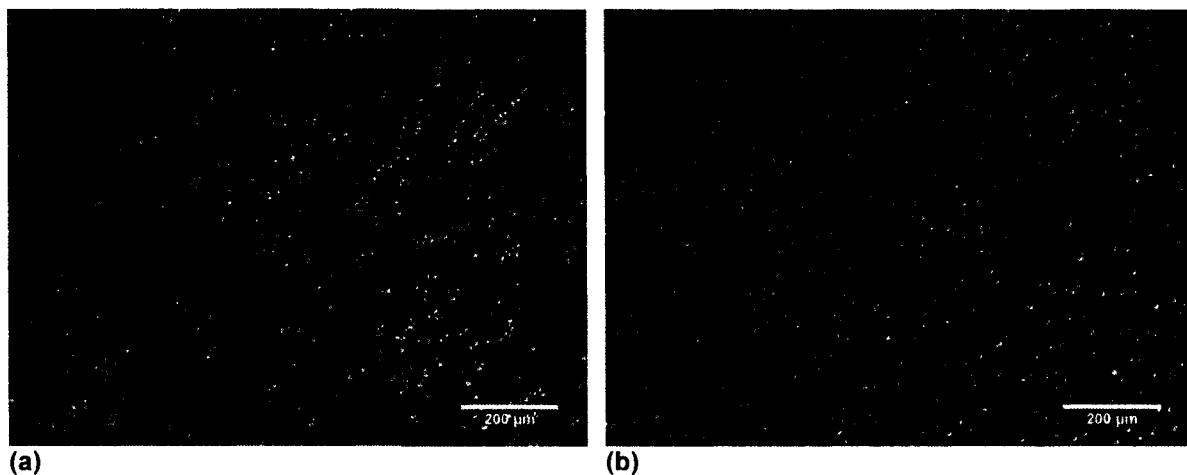
Figure 5-2 Relief contrast images of VICs isolated from distinct regions of collagen matrices: (a) VIC suspension with only obtained using only collagenase digestion and (b) single-cell suspension obtained using a 1:1 collagenase (300 U/mL) and 0.125% trypsin with EDTA mixture.

5.2.5. Immunofluorescent staining of cytoskeletal proteins

VICs in suspension were stained for α–SMA to correlate its expression with cell stiffness. Cells were removed from the collagen substrate as described above and mounted on a glass slide using a cytospin centrifuge (9 minutes at 700 rpm). Following cytospinning, VICs were fixed and permeablized for indirect immunostaining with monoclonal mouse anti-α–SMA primary antibody (α-SMA; Clone 1A4) and goat anti-mouse AlexaFluor 568

secondary antibody, followed by nuclear counterstain with Hoechst 33242 dye, following the protocol in Appendix A.

5.2.6. MA technique

MA testing procedures were followed according to the protocols outlined in Chapter 3 and Appendix A. Cells were held on ice throughout testing. Cells in suspension were placed on the microscope stage for a maximum of 25 minutes at a time and generally were held in the micropipette at a constant pressure for a maximum of 2 minutes. Average applied pressure (ΔP) was 486±11 Pa (mean ± standard deviation) for all collagen gel experiments. Stiffness measurements are reported as instantaneous Young's modulus (E_0) and were analyzed as outlined in Chapter 3.

One trial is defined as MA testing and plating of VICs from a single isolation – a small number of primary VICs from a particular isolation were tested using MA while the remainder were seeded onto collagen matrices and tested 10 -15 days later after aggregates had formed.

5.2.7. Statistical analysis

Values for Young's modulus more than 1.5 times the interquartile range (1.5×IQR) above the 75th percentile or below the 25th percentile were considered outliers and removed from the dataset. All data are presented as mean ± standard error of the mean (mean±SEM).

We repeated the collagen matrix experiments three times and applied statistical tests to the averages between trials. For two of the conditions (aggregates on thin gels and non-aggregate regions on thick gels) we were only able to obtain data from Trials 2 and 3.

Because the primary cell data cannot be considered an independent population from the four cultured conditions, we analyzed the data in two parts. We first tested to see whether

there was a statistical difference between primary (i.e. healthy) VICs and each of the four cultured populations. The Student's t-test was used to evaluate statistically significant differences between groups.

We then used ANOVA and multiple pairwise comparisons (Fischer LSD test) to assess differences between the four cultured VIC groups. P-values less than 0.05 were considered significant.

5.3. Results

5.3.1. α-SMA expression of primary and differentiating VICs

We used immunostaining to assess α-SMA expression in VICs removed from collagen matrices. Primary VICs, as well as those removed from aggregate and non-aggregate areas on both thick and thin gels were mounted on glass slides. Cells appeared rounded (rather than elongated as is normally typical for fibroblasts) because they were held in suspension prior to cytospinning and fixation. As expected, primary VICs did not show evidence of α-SMA expression. In addition, based on nuclear size, primary VICs appeared to be smaller than those cultured on collagen matrices, mirroring the trend observed with VICs cultured on plastic substrates in Chapter 4.

Cells grown on compliant matrices stained weakly positive for α-SMA, while those grown on stiff matrices stained strongly positive. There also appeared to be slight differences between cells isolated from aggregates or non-aggregate regions. VICs isolated from non-aggregate regions on stiff matrices showed the highest α-SMA expression, with the majority of cells staining strongly positive. Within aggregates on stiff matrices, α-SMA expression was high within some cells, but almost entirely absent in others. Some VICs from non-

aggregate regions on compliant matrices showed weak positive staining for α-SMA, although the majority did not express it. VICs within aggregates on compliant matrices showed a slightly higher rate of positive staining, although it was considerably weaker than that observed on stiff matrices
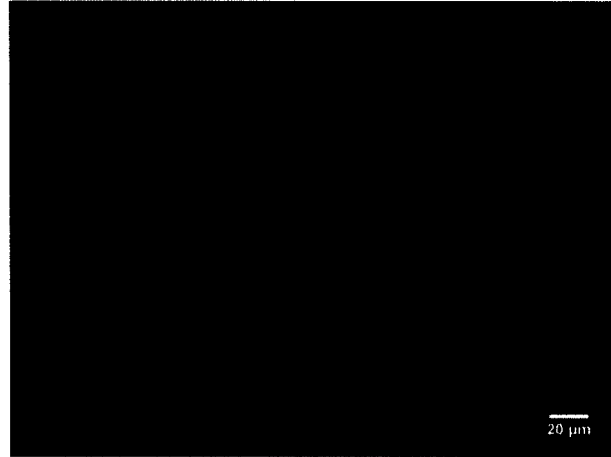
Figure 5-3 Primary VICs stained for α-SMA (red) and nucleus (blue). As expected, α-SMA is not expressed.

(a) (b)
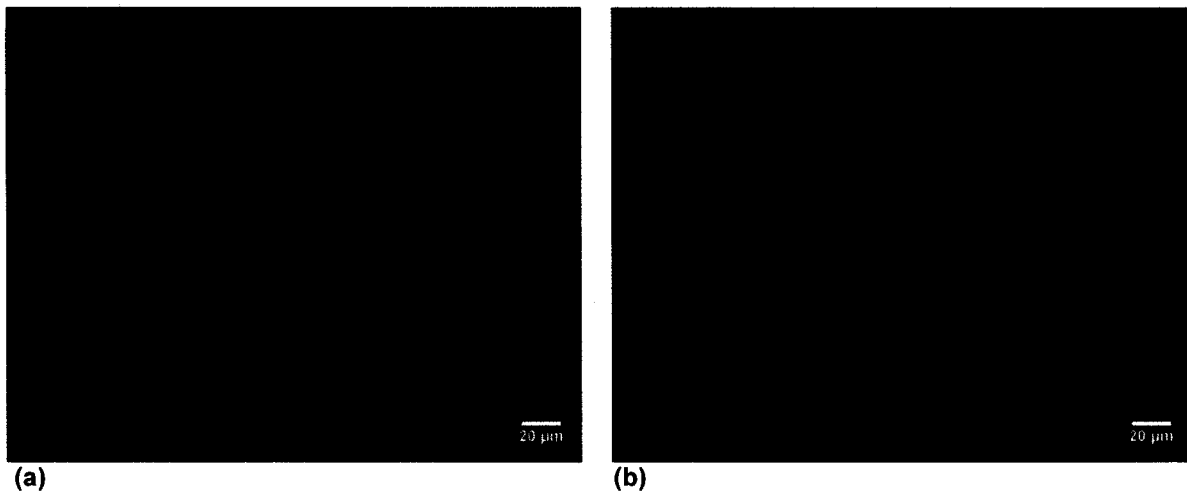
Figure 5-4 α-SMA (red) and nuclear (blue) staining of cells removed from compliant collagen matrices. VICs from (a) aggregates show slightly higher α-SMA expression than those isolated from (b) non-aggregate regions.

(a)   **(b)**
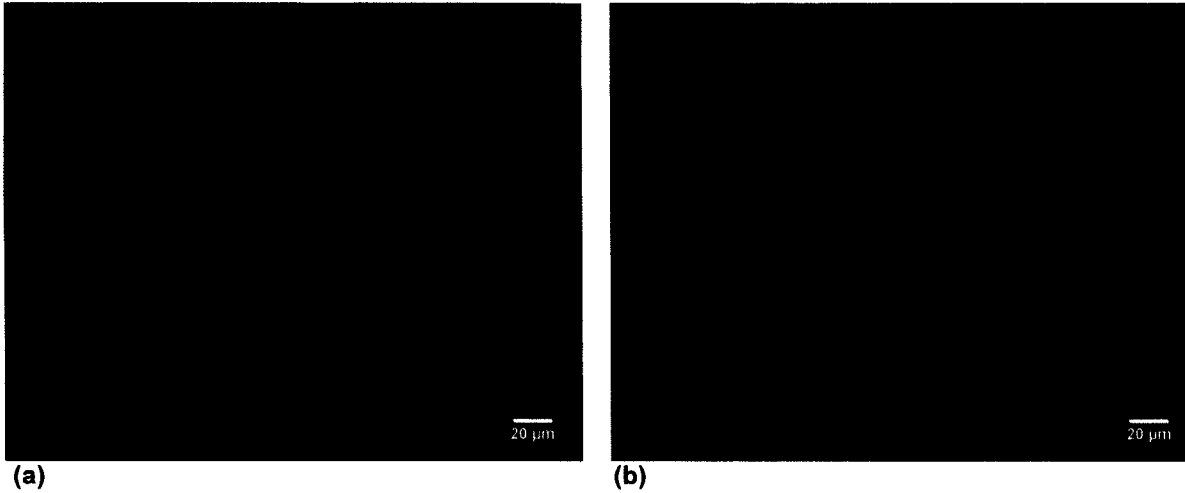
Figure 5-5 α-SMA (red) and nuclear (blue) staining of cells removed from stiff collagen matrices. VICs from (a) aggregates show slightly lower α-SMA expression than those isolated from (b) non-aggregate regions.

5.3.2. MA of calcifying cells

Below are the results and sample sizes for each test within each of the three trials (Figure 5-6 and Table 5-1). For trial 1, it was not possible to conduct MA experiments on VICs removed from non-aggregate regions on thick gels and aggregates on thin gels.

Table 5-1 Mean ± SEM and sample size for each condition within each trial

	Trial 1		Trial 2		Trial 3	
	E_0 [kPa]	# cells	E_0 [kPa]	# cells	E_0 [kPa]	# cells
Primary	2.55±0.18	23	2.52±0.17	19	2.57±0.13	27
Thick matrix						
Aggregate	4.61±0.36	19	5.27±0.47	19	4.03±0.22	24
Non-aggregate	N/A		3.61±0.05	7	3.34±0.17	21
Thin matrix						
Aggregate	N/A		3.86±0.37	14	4.15±0.20	25
Non-aggregate	6.11±0.64	19	5.18±0.46	12	6.37±0.53	27
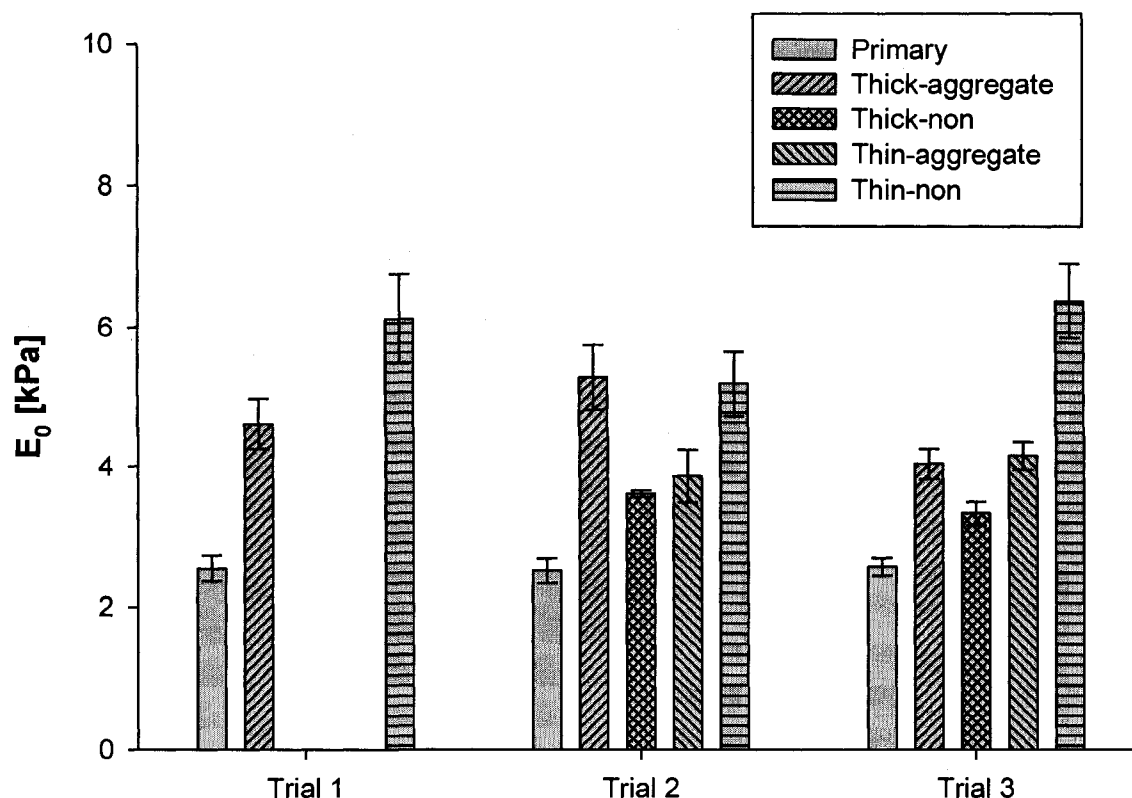
Figure 5-6 Values for Young's modulus for each condition for each of the three trials.

We compared the average stiffness between trials for each test condition (Figure 5-7). Primary VICs were the most compliant at 2.55 ± 0.02 kPa. Among the VICs cultured on gels, stiffest were VICs grown in non-aggregate regions on stiff collagen matrices (5.89 ± 0.36 kPa) and softest were VICs grown in non-aggregate regions on compliant gels (3.47 ± 0.14 kPa). VICs from aggregates on both compliant and stiff matrices had an instantaneous Young's modulus of 4.64 ± 0.36 kPa and 4.01 ± 0.15 kPa respectively.

We first compared the stiffness of primary cells to each of the four culture conditions (Table 5-2). Because we were making multiple comparisons between groups, a p-value of 0.05 might not necessarily indicate a statistical difference between two groups. However, the

p-values obtained were all an order of magnitude smaller (p < 0.005 for all comparisons),

suggesting that stiffness did change with culture on collagen gels.

Table 5-2 Stiffness of primary VICs compared with stiffness of VICs from collagen matrices (mean±SEM). P-values were determined using the Student's t-test for each comparison.

	Average E_0 [kPa]	*Pairwise comparison with primary VICs*
Primary	2.55±0.02	N/A
Thick matrix		
Aggregate	4.64±0.36	p = 0.004
Non-aggregate	3.47±0.14	p = 0.003
Thin matrix		
Aggregate	4.01±0.15	p ≤ 0.001
Non-aggregate	5.89±0.36	p ≤ 0.001

Next, we compared stiffness of VICs among the four culture conditions (Figure 5-7).

Significant differences were observed between VICs from non-aggregate regions on stiff gels

and: i) aggregates on stiff gels (p = 0.008), ii) aggregates on compliant gels (p = 0.026) and

iii) non-aggregate regions on compliant gels (p = 0.002).
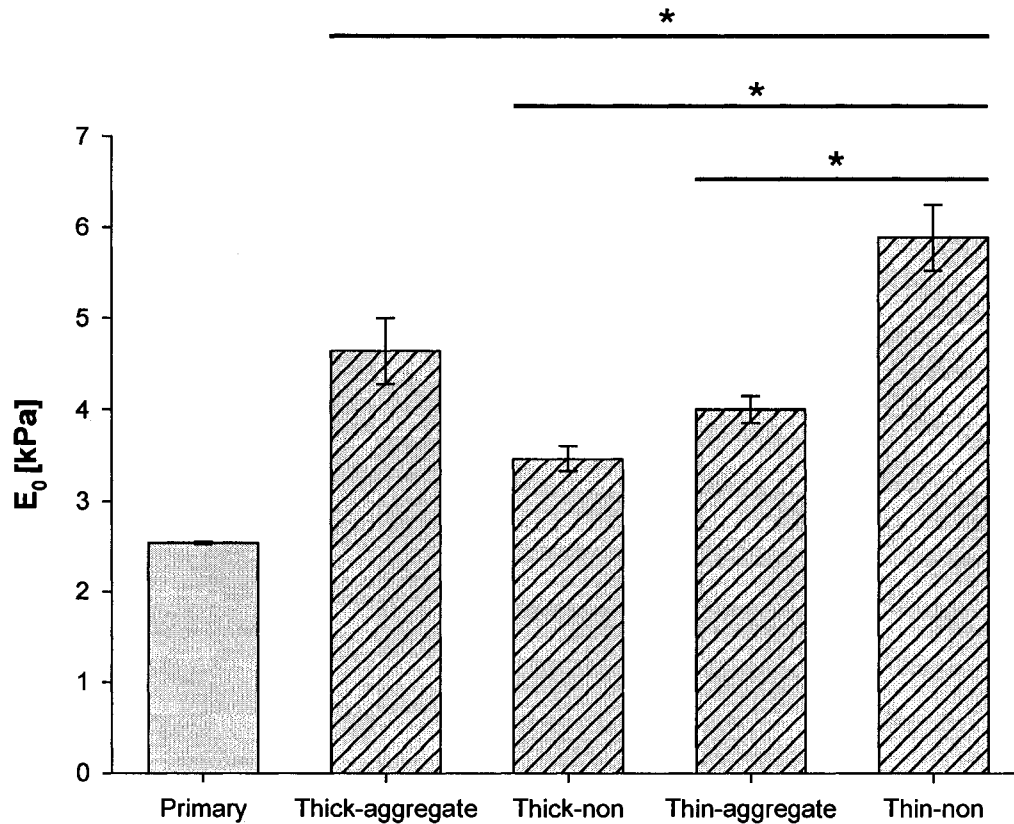
Figure 5-7 Average stiffness of VICs for each condition. Statistically significant differences (p < 0.05) between culture conditions (excluding primary VICs) are indicated.

5.4. Discussion

Mechanical changes at the cellular level are common in many pathological states, [13-15, 17, 140] and are often reflected or influenced by structural changes at the tissue or organ level. Mechanical effects appear to play a substantial role in the initiation and progression of aortic valve sclerosis [58, 59, 88], however whether these changes are evident at the cellular level is uncertain. Known is that valve interstitial cells play an active role in AS [72, 89, 90], and as such may change their mechanical response during pathogenic differentiation. Any changes in cell structure and organization could also be translated to the molecular level through mechanotransduction. Thus, an understanding of how VIC structural

integrity changes with valve pathology could be an important initial step in understanding the mechanistic basis of the disease.

VICs can be induced to form aggregates *in vitro* [89], which are also referred to as bone nodules or calcified nodules due to the presence of calcium deposits and ALP activity [108, 111] and are often used as an *in vitro* model for valve disease. We used an existing collagen matrix system characterized in our lab [119] (described in more detail below) that is capable of differentially mediating pathogenic processes within VICs to assess the changes, if any, of cell stiffness in disease.

5.4.1. Pathogenic differentiation of VICs

The collagen matrix system we used to induce VICs to pathogenic phenotypes has already been characterized from a biological perspective [119]. With the obvious exception of matrix stiffness, VICs seeded and grown in calcifying media on each collagen gel were exposed to identical culture conditions. Preliminary characterization of mechanical properties of these matrices has shown that the elastic modulus of compliant collagen gels is slightly higher than the tensile modulus of normal valve tissue [70], but similar to that of early atherosclerotic lesions [116]. Furthermore, the thin gel appears to be stiff enough to induce myofibrogenic differentiation in VICs, despite an apparent elastic modulus only a few times higher than that of the compliant matrix. Together, these two matrices provide an opportunity to determine how cellular stiffness is affected under two distinct aortic valve pathological processes. The exact differences in biological response are reported in [119] and are summarized in the following paragraphs.

VIC aggregate formation occurred on both matrices after 10-15 days of culture and there was localized calcium deposition characteristic of bone nodules within aggregates

formed on both stiff and compliant matrices. Beyond those similarities however, VICs responded in a noticeably dissimilar manner to the two culture environments. VICs cultured in calcifying media on thick collagen gels tended to differentiate into osteoblast-like cells, characterized by an upregulation of bone matrix proteins osteonectin and osteocalcin. More specifically, aggregates on thick matrices showed localized ALP activity and osteocalcin expression, suggesting that after a requisite culture time, VICs differentiated into two phenotypes on the same matrix – calcifying VICs clustered together within aggregates and VICs more evenly distributed elsewhere (see Figure 5-1). Actin expression within VICs cultured on compliant surfaces included expression of α-SMA in monomeric form, suggesting that the differentiation process these cells were undergoing was not typical of myofibrogenesis. Conversely, VICs cultured on thin matrices preferentially expressed the filamentous α-SMA characteristic of myofibroblasts, particularly among cells not within aggregates [119].

Although VICs cultured on stiff substrates also formed aggregates, the morphology, frequency and biology of these were observed to be distinct from those seen on compliant matrices (see Figure 5-1). In general, VICs on stiff substrates formed fewer aggregates and instead tended to overlap and form ridges. Furthermore, aggregates on thin matrices exhibited a dystrophic calcific phenotype, and VICs within them were either dead or apoptotic, while the cells within aggregates on thick matrices appeared viable and showed no evidence of apoptosis [119].

Overall, the collagen culture system provided us with a tool to examine multiple pathogenic responses of VICs. In particular, cells from aggregates on thick gels appeared to preferentially undergo osteogenic differentiation, while cells from non-aggregate regions on

thin gels appeared more characteristic of myofibroblasts. Perhaps less clear is the biological representation of the remaining two populations – cells from aggregates on thin gels and non-aggregates on thick gels. The former may simply be the final step in myofibrogenic differentiation, in which cells become apoptotic [100], as has been observed *in vivo* in dystrophic valvular calcification [94, 98]. The latter may be representative of a distinct, non-calcific phenotype. Emerging evidence in our lab suggests that the native VIC population contains a subpopulation of mesenchymal progenitor cells [114], which presumably would be present in the heterogeneous VIC population seeded on both matrices. Culture conditions on the softer matrix may induce the osteogenic differentiation of these progenitor cells, which then causes formation of the calcific aggregates observed on compliant matrices. Cells not within aggregates may simply be non-progenitors. This theory is further supported by a study that has shown that bone marrow derived mesenchymal progenitor cells differentiate preferentially to osteoblasts when grown on type I collagen coated polyacrylamide matrices with an elastic modulus similar to that of the compliant collagen matrix [100].

5.4.2. α-SMA expression in primary and differentiating VICs

For our collagen matrix test system, immunofluorescent staining for F-actin and α-SMA on adherent VICs showed that while F-actin formed fibres regardless of matrix stiffness, α-SMA structure and organization were sensitive to changes in substrate stiffness. Monomeric α-SMA expression was observed in cells within aggregates on compliant matrices and filamentous α-SMA expression (or stress fibres formation) was noted in VICs on thin gels, especially in non-aggregate regions [119].

A particular concern for any MA testing of adherent cells is the effect of their removal from the native ECM or the *in vitro* culture substrate. Initially unclear was how the

VIC cytoskeleton reorganized itself upon removal from the collagen substrate. MA tests on VICs from stiff and compliant collagen matrices that differentially alter their cytoskeletal organization following removal from the collagen substrate may not accurately reflect the mechanical changes cells experienced as a result of pathological differentiation.

Because F-actin expression was similar for both culture conditions, we assumed that any changes in structure would be common to all cells tested, whether removed from stiff or compliant gels. However, because α-SMA was differentially expressed in adherent VICs from stiff and compliant cells, we needed to establish that this was still the case once cells were in suspension. Therefore, we processed one set of samples exactly as normally done for MA tests (microdissection of either aggregates or non-aggregate regions, digestion of excess collagen and resuspension in complete media) and used a cytospin centrifuge to mount a cell splatter of each sub-population on glass slides. These cells were subsequently fixed and stained for α-SMA and cell nuclei. The results (section 5.3.1) confirm that the relative amount of α-SMA in primary VICs and each of the four sub-populations appears to be consistent with what was observed in staining of adherent cells. In addition, primary VICs expressed little to no α-SMA, also consistent with what has been observed in intact valve tissue [62].

Suspended VICs grown on stiff matrices do show disruption of the filamentous α-SMA observed in adherent cells, yet even in suspension these VICs exhibit considerably higher α-SMA expression, both in staining intensity and in the number of cells positive for the actin isoform. Among VICs from thick matrices, α-SMA expression was not nearly as high, nor expressed in as many cells, particularly among cells removed from non-aggregate regions. Therefore, we were able to assume that the relative differences in α-SMA content

observed in VICs from the different sub-populations are indeed reflected in the adherent cells.

5.4.3. VIC stiffness changes with pathological differentiation

MA tests indicate a clear change in VIC stiffness with the onset of pathogenic differentiation *in vitro*. VICs from aggregates on compliant matrices were on average 82% stiffer than primary cells and those from non-aggregate regions on stiff matrices were over 130% stiffer. VICs from non-aggregate regions on thick gels and aggregates on thin gels were 36% and 57% stiffer, respectively. Statistical testing between primary VICs and each of the four sub-populations yielded $p < 0.005$ for all comparisons.

Comparison between the four groups of differentiating VICs also showed significant differences in stiffness between cells from non-aggregates on stiff matrices and each of the other sub-groups (p-values of 0.026, 0.002 and 0.008 for VICs from aggregates on compliant matrices, non-aggregates on thick gels and aggregates on thin gels, respectively).

Of particular interest is the fact that VICs undergoing osteogenic differentiation (compliant matrix aggregates) are significantly softer than those undergoing myofibrogenic differentiation (stiff matrix non-aggregate regions). This difference is likely even more pronounced in adherent cell culture, since the formation of α-SMA stress fibres in VICs undergoing myofibrogenic differentiation aids in force generation [101] and increases cytoskeletal tension, considerably affecting (i.e. increasing) cell stiffness. These stress fibres are generally anchored to the substrate via focal adhesions, disruption of which (as caused by removal of the cell from its substrate) can ultimately result in a softening of the cell. Therefore, osteogenic and myofibrogenic differentiation of VICs appears to be differentially mediated from a cellular-level mechanical as well as biochemical perspective. Still unclear is

exactly how these biochemical and mechanical changes are related and whether changes in cellular level stiffness affect the underlying ECM, or whether changes in matrix stiffness causes VICs to reorganize their cytoskeletal arrangement.

Cells tested from aggregate regions on stiff matrices were significantly softer than the other VIC population on the same gel. However, the cells tested may not be entirely representative of the entire aggregate population, limiting the interpretation of these data. Aggregates on thin gels appeared to contain a large number of dead cells (as identified by EthD-1 staining) [119], and although these were not seen in the suspension used for MA testing, it is possible that the dead or dying VICs were lysed in the steps prior to MA testing (initial MA tests of VICs positively stained for EthD-1 showed that these were extremely compliant cells prone to rupture with the application of very small suction pressures – see section 3.3.3.1). Live VICs were most often observed growing on the surface of the aggregates, a substrate that presumably was softer than the stiff collagen matrix. The decrease in substrate stiffness may therefore have resulted in a corresponding drop in cell elasticity.

The final population of VICs, those grown in non-aggregate regions on compliant gels, showed the smallest change in stiffness compared with primary cells, and also showed the lowest expression of α-SMA, making them the most similar to VICs isolated from the valve and perhaps providing the closest representation of an undifferentiated phenotype. Culture in calcifying media may have induced some changes within these cells, possibly accounting for the expression of monomeric α-SMA and the slight increase in Young's modulus. However, VICs grown on compliant matrices in complete (non-calcifying) media may be worth investigating as an *in vitro* model for non-pathogenic VICs, as this culture

system does not appear to induce the myofibrogenic differentiation observed with culture of VICs on tissue-culture plastic.

5.4.4. Study limitations

Perhaps the largest limitation in this study is the small sample size. Trials were only performed three times, and in the case of MA testing of cells from non-aggregate regions on compliant matrices and aggregate regions on stiff matrices, only two trials were performed. Additional trials would undoubtedly strengthen results obtained through statistical testing and perhaps even show differences not observed due to the small sample size. Moreover, each collagen gel experiment is technically challenging, involving a full day of cell isolation and MA testing, followed by up to two weeks of *in vitro* cell culture. In the best case, time constraints prevented the acquisition of more than about 20-30 cells per culture condition – and this was for MA testing conducted over a period of two days (initial attempts to accomplish everything in a single day was the principal reason that no data were acquired for the two conditions mentioned above). Finally, although we tried to test cells from each sub-population from multiple different matrices, this was not always possible, due to both the time constraints mentioned above and a tendency for the thick collagen gels to detach from their culture wells and contract, limiting the number of gels available for testing (if detachment and contraction occurred, the entire gel was discarded and no cells from it were tested).

A further technical difficulty was the microdissection of aggregate regions from non-aggregate regions. Although care was taken to keep the two populations separate, it is impossible to guarantee that cells from one group may not have been in the other. In order to

minimize the effects of any cross-contamination, we needed to test large numbers within each trial, a requirement sometimes made difficult by the above-mentioned time constraints.

In addition to the MA test results described in Chapter 4, ongoing research in our lab suggests that there may be a difference in both biological function and mechanical properties in cells isolated from distinct valve regions (specifically, from the fibrosa and the ventricularis/spongiosa layers). Unclear is whether these differences are inherent characteristics of the two populations, or whether these are acquired as part of existence in a distinct mechanical and biological environment. This raises an important concern in the study of pathological differentiation, since aortic valve lesions and calcification do tend to occur preferentially within the fibrosa [59, 88]. Conceivably, separate *in vitro* culture of these two populations using the collagen matrix system described above may yield different results, both biologically and mechanically. Despite this hypothesis, we were unable to examine the two cell populations separately, largely due to experimental constraints. Optimization of the layer separation technique outlined in Chapter 4 is ongoing and currently involves considerably longer isolation times and lower cell yields as compared to our standard whole-leaflet isolation protocol. These practical limitations have thus far prevented us from inducing a pathogenic response in each of the layer populations separately.

5.4.5. Conclusions

We examined the effect of pathogenic differentiation on VIC mechanical properties using a collagen matrix system capable of inducing both myofibrogenic and osteogenic differentiation. MA tests revealed that healthy VICs were considerably softer than all cultured phenotypes, evidence that similar to valve tissue, VICs stiffen with disease. Furthermore, among the cultured VICs, those undergoing myofibrogenic differentiation were

the stiffest, significantly more so than cells exhibiting an osteogenic phenotype, suggesting that the two pathogenic processes elicit different structural changes at the cellular level.

Chapter 6:   Summary

6.1.   Conclusions

The first objective of this thesis was to design, build and test a custom micropipette aspiration system capable of measuring the mechanical response of multiple cell types and biomaterials at the microscale. This system was then applied specifically to study the mechanical response of aortic valve interstitial cells, both as a function of location in native valve tissue and after the induction of a pathogenic response.

We were able to directly isolate VICs from distinct layers within valve leaflets and subsequently use the MA system to gauge the mechanical properties of each of these two populations. Preliminary evidence suggests cells from the fibrosa layer are stiffer than those from the ventricular/spongiosa layers, an observation which is reflected in tissue-level mechanical properties. However, further testing is required to absolutely confirm this observation at the cellular scale. We also established that standard cell culture methods significantly alter mechanical properties of VICs, more than doubling the instantaneous elastic modulus with extended *in vitro* culture. Because standard tissue culture methods also appear to induce myofibrogenic differentiation of VICs, we determined that there may be a link between VIC stiffness and valve pathology.

Indeed, further MA tests showed that pathological differentiation also appears to induce changes in the mechanical stiffness of VICs. We tested cells undergoing myofibrogenic differentiation on stiff collagen gels in calcifying media and found that these were significantly stiffer than VICs undergoing osteogenic differentiation on compliant matrices in otherwise identical culture conditions. Furthermore, all VICs cultured either on

stiff or compliant collagen matrices in calcifying media showed a significant increase in cell stiffness compared to primary VICs. Aortic valve sclerosis – which often exhibits both calcific and fibrotic tissue - causes tissue-level stiffening of leaflets, again demonstrating that VIC stiffness changes are reflected on the macroscale.

6.2. Future work

6.2.1. Improvements to MA system

Although the MA system designed was functional for all tests conducted, there exist a number of improvements that would streamline data acquisition and analysis. First, although the LabView program was adequate for our needs, optimization of all features was not a large concern during programming. Improvements to data collection methods, file storage and organization, and interface between video camera and computer would likely reduce testing times and simplify use for new users.

Analysis of data for this project primarily involved the manual measurement of aspiration length. This was a fairly time-consuming process, and the recent development within the department of an automated cell contour visual measurement technique that measures cell deformation in real-time [40] would greatly enhance the efficiency of the system and substantially decrease post-processing times. Integration of this technique with our experimental setup should be investigated.

6.2.2. Alternate mechanical tests on VICs

An obvious improvement would be to test the VIC stiffness of adherent cells. Using MA for this purpose was technically challenging, however it may be possible to eliminate some of the problems described in Chapter 3 by changing the orientation of either the pipette or the cell itself so that the micropipette approaches the top rather than the side of the cell.

The inner diameter of the pipette would no longer be limited by cell height, which would hopefully reduce the blebbing phenomenon observed in our initial attempts. However, implementation of such a system comes with its own problems, including the construction of an appropriate device to image the horizontal aspiration length of the cell. The maximum force applied to the cell would also have to be limited to one that does not cause its removal from the substrate, however if cells are very rigid, it may be difficult to see any appreciable deformation at lower suction pressures. In any case, even if MA of adherent cells proves non-feasible, testing of adherent VICs *in vitro* – perhaps with an established technique such as atomic force microscopy – would greatly aid in the interpretation of the MA data presented in this thesis.

6.2.3. Changes to biological tests of VICs

Once the layer separation protocol is optimized, it is recommended that the collagen matrix experiment be repeated for the two separate populations. Preliminary evidence suggests that there is spatial heterogeneity in both VIC biology and mechanical properties – whether inherent or as a result of environmental conditions remains unclear – implying that these two populations may have a distinct pathogenic response, both mechanically and biochemically.

The collagen system may also prove useful in the study of a healthy VIC phenotype. MA and α-SMA staining of VICs isolated from non-aggregate regions on thick matrices revealed that these cells appeared most like the primary VICs. Culture in complete (rather than calcifying) media on thick substrates may therefore inhibit the myofibrogenic differentiation observed using standard cell culture techniques and provide a more physiologically relevant *in vitro* model.

Finally, although immunostaining appeared to show differences in α-SMA expression in the various VIC sub-groups, protein quantification using Western blotting would provide more rigorous validation of any observed differences.

Bibliography

1. Lim, C.T., et al., *Experimental techniques for single cell and single molecule biomechanics.* Materials Science and Engineering C, 2006. **26**(8): p. 1278-1288.

2. Bachrach, N.M., et al., *Changes in proteoglycan synthesis of chondrocytes in articular cartilage are associated with the time-dependent changes in their mechanical environment.* J Biomech, 1995. **28**(12): p. 1561-9.

3. Buschmann, M.D., et al., *Mechanical compression modulates matrix biosynthesis in chondrocyte/agarose culture.* J Cell Sci, 1995. **108 (Pt 4)**: p. 1497-508.

4. Jen, C.J., S.J. Jhiang, and H.I. Chen, *Invited review: effects of flow on vascular endothelial intracellular calcium signaling of rat aortas ex vivo.* J Appl Physiol, 2000. **89**(4): p. 1657-62; discussion 1656.

5. Kuchan, M.J. and J.A. Frangos, *Shear stress regulates endothelin-1 release via protein kinase C and cGMP in cultured endothelial cells.* Am J Physiol, 1993. **264**(1 Pt 2): p. H150-6.

6. Sato, M., M.J. Levesque, and R.M. Nerem, *Micropipette aspiration of cultured bovine aortic endothelial cells exposed to shear stress.* Arteriosclerosis (Dallas, Tex.), 1987. **7**(3): p. 276-286.

7. Lodish, H.F., *Molecular Cell Biology.* 5th ed. 2004, New York: W.H. Freeman and Company. 973.

8. Chen, C.S., J. Tan, and J. Tien, *Mechanotransduction at cell-matrix and cell-cell contacts.* Annual Review of Biomedical Engineering, 2004. **6**: p. 275-302.

9. Wang, J.H. and B.P. Thampatty, *An introductory review of cell mechanobiology.* Biomech Model Mechanobiol, 2006. **5**(1): p. 1-16.

10. Ingber, D.E., *Cellular mechanotransduction: putting all the pieces together again.* Faseb J, 2006. **20**(7): p. 811-27.

11. Orr, A.W., et al., *Mechanisms of mechanotransduction.* Dev Cell, 2006. **10**(1): p. 11-20.

12. Titushkin, I. and M. Cho, *Modulation of cellular mechanics during osteogenic differentiation of human mesenchymal stem cells.* Biophysical journal, 2007. **93**(10): p. 3693-3702.

13. Trickey, W.R., T.P. Vail, and F. Guilak, *The role of the cytoskeleton in the viscoelastic properties of human articular chondrocytes.* Journal of orthopaedic research : official publication of the Orthopaedic Research Society, 2004. **22**(1): p. 131-139.

14. Jones, W.R., et al., *Alterations in the Young's modulus and volumetric properties of chondrocytes isolated from normal and osteoarthritic human cartilage.* Journal of Biomechanics, 1999. **32**(2): p. 119-127.

15. Suresh, S., *Biomechanics and biophysics of cancer cells.* Acta Biomater, 2007. **3**(4): p. 413-38.

16. Cima, L.G., et al., *A hydrodynamic interpretation of crisis in sickle cell anemia.* Microvasc Res, 1994. **47**(1): p. 41-54.

17. Glenister, F.K., et al., *Contribution of parasite proteins to altered mechanical properties of malaria-infected red blood cells.* Blood, 2002. **99**(3): p. 1060-3.

18. Lim, C.T., E.H. Zhou, and S.T. Quek, *Mechanical models for living cells--a review.* J Biomech, 2006. **39**(2): p. 195-216.

19. Hochmuth, R.M., *Micropipette aspiration of living cells.* Journal of Biomechanics, 2000. **33**(1): p. 15-22.

20. Bao, G. and S. Suresh, *Cell and molecular mechanics of biological materials.* Nat Mater, 2003. **2**(11): p. 715-25.

21. Ethier, C.R. and C.A. Simmons, *Introductory biomechanics: from cells to organisms.* 2007, New York: Cambridge University Press. 511.

22. Engstrom, K.G., B. Moller, and H.J. Meiselman, *Optical evaluation of red blood cell geometry using micropipette aspiration.* Blood cells, 1992. **18**(2): p. 241-57; discussion 258-65.

23. Evans, E. and A. Yeung, *Apparent viscosity and cortical tension of blood granulocytes determined by micropipet aspiration.* Biophysical journal, 1989. **56**(1): p. 151-160.

24. Heinrich, V. and W. Rawicz, *Automated, high-resolution micropipet aspiration reveals new insight into the physical properties of fluid membranes.* Langmuir, 2005. **21**(5): p. 1962-1971.

25. Merryman, W.D., et al., *Correlation between heart valve interstitial cell stiffness and transvalvular pressure: implications for collagen biosynthesis.* American Journal of Physiology. Heart and Circulatory Physiology, 2006. **290**(1): p. H224-31.

26. Moussy, F., et al., *Micropipette aspiration technique to investigate the adhesion of endothelial cells.* Colloids and Surfaces B: Biointerfaces, 1994. **2**(5): p. 493-503.

27. Sit, P.S., et al., *Micropipette aspiration on the outer hair cell lateral wall.* Biophysical journal, 1997. **72**(6): p. 2812-2819.

28. Byfield, F.J., et al., *OxLDL increases endothelial stiffness, force generation, and network formation.* J Lipid Res, 2006. **47**(4): p. 715-23.

29. Mitchison, J.M. and M.M. Swann, *The Mechanical Properties of the Cell Surface .1. The Cell Elastimeter.* Journal of Experimental Biology, 1954. **31**(3): p. 443-&.

30. Yeung, A. and E. Evans, *Cortical shell-liquid core model for passive flow of liquid-like spherical cells into micropipets.* Biophysical journal, 1989. **56**(1): p. 139-149.

31. Hochmuth, R.M. and D. Needham, *The viscosity of neutrophils and their transit times through small pores.* Biorheology, 1990. **27**(6): p. 817-28.

32. Alexopoulos, L.G., et al., *Osteoarthritic changes in the biphasic mechanical properties of the chondrocyte pericellular matrix in articular cartilage.* J Biomech, 2005. **38**(3): p. 509-17.

33. Sato, M., et al., *Application of the micropipette technique to the measurement of cultured porcine aortic endothelial cell viscoelastic properties.* Journal of Biomechanical Engineering, 1990. **112**(3): p. 263-268.

34. Byfield, F.J., et al., *Evidence for the role of cell stiffness in modulation of volume-regulated anion channels.* Acta Physiol (Oxf), 2006. **187**(1-2): p. 285-94.

35. Trickey, W.R., et al., *Determination of the Poisson's ratio of the cell: recovery properties of chondrocytes after release from complete micropipette aspiration.* Journal of Biomechanics, 2006. **39**(1): p. 78-87.

36. Ly, H.V., D.E. Block, and M.L. Longo, *Interfacial tension effect of ethanol on lipid bilayer rigidity, stability, and area/molecule: A micropipet aspiration approach.* Langmuir, 2002. **18**(23): p. 8988-8995.

37. Rowat, A.C., J. Lammerding, and J.H. Ipsen, *Mechanical properties of the cell nucleus and the effect of emerin deficiency.* Biophysical journal, 2006. **91**(12): p. 4649-4664.

38. Shao, J.Y. and R.M. Hochmuth, *Micropipette suction for measuring piconewton forces of adhesion and tether formation from neutrophil membranes.* Biophysical journal, 1996. **71**(5): p. 2892-2901.

39. Shao, J.-Y. and J. Xu, *A modified micropipette aspiration technique and its application to tether formation from human neutrophils.* Journal of Biomechanical Engineering, 2002. **124**(4): p. 388-396.

40. Liu, X.Y., Y.F. Wang, and Y. Sun, *Cell contour tracking and data synchronization for real-time, high accuracy micropipette aspiration.* IEEE Trans. Automation Science and Engineering (accepted for publication), 2008.

41. Zhou, E., C. Lim, and S. Quek, *Finite Element Simulation of the Micropipette Aspiration of a Living Cell Undergoing Large Viscoelastic Deformation.* Mechanics of Advanced Materials and Structures, 2005. **12**(6): p. 501-512.

42. Shao, J.-Y., *Finite Element Analysis of Imposing Femtonewton Forces with Micropipette Aspiration.* Annals of Biomedical Engineering, 2002. **30**(4): p. 546-554.

43. Haider, M.A. and F. Guilak, *An axisymmetric boundary integral model for assessing elastic cell properties in the micropipette aspiration contact problem.* Journal of Biomechanical Engineering, 2002. **124**(5): p. 586-595.

44. Haider, M.A. and F. Guilak, *An axisymmetric boundary integral model for incompressible linear viscoelasticity: application to the micropipette aspiration contact problem.* Journal of Biomechanical Engineering, 2000. **122**(3): p. 236-244.

45. Boudou, T., et al., *An extended modeling of the micropipette aspiration experiment for the characterization of the Young's modulus and Poisson's ratio of adherent thin biological samples: numerical and experimental studies.* Journal of Biomechanics, 2006. **39**(9): p. 1677-1685.

46. Baaijens, F.P., et al., *Large deformation finite element analysis of micropipette aspiration to determine the mechanical properties of the chondrocyte.* Annals of Biomedical Engineering, 2005. **33**(4): p. 494-501.

47. Theret, D.P., et al., *The application of a homogeneous half-space model in the analysis of endothelial cell micropipette measurements.* Journal of Biomechanical Engineering, 1988. **110**(3): p. 190-199.

48. Needham, D. and R.M. Hochmuth, *Rapid flow of passive neutrophils into a 4 microns pipet and measurement of cytoplasmic viscosity.* J Biomech Eng, 1990. **112**(3): p. 269-76.

49. Hochmuth, R.M., *Measuring the mechanical properties of individual human blood cells.* Journal of Biomechanical Engineering, 1993. **115**(4B): p. 515-519.

50. Sato, M., M.J. Levesque, and R.M. Nerem, *An application of the micropipette technique to the measurement of the mechanical properties of cultured bovine aortic endothelial cells.* Journal of Biomechanical Engineering, 1987. **109**(1): p. 27-34.

51. Byfield, F.J., et al., *Cholesterol depletion increases membrane stiffness of aortic endothelial cells.* Biophys J, 2004. **87**(5): p. 3336-43.

52. Engler, A.J., et al., *Matrix elasticity directs stem cell lineage specification.* Cell, 2006. **126**(4): p. 677-89.

53. Dahl, K.N., et al., *Distinct structural and mechanical properties of the nuclear lamina in Hutchinson-Gilford progeria syndrome.* Proceedings of the National Academy of Sciences of the United States of America, 2006. **103**(27): p. 10271-10276.

54. Dahl, K.N., et al., *Power-law rheology of isolated nuclei with deformation mapping of nuclear substructures.* Biophys J, 2005. **89**(4): p. 2855-64.

55. Charras, G.T., et al., *Estimating the sensitivity of mechanosensitive ion channels to membrane strain and tension.* Biophysical journal, 2004. **87**(4): p. 2870-2884.

56. Aoki, T., et al., *The pipette aspiration applied to the local stiffness measurement of soft tissues.* Ann Biomed Eng, 1997. **25**(3): p. 581-7.

57. Boudou, T., et al., *Influences of adhesion area and biological sample size on the estimation of Young's modulus and Poisson's ratio assessed by micropipette aspiration technique.* Conference proceedings : ...Annual International Conference of the IEEE Engineering in Medicine and Biology Society.IEEE Engineering in Medicine and Biology Society.Conference, 2007. **1**: p. 5391-5394.

58. Schoen, F.J., *Cardiac valves and valvular pathology: update on function, disease, repair, and replacement.* Cardiovascular pathology : the official journal of the Society for Cardiovascular Pathology, 2005. **14**(4): p. 189-194.

59. Thubrikar, M.J., *The aortic valve.* 1990, Boca Raton, Fla: CRC Press. 221.

60. Butcher, J.T. and R.M. Nerem, *Valvular endothelial cells regulate the phenotype of interstitial cells in co-culture: effects of steady shear stress.* Tissue engineering, 2006. **12**(4): p. 905-915.

61. Rabkin, E., et al., *Activated interstitial myofibroblasts express catabolic enzymes and mediate matrix remodeling in myxomatous heart valves.* Circulation, 2001. **104**(21): p. 2525-32.

62. Rabkin-Aikawa, E., et al., *Dynamic and reversible changes of interstitial cell phenotype during remodeling of cardiac valves.* J Heart Valve Dis, 2004. **13**(5): p. 841-7.

63. Taylor, P.M., S.P. Allen, and M.H. Yacoub, *Phenotypic and functional characterization of interstitial cells from human heart valves, pericardium and skin.* The Journal of heart valve disease, 2000. **9**(1): p. 150-158.

64. Liu, A.C., V.R. Joag, and A.I. Gotlieb, *The Emerging Role of Valve Interstitial Cell Phenotypes in Regulating Heart Valve Pathobiology.* American Journal of Pathology, 2007.

65. Yoganathan, A.P., Z. He, and S. Casey Jones, *Fluid mechanics of heart valves.* Annu Rev Biomed Eng, 2004. **6**: p. 331-62.

66. Simmons, C.A., et al., *Spatial heterogeneity of endothelial phenotypes correlates with side-specific vulnerability to calcification in normal porcine aortic valves.* Circulation research, 2005. **96**(7): p. 792-799.

67. Xing, Y., et al., *Effects of constant static pressure on the biological properties of porcine aortic valve leaflets.* Ann Biomed Eng, 2004. **32**(4): p. 555-62.

68. Stella, J.A. and M.S. Sacks, *On the biaxial mechanical properties of the layers of the aortic valve leaflet.* J Biomech Eng, 2007. **129**(5): p. 757-66.

69. Sacks, M.S., D.B. Smith, and E.D. Hiester, *The aortic valve microstructure: effects of transvalvular pressure.* J Biomed Mater Res, 1998. **41**(1): p. 131-41.

70. Vesely, I. and R. Noseworthy, *Micromechanics of the fibrosa and the ventricularis in aortic valve leaflets.* Journal of Biomechanics, 1992. **25**(1): p. 101-113.

71.   Vesely, I., *The role of elastin in aortic valve mechanics.* J Biomech, 1998. **31**(2): p. 115-23.

72.   Chester, A.H. and P.M. Taylor, *Molecular and functional characteristics of heart-valve interstitial cells.* Philos Trans R Soc Lond B Biol Sci, 2007. **362**(1484): p. 1437-43.

73.   Lindroos, M., et al., *Prevalence of aortic valve abnormalities in the elderly: an echocardiographic study of a random population sample.* J Am Coll Cardiol, 1993. **21**(5): p. 1220-5.

74.   Stewart, B.F., et al., *Clinical factors associated with calcific aortic valve disease. Cardiovascular Health Study.* J Am Coll Cardiol, 1997. **29**(3): p. 630-4.

75.   Mohler, E.R., 3rd, *Are atherosclerotic processes involved in aortic-valve calcification?* Lancet, 2000. **356**(9229): p. 524-5.

76.   O'Brien, K.D., *Pathogenesis of calcific aortic valve disease: a disease process comes of age (and a good deal more).* Arterioscler Thromb Vasc Biol, 2006. **26**(8): p. 1721-8.

77.   Otto, C.M., et al., *Association of aortic-valve sclerosis with cardiovascular mortality and morbidity in the elderly.* The New England journal of medicine, 1999. **341**(3): p. 142-147.

78.   Mohler, E.R., 3rd, et al., *Bone formation and inflammation in cardiac valves.* Circulation, 2001. **103**(11): p. 1522-1528.

79.   Warren, B.A. and J.L. Yong, *Calcification of the aortic valve: its progression and grading.* Pathology, 1997. **29**(4): p. 360-8.

80.   Edep, M.E., et al., *Matrix metalloproteinase expression in nonrheumatic aortic stenosis.* Cardiovasc Pathol, 2000. **9**(5): p. 281-6.

81.   Hinton, R.B., Jr., et al., *Extracellular matrix remodeling and organization in developing and diseased aortic valves.* Circ Res, 2006. **98**(11): p. 1431-8.

82.   Fondard, O., et al., *Extracellular matrix remodelling in human aortic valve disease: the role of matrix metalloproteinases and their tissue inhibitors.* Eur Heart J, 2005. **26**(13): p. 1333-41.

83.   Kaden, J.J., et al., *Expression and activity of matrix metalloproteinase-2 in calcific aortic stenosis.* Z Kardiol, 2004. **93**(2): p. 124-30.

84.   Otto, C.M., et al., *Characterization of the early lesion of 'degenerative' valvular aortic stenosis. Histological and immunohistochemical studies.* Circulation, 1994. **90**(2): p. 844-53.

85.   Otto, C.M., et al., *Prospective study of asymptomatic valvular aortic stenosis. Clinical, echocardiographic, and exercise predictors of outcome.* Circulation, 1997. **95**(9): p. 2262-70.

86.   Freeman, R.V. and C.M. Otto, *Spectrum of calcific aortic valve disease: pathogenesis, disease progression, and treatment strategies.* Circulation, 2005. **111**(24): p. 3316-26.

87.   Robicsek, F. and M.J. Thubrikar, *Role of sinus wall compliance in aortic leaflet function.* Am J Cardiol, 1999. **84**(8): p. 944-6, A7.

88.   Thubrikar, M.J., J. Aouad, and S.P. Nolan, *Patterns of calcific deposits in operatively excised stenotic or purely regurgitant aortic valves and their relation to mechanical stress.* Am J Cardiol, 1986. **58**(3): p. 304-8.

89. Mohler, E.R., 3rd, et al., *Identification and characterization of calcifying valve cells from human and canine aortic valves.* J Heart Valve Dis, 1999. **8**(3): p. 254-60.

90. Roy, A., N.J. Brand, and M.H. Yacoub, *Molecular characterization of interstitial cells isolated from human heart valves.* J Heart Valve Dis, 2000. **9**(3): p. 459-64; discussion 464-5.

91. Taylor, P.M., et al., *The cardiac valve interstitial cell.* The international journal of biochemistry & cell biology, 2003. **35**(2): p. 113-118.

92. Rajamannan, N.M., et al., *Human aortic valve calcification is associated with an osteoblast phenotype.* Circulation, 2003. **107**(17): p. 2181-4.

93. Rajamannan, N.M., et al., *Atorvastatin inhibits hypercholesterolemia-induced cellular proliferation and bone matrix production in the rabbit aortic valve.* Circulation, 2002. **105**(22): p. 2660-5.

94. Tanaka, K., et al., *Age-associated aortic stenosis in apolipoprotein E-deficient mice.* J Am Coll Cardiol, 2005. **46**(1): p. 134-41.

95. Diegelmann, R.F. and M.C. Evans, *Wound healing: an overview of acute, fibrotic and delayed healing.* Front Biosci, 2004. **9**: p. 283-9.

96. Desmouliere, A., C. Chaponnier, and G. Gabbiani, *Tissue repair, contraction, and the myofibroblast.* Wound Repair Regen, 2005. **13**(1): p. 7-12.

97. Desmouliere, A., *Factors influencing myofibroblast differentiation during wound healing and fibrosis.* Cell Biol Int, 1995. **19**(5): p. 471-6.

98. Mohler, E.R., 3rd, *Mechanisms of aortic valve calcification.* The American Journal of Cardiology, 2004. **94**(11): p. 1396-402, A6.

99. Darby, I., O. Skalli, and G. Gabbiani, *Alpha-smooth muscle actin is transiently expressed by myofibroblasts during experimental wound healing.* Lab Invest, 1990. **63**(1): p. 21-9.

100. Tomasek, J.J., et al., *Myofibroblasts and mechano-regulation of connective tissue remodelling.* Nat Rev Mol Cell Biol, 2002. **3**(5): p. 349-63.

101. Hinz, B., et al., *Alpha-smooth muscle actin expression upregulates fibroblast contractile activity.* Mol Biol Cell, 2001. **12**(9): p. 2730-41.

102. Storch, K.N., et al., *Alpha smooth muscle actin distribution in cytoplasm and nuclear invaginations of connective tissue fibroblasts.* Histochem Cell Biol, 2007. **127**(5): p. 523-30.

103. Wang, J., et al., *Smooth muscle actin determines mechanical force-induced p38 activation.* J Biol Chem, 2005. **280**(8): p. 7273-84.

104. Zhao, X.H., et al., *Force activates smooth muscle alpha-actin promoter activity through the Rho signaling pathway.* J Cell Sci, 2007. **120**(Pt 10): p. 1801-9.

105. Serini, G., et al., *The fibronectin domain ED-A is crucial for myofibroblastic phenotype induction by transforming growth factor-beta1.* J Cell Biol, 1998. **142**(3): p. 873-81.

106. Pho, M., et al., *Cofilin is a marker of myofibroblast differentiation in cells from porcine aortic cardiac valves.* Am J Physiol Heart Circ Physiol, 2008. **294**(4): p. H1767-78.

107. Speer, M.Y. and C.M. Giachelli, *Regulation of cardiovascular calcification.* Cardiovasc Pathol, 2004. **13**(2): p. 63-70.

108. Jian, B., et al., *Progression of aortic valve stenosis: TGF-beta1 is present in calcified aortic valve cusps and promotes aortic valve interstitial cell calcification via apoptosis.* Ann Thorac Surg, 2003. **75**(2): p. 457-65; discussion 465-6.

109. Rajamannan, N.M., et al., *Experimental hypercholesterolemia induces apoptosis in the aortic valve.* J Heart Valve Dis, 2001. **10**(3): p. 371-4.

110. Lee, Y.S. and Y.Y. Chou, *Pathogenetic mechanism of senile calcific aortic stenosis: the role of apoptosis.* Chin Med J (Engl), 1998. **111**(10): p. 934-9.

111. Clark-Greuel, J.N., et al., *Transforming growth factor-beta1 mechanisms in aortic valve calcification: increased alkaline phosphatase and related events.* Ann Thorac Surg, 2007. **83**(3): p. 946-53.

112. Mathieu, P., et al., *Calcification of human valve interstitial cells is dependent on alkaline phosphatase activity.* J Heart Valve Dis, 2005. **14**(3): p. 353-7.

113. Osman, L., et al., *Role of human valve interstitial cells in valve calcification and their response to atorvastatin.* Circulation, 2006. **114**(1 Suppl): p. I547-52.

114. Chen, J.-H., et al., *Identification and characterization of aortic valve mesenchymal progenitor cells with robust osteogenic calcification potential.* Submitted, 2008.

115. McDonald, T.O., et al., *Diabetes and arterial extracellular matrix changes in a porcine model of atherosclerosis.* J Histochem Cytochem, 2007. **55**(11): p. 1149-57.

116. Matsumoto, T., et al., *Local elastic modulus of atherosclerotic lesions of rabbit thoracic aortas measured by pipette aspiration method.* Physiol Meas, 2002. **23**(4): p. 635-48.

117. Discher, D.E., P. Janmey, and Y.L. Wang, *Tissue cells feel and respond to the stiffness of their substrate.* Science, 2005. **310**(5751): p. 1139-43.

118. Engler, A., et al., *Substrate compliance versus ligand density in cell on gel responses.* Biophys J, 2004. **86**(1 Pt 1): p. 617-28.

119. Yip, C.Y.Y., et al., *Calcification by valve interstitial cells is regulated by the stiffness of the extracellular matrix.* Submitted, 2008.

120. Fiddes, L., et al., *Augmenting Microgel Flow via Receptor-Ligand Binding in the Constrained Geometries of Microchannels.* Lab on a Chip (accepted for publication), 2008.

121. Cunningham, C.C., *Actin polymerization and intracellular solvent flow in cell surface blebbing.* The Journal of cell biology, 1995. **129**(6): p. 1589-1599.

122. Laster, S.M. and J.M. Mackenzie, Jr., *Bleb formation and F-actin distribution during mitosis and tumor necrosis factor-induced apoptosis.* Microsc Res Tech, 1996. **34**(3): p. 272-80.

123. Zhao, R., *Personal communication.* 2008.

124. Merryman, W.D., et al., *Viscoelastic properties of the aortic valve interstitial cells.* Journal of Biomechanical Engineering, 2008. Accepted for publication.

125. Charras, G.T., et al., *Non-equilibration of hydrostatic pressure in blebbing cells.* Nature, 2005. **435**(7040): p. 365-369.

126. Hagmann, J., M.M. Burger, and D. Dagan, *Regulation of plasma membrane blebbing by the cytoskeleton.* Journal of cellular biochemistry, 1999. **73**(4): p. 488-499.

127. Rentsch, P.S. and H. Keller, *Suction pressure can induce uncoupling of the plasma membrane from cortical actin.* European journal of cell biology, 2000. **79**(12): p. 975-981.

128. Merryman, W.D., et al., *Differences in tissue-remodeling potential of aortic and pulmonary heart valve interstitial cells.* Tissue engineering, 2007. **13**(9): p. 2281-2289.

129. Billiar, K.L. and M.S. Sacks, *Biaxial mechanical properties of the native and glutaraldehyde-treated aortic valve cusp: Part II--A structural constitutive model.* J Biomech Eng, 2000. **122**(4): p. 327-35.

130. Billiar, K.L. and M.S. Sacks, *Biaxial mechanical properties of the natural and glutaraldehyde treated aortic valve cusp--Part I: Experimental results.* J Biomech Eng, 2000. **122**(1): p. 23-30.

131. Huang, H.Y., J. Liao, and M.S. Sacks, *In-situ deformation of the aortic valve interstitial cell nucleus under diastolic loading.* J Biomech Eng, 2007. **129**(6): p. 880-89.

132. Vesely, I., *Reconstruction of loads in the fibrosa and ventricularis of porcine aortic valves.* Asaio J, 1996. **42**(5): p. M739-46.

133. Vesely, I. and A. Lozon, *Natural preload of aortic valve leaflet components during glutaraldehyde fixation: effects on tissue mechanics.* J Biomech, 1993. **26**(2): p. 121-31.

134. Merryman, W.D., et al., *The effects of cellular contraction on aortic valve leaflet flexural stiffness.* Journal of Biomechanics, 2006. **39**(1): p. 88-96.

135. Even-Ram, S., V. Artym, and K.M. Yamada, *Matrix control of stem cell fate.* Cell, 2006. **126**(4): p. 645-7.

136. Desmouliere, A., et al., *Apoptosis mediates the decrease in cellularity during the transition between granulation tissue and scar.* Am J Pathol, 1995. **146**(1): p. 56-66.

137. Arora, P.D. and C.A. McCulloch, *Dependence of collagen remodelling on alpha-smooth muscle actin expression by fibroblasts.* J Cell Physiol, 1994. **159**(1): p. 161-75.

138. Solon, J., et al., *Fibroblast adaptation and stiffness matching to soft elastic substrates.* Biophys J, 2007. **93**(12): p. 4453-61.

139. Bellows, C.G., A.H. Melcher, and J.E. Aubin, *Contraction and organization of collagen gels by cells cultured from periodontal ligament, gingiva and bone suggest functional differences between cell types.* J Cell Sci, 1981. **50**: p. 299-314.

140. Suresh, S., et al., *Connections between single-cell biomechanics and human disease states: gastrointestinal cancer and malaria.* Acta Biomater, 2005. **1**(1): p. 15-30.

Appendix A: Protocols

VIC Isolation

Purpose: To obtain a pure population of valve interstitial cells from porcine aortic valves

Reagents:
- penicillin/streptomycin (P/S) mixture
- sterile and non-sterile PBS with Ca^{2+}/Mg^{2+}
- amphotericin B
- 0.125% trypsin with EDTA (diluted in PBS without Ca^{2+}/Mg^{2+})
- DMEM + 10% FBS +1% P/S
- TES buffer

Equipment:
- large and small dissection scissors
- scalpel
- biohazard waste bags
- dissection tray
- large and small tweezers
- cell strainers
- cell scrapers
- sterile petri dishes

Procedure:
Steps 1-3 can be done outside of cell culture hood
1. Remove heart from non-sterile PBS and cut in half
2. Use large dissection scissors to cut open aorta until all three leaflets
3. Use small scissors and tweezers to remove individual leaflets and hold PBS with Ca^{2+}/Mg^{2+} + 1% P/S + 0.5% amphotericin B
Step 4 and up must be done in cell culture hood
4. Rinse leaflets (2-3 times) with clean, sterile PBS with Ca^{2+}/Mg^{2+} + 1% P/S + 0.5% amphotericin B, hold leaflets in last wash
5. To remove ECs:
6. Place all leaflets (6 leaflets/15mL tube) in 5 mL of 150 U/mL collagenase made with TES buffer
7. Incubate for 20 minutes at 37°C, 5% CO_2
8. Transfer leaflets to new tube containing 0.125% of trypsin with EDTA, incubate for 7 minutes at 37°C, 5% CO_2
9. Vortex at maximum speed for 1 minute
10. In a petri dish, scrape leaflet surfaces using cell scraper
11. In another petri dish, rinse away loose ECs with sterile PBS with Ca^{2+}/Mg^{2+} (2 rinses)
12. In another petri dish, soak leaflets in 0.125% trypsin with EDTA for 1-2 mins
13. Transfer 3 leaflets at a time into a new petri dish, and mince into small pieces with scissors

14. Transfer leaflet pieces to 150 U/mL collagenase solution made with PBS with Ca^{2+}/Mg^{2+}
15. Incubate for 2 hours in collagenase/PBS solution at 37°C, 5% CO_2
16. Following incubation, vortex at maximum speed for 1 minute (be sure that pieces are being agitated)
17. Strain tissue using cell strainers (1 strainer/3 leaflets)
18. Rinse filter once with equal volume of DMEM
19. Centrifuge cells to pellet (large centrifuge: speed 1150 rpm, 7 minutes; small centrifuge: speed 0.9 x g, 5 minutes)
20. Resuspend in supplemented DMEM (DMEM + 10% FBS + 1% P/S) media
21. Strain cell mixture using cell strainers to break up cell clumps
22. Count viable and dead cells with hemocytometer or with Vi-Cell cell viability analyzer
23. If performing MA on primary cells, hold on ice. Plate at 10'000 cells/cm if culturing cells.
24. Two hours after plating, check cells to see if adherent (should be rounded, but not floating)
25. Three hours after plating, cells should be adherent and just starting to spread; note relative number of adherent to floating cells
26. Remove media and dead cells and replace with new media the following day

Type I collagen matrices

Purpose: To make thick and thin collagen gel for 2D cell culture

Reagents:
- 10x concentrated, sterile DMEM
- 0.25M sterile $NaHCO_3$ buffer
- FBS
- Penicillin/streptomycin antibiotic mixture
- 0.01M sterile NaOH
- Vitrogen 100 Type I collagen

Equipment:
- 24-well plate
- 0.18 mm Ø coverslips

Procedure:
1. Sterilize coverslips (e.g. with ethanol burner) and place in 24-well plate
2. For 24-well plate (12 thick and 12 thin gels), combine and vortex to mix:
   1. 0.6 mL of 10X concentrated DMEM
   2. 0.6 mL of 0.25 M NaHCO3 buffer
   3. 0.6 mL of FBS
   4. 0.6 mL of antibiotics mixture
   5. 0.24 mL of 0.01 M NaOH
3. Add 5 ml of Vitrogen 100 Type I collagen, pipette up and down gently to mix. Do NOT vortex.
4. Pipette gel mixture onto plate
   a. Thick gel – 0.5 mL in each well of 24-well plate
   b. Thin gel – 0.5 mL in each well of 24-well plate, let sit for 1 minute and remove excess liquid (can re-used be used for thick gels)
5. Place in incubator at 37°C, 5% CO_2 overnight

Indirect immunostaining protocol

Purpose:
To visualize α-SMA expression of VICs mounted using cytospin centrifuge using fluorescently-labeled antibodies.

Reagents:
- PBS (with Ca^{2+} and Mg^{2+}) for rinsing
- 4% paraformaldehyde (PFA) or 10% neutral buffered formalin
- 0.1% Triton X-100
- 3% bovine serum albumin (BSA) in PBS
- α-SMA primary antibody (Ab)
- Goat anti-mouse secondary Ab, fluorescently conjugated
- 10% serum from host of secondary Ab (goat)
- Permafluor mounting medium
- 10 ug/mL Hoechst nuclear stain

Equipment:
- humidification chamber (e.g., Gladware container with wet paper towels in it)

Procedure:
(I) Fixation and permeabilization
1. Wash cytospin slides twice with PBS for 5 minutes each
2. Fix cells 5-10 minutes in 4% PFA or 10% NBF at room temperature
3. Remove fixative and rinse twice with PBS for 5 minutes
4. Permeabilize with 0.1% Triton X-100 for 5 minutes
5. Rinse twice with PBS for 5 minutes
6. Fixed and permeabilized cells can be stored in PBS at 4°C if necessary

(II) Primary Staining
1. Block with 3% BSA for 20 minutes at 37°C
2. Dilute primary Ab (1:100) in 3% BSA to working concentration
3. Remove blocking solution and apply primary Ab. Use wax pen to mark circle around cell splatter to minimize reagent used.
4. Incubate 30-60 minutes at 37°C.

(III) Secondary Staining (do in dark to avoid photobleaching of fluorophore)
1. Wash slides twice with PBS for 10 minutes
2. Make 10% serum/PBS using serum from host of secondary Ab (eg, for rabbit anti-mouse secondary, make 10% rabbit serum) diluted with PBS
3. Dilute secondary Ab (1:100) in 10% serum to working concentration.
4. Block slides with 10% serum for 30 minutes at room temperature
5. Apply secondary Ab to slides for 1 hour at room temperature in humidified chamber. Again, use wax pen circle to minimize the amount of secondary Ab required.
6. Rinse with PBS 5 minutes
7. Rinse with Hoechst diluted 1:1000 in PBS for 5 min to stain nuclei
8. Rinse with PBS 5 minutes
9. (Optional) Briefly rinse with distilled water to remove salts from PBS.
10. Apply Permaflour mounting medium and mount coverslip.

Micropipette aspiration

Reagents:
- Micropipette aspiration basic setup (should be part of permanent setup near fluorescent microscope
    - Micromanipulator and controller
    - Micromanipulator stand
    - Linear actuator with circuit board, reservoir holder
    - Computer with relevant LabVIEW programs open
    - Built-in tubing: from micromanipulator to variable water reservoir, transducer and fixed reservoir
    - Fluorescent microscope on anti-vibration table
    - 2 50mL conical tubes (fixed and variable reservoir)
- Micropipettes (pulled, forged, heat-polished, bent, Sigmacote treated – see *Micropipette fabrication* protocol below)
- Microfil needles
- 0.22 μm syringe filter
- Distilled water
- 2 beakers (one for waste, one for distilled H_2O)
- PBS without Ca^{2+}/Mg^{2+}
- PBS without Ca^{2+}/Mg^{2+} + 10% FBS
- Syringes
    - 60 mL for filling PBS tubing
    - 60 mL for filling distilled water tubing
    - 1 mL for filling micropipettes
- Beaker lift
- Stand to clamp tubing

Procedure:
System setup
1. Attach any necessary tubing
    a. Transducer
        i. Ensure valves connected to pressure ports on transducer are in proper position (so that zero pressure difference exists between positive and negative ports)
        ii. Tubing leading to negative pressure port should be connected to static reservoir, mounted on beaker lift. Fill tubing with distilled water using 60 mL syringe and place in 50mL conical tube on lift
        iii. Positive pressure port should be connected to variable reservoir (on linear actuator). Fill tubing with distilled water using 60 mL syringe and place in 50mL conical tube on reservoir mount

    iv. Ensure all tubing is liquid-filled and open all ports 4-way valves connecting to transducer

    v. Zero system by allowing water level in each 50 mL conical tube to equilibrate. Keep adjusting height of static reservoir (on beaker mount) until water level is at same height as microscope stage (at initial position, water levels in both reservoirs should be at same height). This is the zero-pressure reference point. Make sure to keep checking this throughout actual experiment and adjust as necessary

    vi. Close connections on 4-way valves between positive and negative ports

  b. Actuator

    i. Attach tubing to variable reservoir and fill with distilled water using 60 mL syringe and 4-way valve closest to actuator

    ii. Make sure to clamp tubing in stand beside actuator (ensure that tubing is not pinched shut), this will lessen the vibration effects due to sudden stops of linear actuator

  c. Stage

    i. Using 60 mL syringe and 4-way valve closest to stage, fill tubing (1/4" ID to 1/8" ID to 1/16" ID) with PBS without Ca^{2+}/Mg^{2+}.

    ii. Attach 1/16" ID tubing to micropipette holder

  d. For steps b and c, make sure 2-way valve in system tubing is closed to prevent accidental leakage

2. Fill pipettes

  a. Have a large number of ready formed, treated, bent and coated pipettes on hand and change frequently during experimental trials (pipettes clog easily – is often easier to change rather than try to remove particles stuck in tip)

  b. Filling

    i. Fill 1 mL syringe with PBS without Ca^{2+}/Mg^{2+} + 10% FBS solution

    ii. Attach 0.22 μm syringe filter and use MicroFil needles to fill micropipettes, make sure droplet or spray of liquid is visible at tip of pipette

    iii. Check tip of pipette for breakage and/or clogging particles before mounting into pipette holder

3. Mount pipettes

  a. Make sure pipette holder is completely liquid filled before inserting pipette (and that somewhere a valve is closed along main tubing line, preventing leakage)

  b. Loosen tip of holder and insert pipette making sure it reaches orange O-ring – ensures complete seal

4. Mount pipette and holder onto micromanipulator

  a. Starting position should always be at far left, far back and top point

  b. Place pipette holder with pipette into micromanipulator holder

      c. Ensure angle of pipette is such that foremost tip can reach surface of glass slide

      d. Once properly placed (i.e. with enough range to reach field of view), tighten all possible screws on micromanipulator

5. Adjust microscope settings

      a. Make sure condenser is at correct height

      b. Make sure 40x RC objective is used, and that all settings are correct.

6. Open all valves

7. Ensure there are no blockages in tubing system

      a. Place a glass slide with a few drops of PBS on scope and manoeuvre pipette into field of view.

      b. Use syringe attached to third port of valve to apply positive and negative pressure and ensure that there is aspiration

      c. Raise pipette to point above water drops and remove testing slide

Micropipette aspiration procedure:

8. Place Sigmacote treated glass slide on stage and add a small amount of cell suspension

9. If solution is too concentrated, dilute with small amount of PBS/10% FBS mixture

10. Approach cell with micropipette – this is easier if there is a slight negative pressure on the micropipette, will draw cell to pipette tip

11. Once cell is at tip of micropipette, switch to LabVIEW program and resize image to appropriate scale (100x100 to 150x150 pixels)

12. Apply tare pressure (up to 60 Pa at 50 Hz) and wait 30-60 seconds

13. Apply test pressure (usually 500 Pa at 500 Hz) and wait up to 2 minutes. Monitor aspiration length and discard data if blebbing occurs or if entire cell is aspirated

14. Bring actuator back to zero level

15. Repeat steps 7-13 for approximately 20-30 minutes and then replace cell suspension on microscope (either on new slide, or unused portion of old slide)

16. Continue collecting data for 2-3 hours, then discard unused cells and dismantle system

17. Delete unnecessary files and convert images to stacks using ImageJ.

18. Analyze data

Micropipette fabrication

Equipment:
- Pipette puller
- Microforge
- Ethanol flame burner
- Capillary glass
- Micropipette holder
- Syringe and tubing to connect to pipette holder
- Large petri dishes and plasticine (to store pipettes)
- Sigmacote

Procedure:
1. Use puller to pull glass capillary tube to a point (1 tube = 2 pipettes)
   - Set heating filament control so that current is no more than 20 A
   - Set solenoid at approx 5-6
2. Turn on microforge, heat glass bead on filament wire (when breaking pipette, should glow a dull red colour)
3. Mount pipette in microforge
4. Bring tip of pipette to a position slightly above glass bead on filament wire and make sure it will hit glass bead when lowered
   - Angle of approach: about horizontal, although slight angle below horizontal may produce at straighter edge for smaller IDs.
5. Turn on forge heat and, lower pipette onto glass bead and turn off heat – retraction of heating filament should cause pipette to break
6. Bring broken tip close to (but not touching) heated filament to round off jagged edges (fire-polishing)
7. Reorient pipette so that is vertical, with broken tip at bottom
8. Bring tip close to glass bead (but not touching) and turn up heat
9. Allow pipette tip to bend – approx 15° from vertical
10. Sigmacote pipette tips
    - Place forged and bent pipette into micropipette holder attached to air-filled syringe
    - Dip tip into Sigmacote solution for several seconds
    - Use syringe to expel any excess solution
    - Allow to dry in hood for several hours
11. Measure pipette ID using fluorescent microscope and QImaging program (very approximate method, will measure more accurately from aspiration images)
12. Store measured pipettes in large petri dishes (place on plasticine strips)

Appendix B: MA equipment

Table B-1 Detailed technical specifications of all relevant MA equipment

Equipment	Relevant technical specifications
Video microscopy system	
Microscope (Olympus Canada Inc, Markham, ON)	IX71 → Manual, inverted → WHN10X eyepieces (F.N. 22)
Objectives (Olympus Canada Inc, Markham, ON)	LUCPLFLN (40× relief contrast) → Correction collar (0-2 mm cover glass thickness) → 0.6 N.A., F.N. 22 CPLFLN (10× relief contrast) → 9 mm W.D., 1.5 cover glass → 0.3 N.A., 22 F. N.
Condenser (Olympus Canada Inc, Markham, ON)	IX-ULWCD condenser → N.A. 0.3 → W.D. 73 mm
Video camera (QImaging, Surrey, BC)	Retiga-2000R (RET-2000R-F-M-12-C) → CCD, Firewire connection, QCapture software provided → C-mount optical format → 10fps at 12 bits (190 fps maximum) → Full resolution: 1600×1200 pixels (pixel size 7.4×7.4 µm) → ROI; 1×1, 2×2, 4×4 binning
Anti-vibration table (Kinetic Systems Inc, Boston, MA)	→ Labmate I anti-vibration table
Hydrostatic system	
Linear actuator (Ultra Motion, Cutchogue, NY)	D-A1.0-HT17-8-1NO-BR/4 → 8" stroke length (8" water = 1.99kPa) → Leadscrew: 1.0" pitch → Bracket mount, magnetic position sensor → ¼-28 tapped hole in shaft end → HT17-075 hybrid step motor → 20-24 in/sec max speed → Maximum starting speed 2 rev /sec (i.e. 2 in/sec) → 8 leads, parallel connected
Step motor driver (Applied Motion Products, Watsonville, CA)	3540M → Requires: 12-42 V power supply → Requires: +5 V DC, 15mA input to activate optoisolation circuits → Step pulses able to sink at least 5 mA → Stepping options: 400, 1000, 2000 and 12800 steps / rev (1 rev corresponds to 1 in linear travel of actuator)
Differential pressure transducer (Validyne Engineering,	P55D-1-N-2-26-S-5-A → Range: ±3.5kPa (±14in H_2O) → 2mV rms output noise (equivalent to 1.4 Pa) → DC output ±5 V signal → Internal zero adjustment (→ Ports: 1/8" NPT female pipe threat, 8-32 bleed screw with gasket
PVC tubing (VWR, McMaster-Carr)	→ 1/8" ID, 1/4" OD (SKU 2127-60985-512) → 1/4" ID, 3/8" OD (SKU 2126-60985-528)

	→ 1/16" ID, 1/8" OD (SKU 2123-60985-502)
Valves	
(Cole-Parmer Canada, Montreal, QC)	→ 4-way stopcock with Luer connections (K-30600-04)
(McMaster-Carr,)	→ 2-way miniature ball valve with ¼" barb connections (4796K71)
Tubing / valve connectors	
(McMaster-Carr,)	→ 1/8" ID to 1/16" ID (5463K142) → 1/4" ID to 1/8" ID (297K261)
(Cole-Parmer Canada, Montreal, QC)	→ Female Luer × 1/4" hose barb (RK-45500-20) → Male Luer with lock ring × 1/4" hose barb (RK-45503-19)

Micropipette preparation and use

Micropipette holder (Harvard Apparatus Canada,	MP-S10A (MP Series holders) → For 1.0 mm OD glass → 1/16" barbed connector (to rest of system)
Capillary glass (Harvard Apparatus Canada,	G100T-4 Premium thin wall borosilicate capillary glass → 1.0mm OD, 0.78 mm ID, 100 mm length
Micromanipulator (Siskiyou Corp., Grants Pass, OR)	MC1000e-J - 3-axis closed loop controller (joystick) → Rapid setting: 1.7 mm/s → Slow setting: 30 µm/s, resolution 0.2µm MX7630 - Micromanipulator → Travel / axis = 20 mm → Minimum controllable motion: 0.1µm → Point-to-point accuracy: ±2 µm → ABP-R mounting plate MXC-45R – Pipette holder → Angle of approach (pipette): 0° - 180° → Clamp for holder with 3-10 mm handle
Micromanipulator stand (Siskiyou Corp., Grants Pass, OR)	→ MX312P-T → MX312P-T - Top plate (3×3") → AS-6.00 – 6" support legs ×4 → AS-2.00 – 2" support legs ×4 → AS-1.50 – 1" support legs ×4
Pipette puller (David Kopf Instruments, Tujunga, CA)	Model 700C
Microforge	DeFonbrune
Microfil needles (pipette filling) (World Precision Instruments, …)	MF34G-5 → Microfil 34AWG 5-pack

Data acquisition system

LabVIEW software and hardware (National Instruments, Austin, TX)	LabVIEW for Windows with multifunction NI DAQ board (PCI-6221 / CB-68LP) - Starter Kit → Analog Input: 8 differential or 16 single-ended → Input range: ±10 V, ±5 V, ±1 V, ±0.2 V (overvoltage protection ±25 V for device on, ±15V for device off) → Analog Output: 2 (16 bit resolution), ±10 V output range, ±5 mA output current drive → Counters: 2, 32 bit resolution (used edge counting) → +5 V power source (used to power step motor driver) → PFI ports – can be configured to digital I/O ports, counter/timer inputs

Appendix C: MA of capsule microgels

In collaboration with a student (Lindsey K. Fiddes) from the Polymers, Interfaces and Materials Science group (principal investigator: E. Kumacheva) we examined the mechanical properties of two types of microgel capsules using our MA setup. The instantaneous shear moduli (G) of the microgel capsules were determined by fitting experimental force-deformation data to a numerically-derived model that accounts for large deformation and gel and pipette geometries. Results are presented in [1].

Table C-1 Instantaneous shear modulus of microgel capsules

	1%	4%
Average	1.63 kPa	2.99 kPa
Standard deviation	0.52 kPa	1.70 kPa
Standard error	0.21 kPa	0.64 kPa

p-value (two tailed t-test assuming equal variance) = 0.089
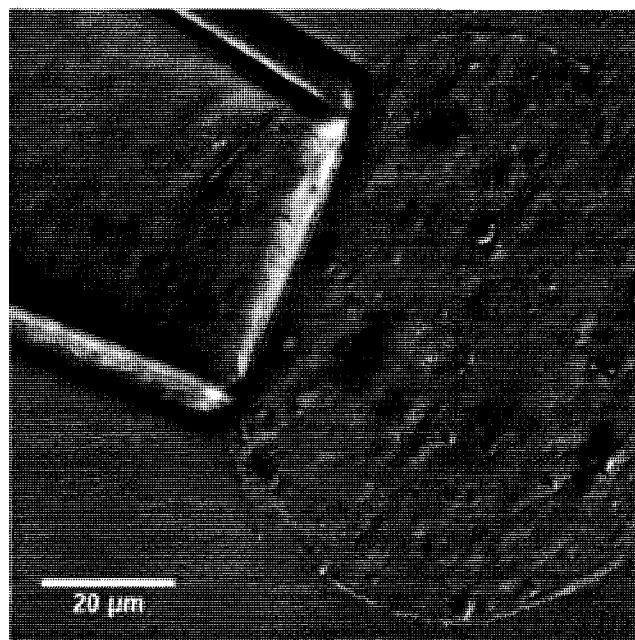
Figure C-1 MA of a capsule microgel

1. Fiddes, L.; Chan, Ho Ka (Carol), Wyss, K.; Simmons, C. A.; Wheeler, A.; Kumacheva, E. *Augmenting Microgel Flow via Receptor-Ligand Binding in the Constrained Geometries of Microchannels*. Lab on a Chip, 2008. Accepted for publication.